**UNIVERSIDADE FEDERAL DE MINAS GERAIS**
**Instituto de Ciências Exatas**
**Programa de Pós-graduação em Física**

Rodrigo Ferreira Saliba

# NUMERICAL SOLUTIONS TO OPEN HUBBARD MODELS

Belo Horizonte
2023

Rodrigo Ferreira Saliba

# NUMERICAL SOLUTIONS TO OPEN HUBBARD MODELS

Dissertação apresentada ao Programa de Pós-Graduação em Física do Instituto de Ciências Exatas da Universidade Federal de Minas Gerais como requisito parcial para obtenção do título de Mestre em Ciências.

Supervisor: Raphael Campos Drumond

Belo Horizonte
2023

Dados Internacionais de Catalogação na Publicação (CIP)

S165n Saliba, Rodrigo Ferreira.
Numerical Solutions to Open Hubbard Models/ Rodrigo Ferreira Saliba –.2023.
98 f. : il.

Orientador: Raphael Campos Drumond.
Dissertação (mestrado) – Universidade Federal de Minas Gerais, Departamento de Física.
Bibliografia: f. 67-71.

1. Hubbard, Modelo de. 2. Física do estado sólido.
I.Título. II. Drumond, Raphael Campos. III. Universidade Federal de Minas Gerais, Departamento de Física.

CDU – 539.2 (043)

Ficha catalográfica elaborada por Gislene Rodrigues CRB6/MG-3293/ Biblioteca Professor Manoel Lopes de Siqueira da UFMG.

UNIVERSIDADE FEDERAL DE MINAS GERAIS
INSTITUTO DE CIÊNCIAS EXATAS
PROGRAMA DE PÓS-GRADUAÇÃO EM FÍSICA

## ATA DE DEFESA DE DISSERTAÇÃO

**ATA DA SESSÃO DE ARGUIÇÃO DA 704ª DISSERTAÇÃO DO PROGRAMA DE PÓS-GRADUAÇÃO EM FÍSICA, DEFENDIDA POR RODRIGO FERREIRA SALIBA**, orientado pelo professor Raphael Campos Drumond, para obtenção do grau de **MESTRE EM FÍSICA**. Às 13 horas de dezesseis de agosto de 2023, por videoconferência, reuniu-se a Comissão Examinadora, composta pelos professores **Raphael Campos Drumond** (Orientador - Departamento de Matemática/UFMG), **Emmanuel Araújo Pereira** (Departamento de Física/UFMG), **Gabriel Teixeira Landi** (Instituto de Física/USP) e o doutor **Adalberto Deybe Varizi** (Departamento de Ciências Exatas/UESC) para dar cumprimento ao Artigo 37 do Regimento Geral da UFMG, submetendo o bacharel **RODRIGO FERREIRA SALIBA** à arguição de seu trabalho de dissertação, que recebeu o título de **"Numerical Solutions to Open Hubbard Models"**. O candidato fez uma exposição oral de seu trabalho durante aproximadamente 50 minutos. Após esta, os membros da comissão prosseguiram com a sua arguição e apresentaram seus pareceres individuais sobre o trabalho, concluindo pela aprovação do candidato.

Belo Horizonte, 16 de agosto de 2023.

Prof. Raphael Campos Drumond
Orientador do aluno
Departamento de Matemática/UFMG

Prof. Emmanuel Araújo Pereira
Departamento de Física/UFMG

Prof. Gabriel Teixeira Landi
Instituto de Física/USP

Dr. Adalberto Deybe Varizi
Departamento de Ciências Exatas/UESC

**Candidato:** Rodrigo Ferreira Saliba

Documento assinado eletronicamente por **Rodrigo Ferreira Saliba**, **Usuário Externo**, em 17/08/2023, às 09:00, conforme horário oficial de Brasília, com fundamento no art. 5º do Decreto nº 10.543, de 13 de novembro de 2020.

Documento assinado eletronicamente por **Gabriel Teixeira Landi**, **Usuário Externo**, em 17/08/2023, às 13:15, conforme horário oficial de Brasília, com fundamento no art. 5º do Decreto nº 10.543, de 13 de novembro de 2020.

Documento assinado eletronicamente por **Emmanuel Araujo Pereira**, **Membro de comissão**, em 17/08/2023, às 15:03, conforme horário oficial de Brasília, com fundamento no art. 5º do Decreto nº 10.543, de 13 de novembro de 2020.

Documento assinado eletronicamente por **Raphael Campos Drumond**, **Professor do Magistério Superior**, em 18/08/2023, às 13:05, conforme horário oficial de Brasília, com fundamento no art. 5º do Decreto nº 10.543, de 13 de novembro de 2020.

Documento assinado eletronicamente por **Adalberto Deybe Varizi**, **Usuário Externo**, em 21/08/2023, às 07:29, conforme horário oficial de Brasília, com fundamento no art. 5º do Decreto nº 10.543, de 13 de novembro de 2020.

A autenticidade deste documento pode ser conferida no site https://sei.ufmg.br/sei/controlador_externo.php?acao=documento_conferir&id_orgao_acesso_externo=0, informando o código verificador **2549597** e o código CRC **E20E4154**.

**Referência:** Processo nº 23072.249759/2023-45 SEI nº 2549597

# Acknowledgements

Agradeço à minha mãe, Angelica, e à minha irmã, Mell, pelo imenso apoio e incentivo ao longo da minha trajetória acadêmica. Também agradeço aos meus tios, Regina e Libério, por terem me dado o suporte necessário para que eu pudesse concluir este trabalho.

Agradeço ao meu orientador, Raphael Campos Drumond, pela paciência e excelente orientação.

A Lucas e Luis, vocês definitivamente são dois amigos.

À Capes, cuja ajuda financeira foi essencial para que este trabalho pudesse ser concluído.

Por fim, gostaria de agradecer a minha namorada, Paola, por ter sido uma fonte de amor e paz ao longo do mestrado.

# Resumo

A dinâmica de sistemas quânticos fechados (ideais), i.e., sistemas em que não consideramos interações com um meio externo (ambiente), é governada por uma evolução unitária, que pode ser geralmente descrita pela equação de Schrödinger - ou, na linguagem de operadores densidade, a equação de von-Neumann. No entanto, sistemas reais, ou seja, sistemas que podem ser medidos no laboratório, nunca estão completamente fechados e inevitavelmente irão interagir com os diversos graus de liberdade de seus ambientes. Nesse cenário, a equação de Schrödinger é apenas uma descrição válida da evolução do sistema por pequenos períodos de tempo, e uma nova descrição se torna necessária. Uma das formas de fazer isso é através do uso de equações mestras, que são equações de movimento que consideram os efeitos dissipativos no sistema devido às interações com o ambiente. Entre as possiveis formas das equações mestras, a equação de Lindblad é uma das mais extensivamente estudadas. Ela descreve evoluções markovianas, que geralmente são válidas no regime de interações fracas entre sistema e ambiente. Nessa perspectiva, ela tem sido aplicada com sucesso em muitos contextos, como medição contínua e ótica quântica. No contexto de problemas de sistemas quânticos abertos de muitos corpos, nem sempre é possível descrever a dinâmica dos sistemas através de uma equação mestra na forma de Lindblad. No entanto, essa aproximação pode ser usada em uma classe especial de sistemas atômicos, moleculares e ópticos (AMO). O objetivo desta dissertação é estudar a dinâmica de sistemas quânticos abertos de muitos corpos AMO, que são aproximadamente descritos pelo modelo de Hubbard, através do uso de métodos numéricos. Para isso, vamos focar nossa atenção em uma técnica de simulação particular conhecida como trajetórias quânticas, que em muitos contextos se mostra muito eficiente - o que pode ser melhorado se integrarmos esse método com outros, como Tensor Networks, t-DMRG e diagonalização exata.

**Palavras-chave**: sistemas quânticos abertos; sistema quânticos de muitos corpos; modelo de Hubbard; trajetórias quânticas; sistemas quânticos de muitos corpos abertos; efeito Zenão contínuo; preparação de estados.

# Abstract

The dynamics of closed (ideal) quantum systems, i.e., systems which are not considered to be interacting with an external media (environment), are governed by unitary evolution which can be generally described by the Schrödinger -or, in the language of density operators, the von-Neunmann - equation. Nevertheless, real systems, i.e., systems which can be measured in the laboratory, are never completely closed and are inevitably going to interact with the various degrees of freedom of their environments. In this scenario, Schrödinger's equation is only a valid description of the system's evolution for small periods of time and a new description of its dynamics becomes necessary. One of the ways to do this is through the use of master equations, which are equations of motion that consider the dissipative effects in the system due to interactions with its environment. The Lindblad master equation is one of the most extensively studied. It describes Markovian evolutions, which are usually the case in the regime of weak interactions between system and environment. It has been successfully applied in many contexts, such as those of continuous measurement and quantum optics. In the context of open quantum many body problems it is not always possible to describe the system dynamics through a master equation in Lindblad form. Nonetheless, this approxmation can be used in a special class of atomic, molecular and optical (AMO) systems. The goal of these thesis is to study the dynamics of open many body quantum AMO systems which are approximately described by the Hubbard model through the use of numerical methods. To that end we will focus our attention on a particular simulational technique known as quantum trajectories which in many contexts proves to be very efficient - even more so if we integrate this method with others such as Tensor Networks, t-DMRG and exact diagonalization.

**Keywords**: Open quantum systems; many body quantum systems; Hubbard model; quantum trajectories; open many body quantum systems; continuous quantum Zeno effect; state preparation.

# List of Figures

# Contents

# 1 Introduction

The study of open quantum systems has great impact in many areas of physics, such as quantum optics, continuous measurements, quantum information and quantum computation. The application of its results have proved to offer new insights in both theoretical and experimental setups.

In an ideal setup, where no interaction with the system's environment is considered, the dynamics of the state of the system is described by unitary evolution, i.e. by Shcrödinger's equation. Nevertheless, this description does not hold for long when we study open quantum systems, i.e., real quantum systems, whose interactions with an environment have to be considered. In the real world, no system measured is completely closed and, therefore, a more precise description of the system dynamics when in contact with its environment is required in order to make correct predictions and have a deeper understanding of the system's dynamics mechanisms.

In this spirit, many formalisms were created in order to describe these systems, such as quantum maps and master equations. The latter are equations of motion analogous to the Schrödinger equation, which take into consideration the coupling between system and environment, and may describe markovian or non-markovian dynamics depending on the system under consideration [11].

In this regard, even though non-markovian dynamics is dominant in physical systems, there are many fields, such as quantum optics and continuous measurements, in which important approximations may be done to consider the evolution of systems as being markovian. The extensive studies over such markovian master equations led to many methods to numerically solve them. One of these methods, the so called quantum trajectories technique, will be one of the focus of this thesis.

In recent years, advances in the control over many body systems composed of ultracold atoms and molecules, as well as trapped ions and optical systems (usually known as AMO systems) have brought interest in their application to the study of many areas, such as analog quantum simulation [5, 12], quantum computation [13] and quantum information [14, 15].A great example is that of the study on optical cavities done by *Haroche et al* [1], where detection of single photons were made by continuously probing the state of the cavity with two level atoms - the so called quantum non-demolition measurements(QND). The fact that, under the right parameter range, these systems dynamics may be described by well known models in quantum many body problems, e.g., the Hubbard and Heisenberg models, and also that their open dynamics may be described by markovian master equations turned their research very appealing, since many techniques

used to study open quantum systems, such as numerical methods and theoretical results, may be conveniently used in this many body context.

In this thesis we shall focus our attention on the study of open many body AMO systems whose dynamics may be described by the Hubbard model, giving emphasis in the quantum trajectories numerical method as a means to obtain results about them. In Chapter 2, we cover the fundamental notions of open quantum systems, introducing the quantum trajectories technique and discussing some results on master equations through it. In Chapter 3, we give an overview of quantum many body systems focusing our attention on the Hubbard model and AMO systems. In Chapter 4.1, we present a review of the progress of open many body AMO systems and the use of quantum trajectories to study them. We focus our attention on two specific features caused by dissipation on those systems, namely, the continuous quantum Zeno effect and state preparation. Finally, in Chapter 5, we give our final considerations and conclusions on this work.

# 2 Open Quantum Systems

The postulates of quantum mechanics are usually formulated in an ideal setup, i.e., an isolated system that does not interact with the environment around it. This idealization is an important step towards understanding the causes of numerous quantum phenomena and also provides us with a mathematical framework for the development of physical theories [16]. Nevertheless, in reality there are no isolated systems and interactions with the various degrees of freedom of the environment are inevitable. In this viewpoint, the system evolution can only be accurately described by Shrödinger's (or von-Neumann's) equation for very short timescales before the dynamics of the open quantum system becomes dominated by its coupling with the environment, which will lead to decoherence and a more classical behavior ( [9], [11]. A clear example of an open system, given by *Nielsen et al* [16], can be seen in the context of quantum information. If we consider the state of a qubit to be represented by two positions of an electron in an atom, the interactions with the electric and magnetic fields of other particles will become an uncontrollable source of noise and affect the system state.

In this context, a number of formalisms to describe open quantum systems were developed such as quantum maps (also known as quantum operators), that describe the evolution of an open system in discrete time intervals, and master equations which allow us to evolve the system state continuously. We shall briefly describe them.

## 2.1 Quantum Maps

In the quantum maps formalism we consider a composite system $\mathcal{H}_s \otimes \mathcal{H}_e$ formed by the system Hilbert space $\mathcal{H}_s$ and the environment Hilbert space $\mathcal{H}_e$. We then consider the composite system as a closed system - described by the postulates of quantum mechanics- which implies that the system will undergo unitary dynamics. Thus, if the initial state of the composite system is $|\psi_s\rangle \otimes |\psi_e\rangle$ the evolution of the system will be given by:

$$|\psi_s\rangle \otimes |\psi_e\rangle \to U_{se} |\psi_s\rangle \otimes |\psi_e\rangle \tag{2.1}$$

where $U_{se}$ is a unitary operator. Let $\{|m_s\rangle\}$ and $\{|m_e\rangle\}$ be an orthonormal basis for the system and environment, respectively. If we use the explicit identity $I_e = \sum_m |m_e\rangle \langle m_e|$ in equation 2.1 we get:

$$\begin{gathered}(U_{se} |\psi_s\rangle \otimes |\psi_e\rangle) = (I_s \otimes I_e) U_{se}(|\psi_s\rangle \otimes |\psi_e\rangle) \implies \\ U_{se}(|\psi_s\rangle \otimes |\psi_e\rangle) = (I_s \otimes \textstyle\sum_m |m_e\rangle \langle m_e|) U_{se}(|\psi_s\rangle \otimes |\psi_e\rangle).\end{gathered} \tag{2.2}$$

Defining the operator:

$$\langle m_e| U_{se}(|\psi_s\rangle \otimes |\psi_e\rangle) \in \mathcal{H}_s := A_m |\psi_s\rangle \tag{2.3}$$

we can rewrite the equation 2.2 as:

$$U_{se}(|\psi_s\rangle \otimes |\psi_e\rangle) = \sum_m A_m |\psi_s\rangle \otimes |m_e\rangle \tag{2.4}$$

where $\sum_m A_m^\dagger A_m = I_s$. Thus, we have the map:

$$\mathcal{T}(\rho = |\psi_s\rangle \langle\psi_s|) \rightarrow \ \mathrm{Tr}_e\Big[\sum_m \sum_{m'} A_m |\psi_s\rangle \otimes |m_e\rangle \langle m'_e| \otimes \langle\psi_s| A_{m'}^\dagger\Big] \ = \sum_m A_m \rho_s A_m^\dagger \tag{2.5}$$

where the trace $\mathrm{Tr}_e$ is taken over the environment. Equation 2.5 is called the Kraus representation for the quantum map:

$$\mathcal{T}(\rho) = \sum_m A_m \rho A_m^\dagger \tag{2.6}$$

It is also possible to define a quantum map through the use of three axioms [16, 17]:

1. $0 \leq \mathrm{Tr}[\mathcal{T}(\rho)] \leq 1$ e $\mathrm{Tr}[\mathcal{T}(\rho)]$ represents the probability the process has happened.
2. $\mathcal{T}(\rho)$ is convex-linear:
$$\mathcal{T}(\sum_i p_i \rho_i) = \sum_i p_i \mathcal{T}(\rho_i) \tag{2.7}$$
3. The map $\mathcal{T}$ must be completely positive, that is, $\mathcal{T}(\chi)$ must be positive for any positive operator $\chi$. If we introduce a new system, $M$, it must be true that $I_M \otimes \mathcal{T}(\chi)$ is also positive.

A simple example of a quantum map are generalized measurements (also known in some contexts as Positive Operator Valued Measurement, or POVM) which are essential in the context of continuous measurements [18], and can be defined as follows:

- A generalised measurement is composed by operators $\{\Omega_m\}$, which satisfy $\sum_m \Omega_m^\dagger \Omega_m = I$ where the index $m$ indicates the possible measurement results. If the state of the system before the measurement is $\rho$ then we have that:
- the probability of obtaining the result $m$ is given by $\mathrm{Tr}[\Omega_m^\dagger \Omega_m \rho]$.
- the state after the measurement is given by $\frac{\Omega_m \rho \Omega_m^\dagger}{\mathrm{Tr}[\Omega_m^\dagger \Omega_m \rho]}$.

## 2.2 Master Equations

Another important formalism that gives us a mechanism to evolve an open quantum system are the master equations. It consists of deriving an equation of motion for the system state $\rho$, where the dissipative effects due to coupling with the environment are taken into consideration. The state of the system is defined as the trace over the degrees of freedom of the environment for the density operator $\rho_{total}$ of the total (closed) composite system, i.e. $\rho = \mathrm{Tr}_{env}[\rho_{total}]$, as in the last section.

Generally, a master equation may take a very complicated form, since the state of the system at a specific time, $\rho_s(t_n)$, may depend on the state at previous times $(\rho(t_1), \rho(t_2), ...)$, i.e., the equation may be non-Markovian. Nevertheless, on specific regimes it is possible to approximate the dynamics as Markovian, which makes it easier to derive a master equation for it. This can be done through different routes [11, 19, 20] (see B for one of such routes).

The most general representation of the systems equation of motion for a Markovian evolution take the Lindblad form:

$$\dot{\rho} = -\frac{i}{\hbar}[H, \rho] - \frac{1}{2}\sum_m \gamma_m [C_m^\dagger C_m \rho + \rho C_m^\dagger C_m - 2C_m \rho C_m^\dagger] \tag{2.8}$$

where $H$ is the system Hamiltonian, the operators $C_m$ are called Lindblad operators (or jump operators) and describe the dissipative dynamics which happen at rates $\gamma_m$. The initial state is usually assumed to be uncorrelated, i.e., $\rho_{total} = \rho \otimes \rho_{env}$. We can absorb the term $\gamma_m$ into the operators $C_m$ making $l_m = \sqrt{\gamma_m} C_m$ in order to simplify the equation:

$$\dot{\rho} = -\frac{i}{\hbar}[H, \rho] - \frac{1}{2}\sum_m [l_m^\dagger l_m \rho + \rho l_m^\dagger l_m - 2 l_m \rho l_m^\dagger]. \tag{2.9}$$

Another representation of 2.8 is:

$$\dot{\rho} = -\frac{i}{\hbar}(H_{eff}\rho - \rho H_{eff}^\dagger) + \sum_m l_m \rho l_m^\dagger, \tag{2.10}$$

where $H_{eff}$ represents a non hermitian Hamiltonian which accounts for the effects of dissipation and decoherence and is given by

$$H_{eff} = H - \frac{i}{2}\sum_m l_m^\dagger l_m. \tag{2.11}$$

This definition of the effective Hamiltonian is very useful for the implementation of numerical methods such as the quantum trajectories technique. The second term on the right handside of equation 2.10($\sum_m l_m \rho l_m^\dagger$) is also called the *recycling term* since it recycles the lost population of states after the action of the non-Hermitian effective Hamiltonian.

## 2.3 Quantum Trajectories

The term *quantum trajectories* was first coined by Carmichael [21] for the numerical technique designed to obtain the evolution of a master equation as stochastic averages over individual evolution of pure initial states (i.e. individual trajectories) in his studies of generation of non-classical states of light. Similar methods have been developed parallel to his work by different research groups under different names such as the Monte Carlo Wave Function method [22–24]. The numerical technique presented advantages in comparison to solving the master equation exactly when the dimensions of the Hilbert spaces involved in the calculation were significantly large. This is because instead of evolving an object of size $D^2$ (where $D$ is the dimension of the Hilbert space), which becomes very costly as the dimensions of the space become larger, an object of size $D$ was evolved which, depending on the system, would cost much less memory.

The quantum trajectory method is more easily understood in the viewpoint of M∅lmer *et al* [22, 23]. We begin by expanding the master equation

$$\frac{d\rho}{dt} = -\frac{i}{\hbar}[H, \rho] + L(\rho) \tag{2.12}$$

where $\rho$ is the system state, $H$ the system Hamiltonian and $L$ is the Liouvillian superoperator:

$$L = -\frac{1}{2}\sum_m (l_m^\dagger l_m \rho + \rho l_m^\dagger l_m) + \sum_m l_m \rho l_m^\dagger \tag{2.13}$$

to first order, representing the state in an equivalent vector form. Suppose the system state at time $t$ is $|\phi(t)\rangle$. The idea is to define a stochastic process for the state vector, such that, for every instant of time, its average over all realization matches the solution of the Linblad equation at that instant of time. Then, to first order in $\delta t$, we have

$$\left|\phi^{(1)}(t+\delta t)\right\rangle = \left(1 - \frac{iH_{eff}\delta t}{\hbar}\right)|\phi(t)\rangle\,. \tag{2.14}$$

Since $H_{eff}$ is non-Hermitian the state $\left|\phi^{(1)}(t+\delta t)\right\rangle$ is not normalized and

$$\begin{gathered}\left\langle\phi^{(1)}(t+\delta t)\middle|\phi^{(1)}(t+\delta t)\right\rangle = \\ \langle\phi(t)|\left(1 + \tfrac{iH_{eff}^\dagger\delta t}{\hbar}\right)\left(1 - \tfrac{iH_{eff}\delta t}{\hbar}\right)|\phi(t)\rangle = 1 - \delta p,\end{gathered} \tag{2.15}$$

where

$$\begin{aligned}\delta p &= \delta t \tfrac{i}{\hbar}\langle\phi(t)|\, H_{eff} - H_{eff}^\dagger\,|\phi(t)\rangle \\ &= \textstyle\sum_m \delta p_m\end{aligned} \tag{2.16}$$

and $\delta p_m = \delta t\,\langle\phi(t)|\, l_m^\dagger l_m\,|\phi(t)\rangle$. After the evolution we randomly decide whether a quantum jump will occur. This is done by choosing a uniformly distributed random number $\epsilon$ in the

interval [0,1] and using the following rule:

$$|\phi(t+\delta t)\rangle = \begin{cases} \frac{\left|\phi^{(1)}(t+\delta t)\right\rangle}{\sqrt{(1-\delta p)}} \text{ if } \epsilon \geq \delta p, \\ l_m \left|\phi(t)\right\rangle, \text{ otherwise.} \end{cases} \tag{2.17}$$

where we choose the operator $l_m$ with probability

$$\Pi_m = \frac{\delta p_m}{\delta p}. \tag{2.18}$$

Therefore after a time interval $\delta t$ the state of the system is randomly chosen to be one of the possible states in equation 2.17. Since it is a first order approximation this procedure is only valid for intervals $\delta t$ such that $\delta p \ll 1$.

This process should then be repeated to the point that the average over an infinite number of trajectories converge to the solution of the master equation.

### 2.3.1 Equivalence to the Master Equation

To show that the stochastic average over trajectories lead to the solution of the master equation we consider the density operator $\sigma(t) = |\phi(t)\rangle \langle\phi(t)|$.The propagation of $\sigma(t)$ is given by:

$$\begin{aligned} \sigma(t+\delta t) \quad &= (1-\delta p)\frac{\left|\phi^{(1)}(t+\delta t)\right\rangle}{\sqrt{(1-\delta p)}} \frac{\left\langle\phi^{(1)}(t+\delta t)\right|}{\sqrt{(1-\delta p)}} \\ &+\delta p \textstyle\sum_m \Pi_m \frac{l_m|\phi(t)\rangle}{\sqrt{(\frac{\delta p_m}{\delta p})}} \frac{\langle\phi(t)|l_m^\dagger}{\sqrt{(\frac{\delta p_m}{\delta p})}} \end{aligned} . \tag{2.19}$$

Using definitions 2.14 2.13 2.11 we get:

$$\sigma(t+\delta t) = \sigma(t) + \left(\frac{i\delta t}{\hbar}\right)[\sigma(t), H] + \delta t L(\sigma(t)). \tag{2.20}$$

Therefore we see that taking the stochastic average over trajectories we have

$$\frac{d\overline{\sigma}}{dt} = \frac{i}{\hbar}[\overline{\sigma}, H_s] + L(\overline{\sigma}), \tag{2.21}$$

where $\overline{\sigma}$ indicates the average. This shows that the quantum trajectories technique gives the solution of the master equation.

In order to obtain the values of observables a similar approach as the one described above can be taken. For several trajectories,$|\phi^i(t)\rangle$, the expected value of an observable $A$ is calculated, i.e.$\langle\phi^i(t)| A |\phi^i(t)\rangle$. Defining the stochastic average over trajectories for the observable as

$$\langle A\rangle_n(t) = \frac{1}{n}\sum_{i=0}^{n} \left\langle\phi^i(t)\right| A \left|\phi^i(t)\right\rangle \tag{2.22}$$

where $n$ is the number of trajectories that have been run in the simulation. As a consequence of equation 2.21 and from the definition of the quantum mechanical expectation value $\langle A\rangle = \mathrm{Tr}\{\rho A\}$, in the limit of $n \gg 1$ we have

$$\langle A\rangle_n(t) \approx \langle A\rangle(t). \tag{2.23}$$

According to Dallibard et al [22] and Daley [9] we can also have a direct physical interpretation of the numerical technique, in the sense that we have a system evolving under the Hamiltonian $H_{eff}$ and there is the possibility of a quantum jump happening with a certain probability. The interpretation is clearer when we consider the example of a two level atom whose ground and excited states are $|g\rangle$ and $|e\rangle$, respectively. The system Hamiltonian is given by:

$$H = \hbar\omega_0\sigma^+\sigma^- \tag{2.24}$$

where

$$\sigma^+ = |e\rangle\langle g|\,,\ \sigma^- = |g\rangle\langle e|\,, \tag{2.25}$$

and $\hbar\omega_0$ is the difference in energy between the two states.

Let the state of the system, $|\psi(t)\rangle$, at $t = 0$ be given by the superposition:

$$|\psi(0)\rangle = \alpha_0|g\rangle + \beta_0|e\rangle\,. \tag{2.26}$$

Assuming the system undergoes a process analogous to the one descibed in equation 2.12, the effective Hamiltonian is, then, given by:

$$H_{eff} = \hbar\omega_0\sigma^+\sigma^- - \frac{i\hbar\Gamma}{2}\sigma^+\sigma^-, \tag{2.27}$$

where $\Gamma$ is the decaying rate of the two level atom.

After a sufficiently long time, interaction with the environment will lead the atom to decay into the ground state. Evolving the state $|\psi(0)\rangle$ for a time interval $\delta t$ we have

$$\left|\psi^{(1)}(\delta t)\right\rangle = \alpha_0|g\rangle + \beta_0\exp(-i\omega_0\delta t)\exp\left(-\frac{\Gamma}{2}\delta t\right)|e\rangle \tag{2.28}$$

and

$$\delta p = \delta t\Gamma\langle\psi(0)|\sigma^+\sigma^-|\psi(0)\rangle = \delta t\Gamma|\beta_0|^2, \tag{2.29}$$

with $\delta p$ being the the probability of a photon being emitted on the time interval $\delta t$. Therefore, we can see that obtaining a random number $\epsilon < \delta p$ corresponds to the detection of a photon emitted by the atom (a quantum jump), whereas if we have $\epsilon > \delta p$ the system state will be proportional to $\left|\psi^{(1)}(\delta t)\right\rangle$ and, using the fact that $\delta t$ is small, it can be rewritten as (see [22]):

$$|\psi(\delta t)\rangle = \alpha_0\left(1 + \frac{\Gamma}{2}\delta t|\beta_0|^2\right)|g\rangle + \beta_0\left(1 - \frac{\Gamma}{2}\delta t|\alpha_0|^2\right)\exp(-i\omega_0\delta t)|e\rangle\,. \tag{2.30}$$

This manner of writing the evolved state after no photon is detected is crucial in order to get the realistic solution to the dynamics of the system. Note that if we had written the normalized evolved state as

$$|\psi(\delta t)\rangle = \alpha_0 |g\rangle + \beta_0 \exp(-i\omega_0 \delta t) |e\rangle , \tag{2.31}$$

the probability of having a quantum jump in the interval $(0, \delta t)$ would be the same as in the interval $(\delta t, 2\delta t)$, meaning there would be no real change in the probability the system is in the excited state since the state would change only by a global phase, i.e.,

$$| \langle e|\psi(\delta t)\rangle |^2 = |\beta_0^2|(\exp\{i\omega_0 \delta t\} \exp\{(-i\omega_0 \delta t)\}) = |\beta_0^2|. \tag{2.32}$$

Thus, in this scenario the only possible way for the system to decay into the ground state would be by photon emition. But in the physical evolution there is a probability for the system decaying to its ground state without emitting a photon. Therefore the states are coupled and their accurate evolved representation should be given by (2.30). The probability of the atom being in each state is then time dependent and the evolution of the parameters $\alpha_0$ and $\beta_0$ are given by:

$$\alpha(t) = \alpha_0[|\alpha_0|^2 + |\beta_0|^2 \exp(-\Gamma t)]^{-\frac{1}{2}} \tag{2.33}$$

$$\beta(t) = \beta_0 \exp(-\Gamma/2t)[|\alpha_0|^2 + |\beta_0|^2 \exp(-\Gamma t)]^{-\frac{1}{2}} \tag{2.34}$$

and the probability that no quantum jump occur in the time interval $(0, t)$ is given by:

$$P(t) = |\alpha_0|^2 + |\beta_0|^2 \exp(-\Gamma t) \tag{2.35}$$

and, hence, there is a probability $|\alpha_0|^2$ that no photon will be detected in the interval $(0, \infty)$.

### 2.3.2 Statistical Errors

Assuming the random numbers generated in the numerical calculation of the trajectories are statistically independent, the expected value $\langle \Omega \rangle$ of an operator should be approximately described by the mean:

$$\bar{\Omega} = \frac{1}{N} \sum_i \Omega_i = \frac{1}{N} \sum_i \langle \psi_i(t)| \, \Omega \, |\psi_i(t)\rangle \tag{2.36}$$

where the subscript $i$ indicates the $i$-th trajectory and $N$ is the total number of trajectories used in the estimate.

For sufficiently large $N$ the central limit theorem tells us that the probability distribution for $\bar{\Omega}$ is approximately Gaussian with mean $\langle \Omega \rangle$. The statistical error of this

distribution is, then, calculated in terms of the variance of $\bar{\Omega}$:

$$\begin{aligned}\mathrm{Var}[\bar{\Omega}] &= \left\langle (\bar{\Omega} - \langle\Omega\rangle)^2 \right\rangle = \left\langle \left( \tfrac{1}{N}\sum_{i=1}^{N}\Omega_i \right)^2 - 2\bar{\Omega}\langle\Omega\rangle + \langle\Omega\rangle^2 \right\rangle \\ &= \tfrac{1}{N^2}\sum_{i=1}^{N}\sum_{j=1}^{N}\langle\Omega\rangle - \langle\Omega\rangle = \tfrac{1}{N^2}\sum_{i=1}^{N}\langle\Omega_i^2\rangle + \tfrac{1}{N^2}\sum_{i=1}^{N}\sum_{j=1}^{N}\langle\Omega_i\rangle^2\langle\Omega_{j\neq i}\rangle^2 - \langle\Omega\rangle^2 \\ &= \tfrac{1}{N^2}\sum_{i=1}^{N}\langle\Omega_i^2\rangle + \tfrac{N^2-N}{N^2}\langle\Omega_i\rangle^2 - \langle\Omega\rangle^2 = \tfrac{1}{N^2}\sum_{i=1}^{N}\langle\Omega_i^2\rangle + \tfrac{N-1}{N}\langle\Omega\rangle^2 - \langle\Omega\rangle^2 \\ &= \tfrac{1}{N}(\langle\Omega^2\rangle - \langle\Omega\rangle^2) = \tfrac{1}{N}\mathrm{Var}[\Omega].\end{aligned} \tag{2.37}$$

where we have assumed $\langle\Omega_i\Omega_{j\neq i}\rangle = \langle\Omega_i\rangle\langle\Omega_{j\neq i}\rangle$ and $\langle\bar{\Omega}\rangle = \langle\Omega\rangle$. It can be shown that we could use the approximator [25]

$$\mathrm{Var}[\Omega] \approx \frac{\sum_{i=1}^{N}(\Omega_i - \bar{\Omega})^2}{N-1}. \tag{2.38}$$

The statistical error is, then, the standard deviation of the values $\Omega_i$ which is given by:

$$\sigma = \frac{\Delta O}{\sqrt{N}}, \tag{2.39}$$

where $\Delta O = \sqrt{\mathrm{Var}[\langle O\rangle]}$ the standard deviation of the observable $O$.

The number of trajectories needed for good conversion will depend on the kind of variable being measured. Tipically, it is desired that $\frac{\sigma}{\langle O\rangle} \ll 1$ which leads to the conclusion that

$$\sqrt{N} \gg \frac{\Delta O}{\langle O\rangle}. \tag{2.40}$$

### 2.3.3 High Rank quantities vs Low Rank quantities

According to Mølmer et al [22] there is a difference in the number of trajectories needed in order to estimate high rank and low rank quantities. High rank quantities such as the total energy of the system $O_G = E_{tot}$ should need a number of trajectories that has no dependence on the size of the Hilbert space associated with the system. One example given by Daley et al [9] is the brownian motion of a particle in a thermalized system at temperature $T$, whose energy expectation value is $\langle E_{tot}\rangle \approx \frac{3}{2}k_BT$ where $k_B$ is the Boltzmann constant. In this case the requirement on the number of trajectories should be $N \gg 1$ and the estimative for the error should be approximately given by $\frac{1}{\sqrt{N}}$.This is also expected in Many body systems where we expect global averages involving all the particles in the system to be efficiently calculated with quantum trajectories.

The situation is different for low rank quantities in single particles systems, such as the population of a given eigenstate of $O$. In this case the mean and variance of the

observable will scale with the inverse of the number of quantum levels -size of the Hilbert space of the system- involved in the simulation [22], then it will be expected that the number of trajectories needed for good accuracy of the solution will be given by $N \gg D$, where $D$ is the dimension of the Hilbert space of the system. This follows from the observation that low rank quantities should behave as $\langle O_L \rangle \sim 1/D$ and $\Delta\langle O_L \rangle \sim 1/\sqrt{D}$. Substitution of this result in equation 2.40 leads to $\sqrt{N} \gg \sqrt{D}$.

In the case of many particle systems the behavior of low rank quantities may not be so clear as when dealing with single particle systems. If we try to calculate the population of an eigenstate of some local many body observable out of D many body eigenstates of that observable the situation is the same. On the other hand, if the quantities of a finite-size system are local in momentum or space they will often scale as the size of the system L. In this perspective, quantities such as the local occupation on a site in a lattice with L sites tend to scale as $\langle O_L \rangle \sim \frac{1}{L}$ and we require a number of trajectories $N \gg L$ for good convergence. Even though more trajectories will be needed than in the case of high rank quantities it is still advantageous to use quantum trajectories in the case of these local quantities.

### 2.3.4 Alternative formulation

The method of evolving the trajectories given in the beginning of this section is only accurate to first order in $t$. It may be possible to use this first order time step for dissipative dynamics if dissipation is much slower then the dynamical timescales of the system. However, the fact that it takes an entire time step $\delta t$ for a quantum jump to occur leads to a systematic overestimation of jumping rates.

An improved algorithm has been developed by Dum et al. [24], which is approached by the viewpoint of continuous measurement [18]. The algorithm steps are the following

1. Sample the initial state and evolve it under the effective Hamiltonian $H_{eff}$ as in Eq. (2.14)
2. Sample a random number $\epsilon$, uniformly distributed between 0 and 1
3. Numerically solve the equation:
$$\left\| \exp\left\{ -\frac{i}{\hbar} H_{eff} t_1 \right\} |\psi(t_0)\rangle \right\|^2 = \epsilon \tag{2.41}$$
in order to find the time $t_1$ at which the next jump occurs given that the last jump or the beginning of the calculations occurred at time $t_0$
4. $|\psi(t)\rangle$ is then calculated in the time interval $[t_0, t_1]$ as
$$|\psi(t)\rangle = \frac{\exp\left\{ -\frac{i}{\hbar} H_{eff}(t - t_0) \right\} |\psi(t_0)\rangle}{\left\| \exp\left\{ -\frac{i}{\hbar} H_{eff}(t - t_0) \right\} |\psi(t_0)\rangle \right\|} \tag{2.42}$$

5. At time $t_1$ a quantum jump is applied, with probabilities of using each $l_m$ given by the second step of the method in the beginning of this section, i.e., choosing $l_m$ with probabilities

$$P_m = \frac{\delta p_m}{\delta p}, \tag{2.43}$$

and apply the jump as:

$$|\psi(t_1)_a\rangle = \frac{l_m |\psi(t_1)_b\rangle}{\|l_m |\psi(t_1)_b\rangle\|}, \tag{2.44}$$

where $|\psi(t_1)_a\rangle$ is the state of the system after applying the jump and $|\psi(t_1)_b\rangle$ is the state of the system after the evolution under the effective Hamiltonian up to time $t_1$.

6. Repeat the process from step 2 choosing a new random number $\epsilon$.

This algorithm will be the only one used throughout this text.

### 2.3.5 Examples

- **Optical Bloch Equations**

To give a better understanding of the method we begin by studying the simple dissipative single particle system, a two level atom coupled to a (classical) laser field [26], with detuning $\Delta$ between the laser frequency and the frequency associated with the atomic transition. In the case where there is no dissipation the atom undergoes Rabi oscillations between the excited and ground states, $|e\rangle, |g\rangle$, respectively. This leads to the Rabi Hamiltonian for spin half systems. When the system goes through spontaneous emissions( in the presence of damping) it can be described by the following master equation:

$$\dot{\rho} = -\frac{i}{\hbar}[H_{opt}, \rho] + \frac{\Gamma}{2}(2\sigma_-\rho\sigma_+ - \{\sigma_+\sigma_-, \rho\}) \tag{2.45}$$

where

$$H_{opt} = -\frac{\Omega}{2}\sigma_x - \Delta\sigma_+\sigma_-. \tag{2.46}$$

This master equation leads to the so-called optical Bloch equations which are the differential equations that govern the dynamics of the matrix elements of $\rho$.

We show on Fig 1 the solutions of the master equation using the quantum trajectory technique. As it can be seen in the in Fig 1-a the single trajectories undergo rabi oscillations and quantum jumps to the ground state are happening stochastically. In Fig 1-b shows the comparison of the solution of the master equation for an average over 500 trajectories and the exact solution of the master equation.

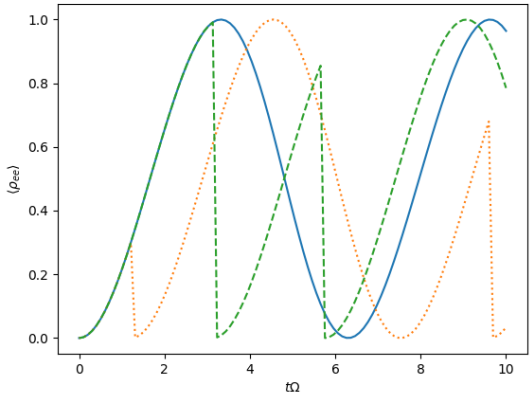


(a)

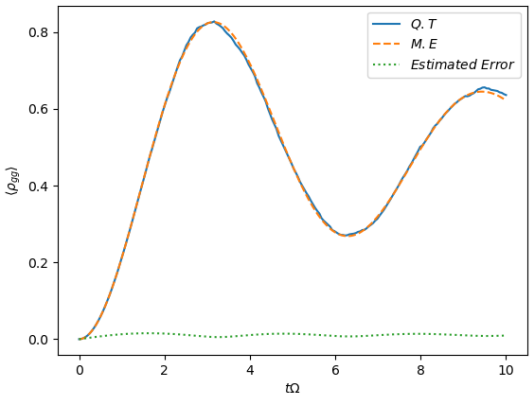


(b)

Figure 1 – Illustrative example of quantum trajectories averaging for a two-level system. (a) Probability of finding the atom in the excited state, $\rho_{ee}$, as a function of time $t\Omega$, for three example trajectories (with blue solid, green dashed and orange dotted lines showing different random samples). We see the effect of quantum jumps, where the atom is projected onto the ground state. Here the detuning $\Delta = 0$, and $\Gamma = \Omega/6$. (b) Expected value of $\rho_{ee}$ averaged over 500 sample trajectories (dotted line), compared with the exact result from direct integration of the master equation (solid line). We have also estimated the error over the number of trajectories used (doted green line).

- **Dephasing for hardcore lattice Bosons**

  A second example is a gas of hard-core bosons which move on a lattice. The effective model for this many body system can be given by the Hubbard Model(see section 3.5):

$$H_{BH} = -J \sum_{\langle j,l \rangle} a_j^\dagger a_l + \frac{U}{2} \sum_l a_l^\dagger a_l (a_l^\dagger a_l - 1) \tag{2.47}$$

  where $a_i$, $a_i^\dagger$ are the annihilation and creation operators, respectively (see C.3), on site $i$, $J$ is the hopping amplitude and $U$ is the on-site interaction.

  In this model the first term is associated with the hopping of particles between lattice sites and the second term is associated with the on-site interaction. Effectively, we can describe the system of a gas of hard-core bosons by taking the limit $\frac{U}{J} \to \infty$ so that conservation of energy strongly defavors double occupancy on one site. Considering a one dimensional system, this leads to the following Hamiltonian for the system:

$$H = -J \sum_l (a_l^\dagger a_{l+1} + a_{l+1}^\dagger a_l) \tag{2.48}$$

  and we apply the constraint $(a^\dagger)^2 := 0$

  An example of dissipative process occurs when we consider spontaneous emission in the system, i.e., incoherently scattering light from lattice lasers, for example. This tends to localize particles in the system, providing the environment with information about the location of the particles. A master equation that describe such process is given by:

$$\dot{\rho} = -\frac{i}{\hbar}[H, \rho] + \sum_l \frac{\Gamma}{2} (2 n_l^2 \rho n_l^2 - \{n_l^2, \rho\}) \tag{2.49}$$

  where $H$ is the Hamiltonian given by equation 2.48 and $n_l = a_l^\dagger a_l$ is the number operator. This equation may be solved numerically using quantum trajectories technique and we may calculate quantities considered global (such as the total energy of the system) and local (such as the occupation density). In figure 2 we show the results for the evolution of the total energy starting from the ground state of the Hamiltonian 2.48. From figure 2-a we see the evolution of random single trajectories and in Fig 2 -b we see the comparison between the average over 1000 trajectories and the exact evolution of the master equation. It is clear that there is very good agreement between the two methods.

  In order to study local quantities in this system we take as an example the evolution of the occupation density on site 5 of the lattice (see Fig. 3).The evolution for three different randomly chosen trajectories are shown in figure 3-a. The results of figure 3-b show that the average over 1000 trajectories agrees with the exact results from direct integration of the master equation within statistical errors, thus, proving

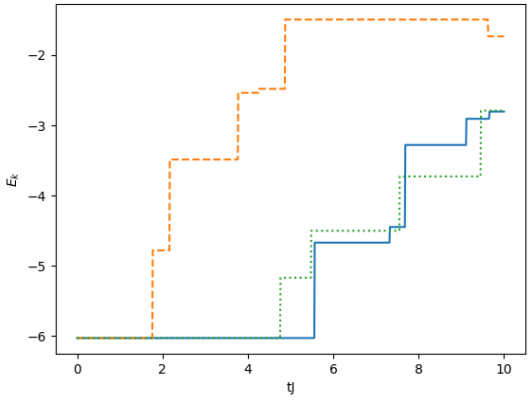


(a)

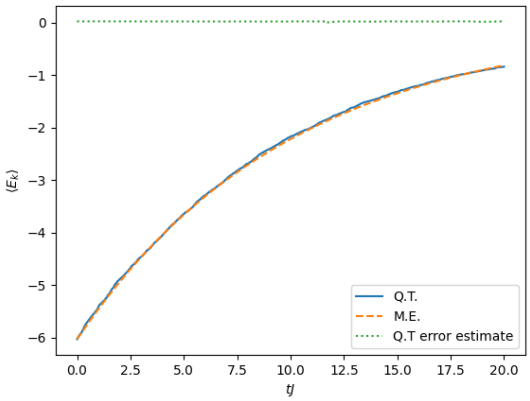


(b)

Figure 2 – Illustrative example of quantum trajectories averaging for a gas of hard-core bosons on a lattice, analogous to the example for a two-level system in Fig. 3. Here we show results from exact diagonalisation calculations with 5 particles on 10 lattice sites. (a) Kinetic energy of the system of hard-core bosons as a function of time $tJ$ for two example trajectories (with blue solid and red dashed lines showing different random samples). We see the effect of quantum jumps, where the kinetic energy increases as individual atoms are localised in space. Here the scattering rate $\Gamma = 0.1J$. (b) Values for the kinetic energy averaged over 1000 sample trajectories, compared with the exact result from eq. (50).

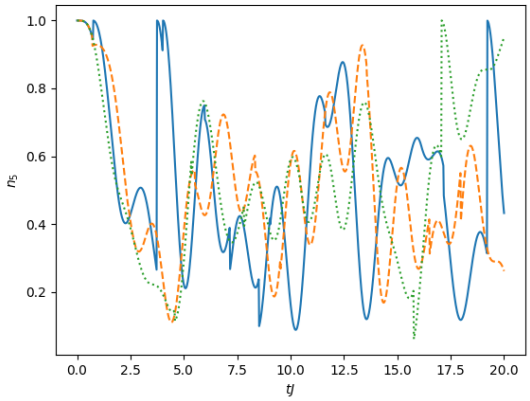


(a)

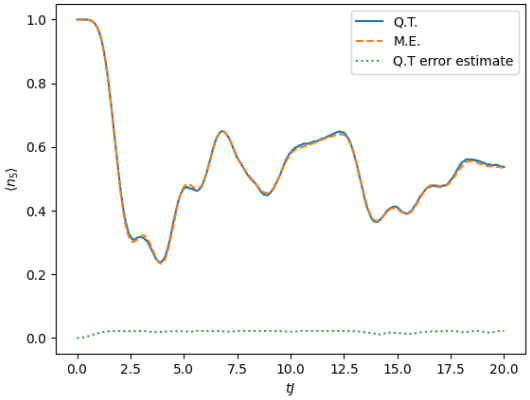


(b)

Figure 3 – Illustrative example of quantum trajectories averaging for a gas of hard-core bosons on a lattice, showing results form calculations of the occupation density with 5 particles on 10 lattice sites, as in Fig. 5. (a) Density on site 5 of the lattice as a function of time tJ for two example trajectories (with blue (solid), red (dashed) and green (dotted) lines showing different random samples). We see the effect of quantum jumps, where nearby jumps give rise to fluctuations either up or down of the local mean density. (b) Values for $\langle n5 \rangle$ averaged over 1000 sample trajectories, and compared with the exact results computed through direct integration of the master equation. We have also estimated the error over the number of trajectories used (doted green line).

that quantum trajectories may be advantageous when working with certain local quantities (as was explained in the last sections).

## 2.4 Quantum Trajectories: Physical Viewpoint

It is important to emphasize that the quantum trajectories technique is not simply a mathematical tool to obtain the evolution of master equations. It can be interpreted experimentally as a physical process used to obtain the dynamics of the expectation values

of observables. This interpretation can be more readily seen in the context of continuous measurement, where weak measurements[1] are used in very small timesteps to monitor observables in repeated experiments (a process which may be understood as quantum trajectories). Averaging over the experiments(trajectories) leads to the dynamical evolution of the expected value of the observable being monitored.

To see this more clearly we use the example of *Haroche et. al.* [1], in which by continuously monitoring an optical cavity they were able to detect the decay of a photon inside it. The experiment setup (shown in Fig. 4) was done using a method of detection which consisted of sending a beam of two level atoms in a specific superposition of its states through the cavity and detecting phase shifts produced by the photon on the atoms as they exit the cavity.

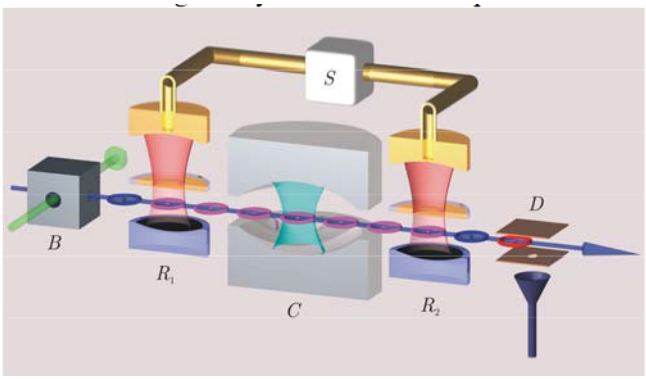


Figure 4 – Experiment setup used by *Haroche et. al.* to detect the creation and destruction of photons inside a resonant cavity. A beam of two level atoms are ejected from B. The atoms are configured in a specific superposition of their states in the microwave cavity R1 before entering the cavity optical cavity C. Upon interaction with the cavity the atoms are reconfigured in R2 in order to be detected on D. Image extracted from [1]

Preparing the optical cavity with a single photon[2] it was possible to use the apparatus to monitor the existence of the photon and its decay over a time period. The dynamics of each repetition of the experiment represent single trajectories. Averaging over trajectories it was possible to obtain expectation value for the photon number inside the cavity over time $\langle P(t)\rangle$, which is shown in Fig.5 for different number of trajectories.

[1] In the context of continuous measurements these measurements are usually POVM's. The measurements, therefore, do not project the system into specific states, causing only small disturbances to its evolution.

[2] The experiment was configured so there was at most one photon inside the cavity

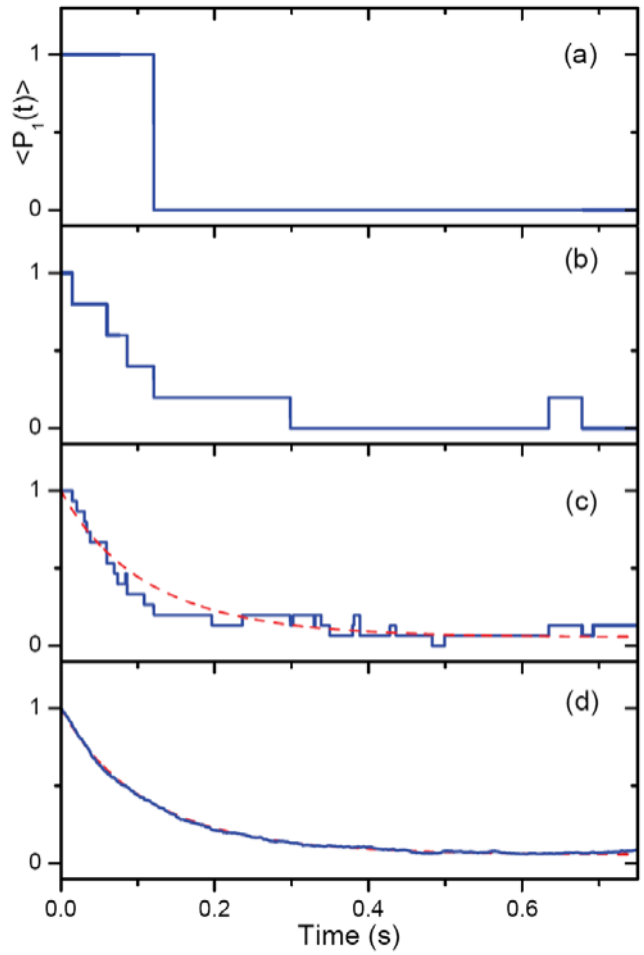


Figure 5 – Expectation value of the photon number inside the optical cavity for different number of trajectories.(a) A typical trajectory obtained in the experiment.(b)-(d) averages over 5, 15 and 904 quantum trajectories. The dashed line in (c) and (d) represent the theoretical evolution of the photon number obtained by solving the problem's master equation with the experimental parameters.

# 3 Many Body Quantum Systems

The possibility of representing the evolution of a certain class of AMO (atomic, molecular and optical) many body quantum systems with master equations opened the opportunity to understand open many body quantum systems dynamics much more deeply. This is because well understood techniques already applied to study single or few particle quantum systems with such equations can be extended to the context of many body physics.

Many body quantum systems are studied in a variety of setups, such as in condensed matter physics or statistical mechanics, in order to understand macroscopic observed effects that emerge out of specific microscopic configurations. Here we shall focus on magnetic models such as the transverse Ising and Heisenberg models, which are instances of the so-called quantum spin systems. Another model which will be the main focus of this work is the Hubbard model, which was first thought of as a model that could describe the origin of superconductivity in matter. Under some regimes of AMO systems this model can approximately describe their dynamics and can be used in order to study how these systems are affected by dissipation.

## 3.1 Many Body Quantum Systems

The field of many body quantum physics focuses on understanding the problem of emergent macroscopic phenomena on systems with many interacting building particles at a microscopic scale, and has a wide range of applications from the electronic structure problems (that are of great importance on chemistry and drug development [27]), to the development of new quantum technologies [16].

The starting point is that, in order to completely describe a material (e.g. a metal) and its properties it is virtually impossible to take into consideration every possible variable that is playing a role in its state [2]. This happens due to the number of degrees of freedom and possible interactions happening at each moment in the material, which are essentially impossible to compute since we would need to know the state of each atom in the the material and that would require knowing the state of each electron and nucleus. Also, the geometry of the material would be of great importance for its description and, generally, it is highly irregular, augmenting the complexity of this complete description (the complexity may go even deeper if we consider interactions with the materials environment, the behavior of the protons and neutrons in the nucleus and so on). Thus approximations ought to be made in order to have a grasp of how a many body system behaves. Moreover,

the description of important classes of properties of theses systems might emerge from (very) simplified models built with the intent of describing them. In this perspective, one way in which this models may be built is through discretizing space and building the systems dynamics in the so called point lattice models. These models have been successfully applied to explain properties such as magnetism, superconductivity and Bose-Einstein condensation [2].

Nevertheless, even in such systems computation of dynamics may become unfeasible very fast. In fact if we consider a system composed of $N$ particles each of which with $k$ available states (and considering no other constraints), the number of possible configurations in this system is $k^N$ i.e. there is an exponential growth of computational complexity with the number of particles for such systems.

For instance a one dimensional spin $\frac{1}{2}$ chain, whose possible local states are $\{\uparrow, \downarrow\}$ have $2^{10} = 1024$ possible configurations with only 10 particles in the system and a $1024 \times 1024$ Hamiltonian matrix would be needed to describe its dynamics. In this perspective the computational cost of even such system may become highly dependent on their size.

This problem has led to the search and development of efficient numerical techniques in order to calculate dynamics such as exact diagonilization, which is a technique specially useful to obtain eigenvalues and eigenvectors of the systems Hamiltonian, density matrix normalization groups (DMRG) methods and tensor networks.

## 3.2 Quantum Spin Systems

One of the simplest examples of a many body models are quantum spin systems. Such idealized systems are used in order to understand quantum magnetism. In real materials the relevant spin-spin interacting source for the emergence of magnetism is given by electrons, whose spin quantum number is 1/2 (eventhough this quantum number may be effectively different in some atoms [2]). Therefore, the most simple ideal example of a system whose constituent parts can give rise to magnetism is composed of a collection of spin 1/2 systems, each of which have a two dimensional Hilbert space.

### 3.2.1 Lattice and Spin States

To define a quantum spin system we begin with a definition for a lattice. Let $\Lambda$ be an arbitrary finite set whose elements are called sites. Typically, each site is associated with an atom in a magnetic material. We shall fix a spin quantum number $S = 1/2, 1, 3/2...$ and assume that each site $i \in \Lambda$ has a spin quantum number $S$.

Associated with each site ($i \in \Lambda$) there is a Hilbert Space $h_i$ with dimension $(2S+1)$

and the state of the site $i$ is defined as $|\psi^{\sigma_i}\rangle$ where $\sigma_i = -S, ..., S-1, S$ is associated with its spin. The Hilbert space of the spin system on $\Lambda$ is $\mathcal{H} := \bigotimes_{i\in\Lambda} h_i$ and its dimension is $(2S+1)^{|\Lambda|}$ where $|\Lambda|$ is the number of elements of $\Lambda$.

A possible basis state is given by $|\mathbf{\Psi}^{\sigma}\rangle := \bigotimes_{i\in\Lambda} |\psi_i^{\sigma_i}\rangle$ where $\sigma := (\sigma_i)_{i\in\Lambda}$. As an example, consider a spin system with $S = 1/2$. If we have $\Lambda = \{1, 2\}$ then one possible basis state is $\left|\mathbf{\Psi}^{(\uparrow,\downarrow)}\right\rangle = |\uparrow\rangle_1 \otimes |\downarrow\rangle_2$ where $\uparrow, \downarrow$, are $\sigma = 1/2$ and $\sigma = -1/2$, respectfully.

A bond $\{j, l\} \subset \Lambda, j \neq l$ is a set of two sites in $\Lambda$. Defining $\mathcal{B}$ to be a set of bonds in $\Lambda$, the pair $(\Lambda, \mathcal{B})$ determines the structure of the lattice.

### 3.2.2 The Spin Operator on a Lattice

The spin operator represent the (quantum mechanical) spin angular momentum and can be defined as $\hat{\mathbf{S}} = (\hat{S^{(x)}}, \hat{S^{(y)}}, \hat{S^{(z)}})$ where $x, y, z$ are three mutually orthogonal directions. From elementary theory of quantum angular momentum the operators that constitute the spin operator are self-adjoint and satisfy the commutation relations

$$[\hat{S^{(\alpha)}}, \hat{S^{(\beta)}}] = i \sum_{\gamma=x,y,z} \epsilon_{\alpha\beta\gamma} \hat{S^{(\gamma)}} \tag{3.1}$$

for $\alpha, \beta = x, y, z$ where $\epsilon$ is the Levi Civita tensor(to work with the tensor we consider $x = 1, y = 2$ and $z = 3$). $\hat{\mathbf{S}}$ is such that the relation $\hat{\mathbf{S}}^{\mathbf{2}} = S(S+1)$ where $S$ is the spin quantum number, holds for all $S$.

The spin operators act on a $(2S+1)$ Hilbert space and their action on the basis states are characterized by the properties

$$\hat{S}^{(z)} |\Psi^{\sigma}\rangle = \sigma |\Psi^{\sigma}\rangle , \tag{3.2}$$

and

$$\hat{S}^{\pm} |\Psi^{\sigma}\rangle = \sqrt{S(S+1) - \sigma(\sigma \pm 1)} \left|\Psi^{\sigma\pm1}\right\rangle . \tag{3.3}$$

Considering the $\{|\uparrow\rangle, |\downarrow\rangle\}$ basis for $S = 1/2$ we can extract spin operators in matrix form, obtaining:

$$\hat{S}^{(x)} = \frac{1}{2}\begin{bmatrix} 0 & 1 \\ 1 & 0 \end{bmatrix}, \hat{S}^{(y)} = \frac{1}{2}\begin{bmatrix} 0 & -i \\ i & 0 \end{bmatrix}, \hat{S}^{(z)} = \frac{1}{2}\begin{bmatrix} 1 & 0 \\ 0 & -1 \end{bmatrix}. \tag{3.4}$$

We may define operators which rotate the spin states by an arbitrary angle $\theta$ about one of the axis by $\hat{U}_{\theta}^{(\alpha)} := \exp\left(-i\theta\hat{S}^{(\alpha)}\right)$ where $\alpha \in \{x, y, z\}$ and we define the exponential of an operator $\hat{A}$ by the series expansion:

$$\exp\left(\hat{A}\right) := \sum_{n=0}^{\infty} \frac{1}{n!} \hat{A}^n \tag{3.5}$$

where 3.5 will always converge on a finite Hilbert space.

From the properties of the exponential of an operator (see for example [2] we have that $\hat{U}_\theta^{(\alpha)}\hat{U}_\phi^{(\alpha)} = \hat{U}_{\theta+\phi}^{(\alpha)}$. From the definition of the rotation operator e also have $(\hat{U}_\theta^{(\alpha)})^\dagger = \hat{U}_{-\theta}^{(\alpha)}$. It is also possible to show that the operators $\hat{U}_\theta^{(\alpha)}$ form a representation of an $SU(2)$ group [1].

### 3.2.3 Spin Operators on Lattices

Spin operators may also be defined on lattices by denoting $\hat{S}_j^{(\alpha)}$ the spin operator which acts nontrivially only on site $j$ i.e.

$$\hat{S}_j^{(\alpha)} = \hat{\mathbf{1}} \otimes \hat{\mathbf{1}} \otimes \hat{\mathbf{1}} \otimes \cdots \otimes \hat{S}^{(\alpha)} \otimes \cdots \otimes \hat{\mathbf{1}} \otimes \hat{\mathbf{1}} \otimes \hat{\mathbf{1}} \tag{3.6}$$

where $\hat{S}^{(\alpha)}$ acts on the sites Hilbert space $h_j$. We may then write $\hat{\mathbf{S}}_j = (\hat{S}_j^{(x)}, \hat{S}_j^{(y)}, \hat{S}_j^{(z)})$. The commutation relations for spin operators on a lattice are given by:

$$[\hat{S}_j^{(\alpha)}, \hat{S}_l^{(\beta)}] = i\delta_{j,l} \sum_{\gamma=x,y,z} \epsilon_{\alpha,\beta,\gamma} \hat{S}_j^{(\gamma)} \tag{3.7}$$

for any $j, l \in \Lambda$ and $\alpha, \beta = x, y, z$. An important quantity is the total spin operator, whose definition is given by:

$$\hat{\mathbf{S}}_{tot} := \sum_{j\in\Lambda} \hat{\mathbf{S}}_j \tag{3.8}$$

and write $\hat{\mathbf{S}}_{tot} = (\hat{S}_{tot}^{(x)}, \hat{S}_{tot}^{(y)}, \hat{S}_{tot}^{(z)})$ to define

$$\hat{S}_{tot}^{\pm} = \hat{S}_{tot}^{(x)} \pm i\hat{S}_{tot}^{(y)} = \sum_{j\in\Lambda} \hat{S}_j^{\pm} \tag{3.9}$$

where $\hat{S}_j^{\pm} = \hat{S}_j^{(x)} \pm i\hat{S}_j^{(y)}$. As in the case of a single spin, we also define the eigenvalue of $(\hat{\mathbf{S}}_{tot})^2$ as $S_{tot}(S_{tot}+1)$. A state such that $(\hat{\mathbf{S}}_{tot})^2 |\psi\rangle = S_{tot}(S_{tot}+1)|\psi\rangle$ is said to have a total spin $S_{tot}$. It holds that $S_{tot}$ may take $|\Lambda|$ values and there are $2|\Lambda|S+1$ possible eigenvalues $M$ of $S_{tot}^{(z)}$. It is also possible to define a rotation operator of the total spin state:

$$\hat{U}_\theta^{(\alpha)} := \exp\Big(-i\theta\hat{S}_{tot}^{(\alpha)}\Big) = \prod_{j\in\Lambda} \exp\Big(-i\theta\hat{S}_j^{(\alpha)}\Big). \tag{3.10}$$

### 3.2.4 The Operator $\hat{\mathbf{S}}_j \cdot \hat{\mathbf{S}}_l$

An important operator in the context of quantum spin systems is given by $\hat{\mathbf{S}}_j \cdot \hat{\mathbf{S}}_l = \sum_{\alpha=x,y,z} \hat{S}_j^{(\alpha)}\hat{S}_l^{(\alpha)}$ for $j \neq l$. This operator is applied to some Hamiltonian models and has interesting properties. A useful representation of such an operator is given by

$$\hat{\mathbf{S}}_j \cdot \hat{\mathbf{S}}_l = \frac{1}{2}(\hat{S}_j^+\hat{S}_l^- + \hat{S}_j^-\hat{S}_l^+) + \hat{S}_j^{(z)}\hat{S}_l^{(z)}. \tag{3.11}$$

[1] A $SU(2)$ group is a special group whose elements are unitary matrices and have determinant 1, for a definintion on groups and their properties see for example [28]

It is also possible to show that

$$[\hat{\mathbf{S}}_j \cdot \hat{\mathbf{S}}_l, \hat{S}_{tot}^{(\alpha)}] = 0, \tag{3.12}$$

for any $\alpha = x, y, z$, which means $\hat{\mathbf{S}}_j \cdot \hat{\mathbf{S}}_l$ is $SU(2)$ invariant[2].

We can also obtain the eigenvalues of $\hat{\mathbf{S}}_j \cdot \hat{\mathbf{S}}_l$ from the relation:

$$\hat{\mathbf{S}}_j \cdot \hat{\mathbf{S}}_l = \frac{1}{2}[(\hat{\mathbf{S}}_j + \hat{\mathbf{S}}_l)^2 - (\hat{\mathbf{S}}_j)^2 - (\hat{\mathbf{S}}_l)^2] = \frac{1}{2}(\hat{\mathbf{S}}_j + \hat{\mathbf{S}}_l)^2 - S(S+1). \tag{3.13}$$

From equation 3.13 and the theory of addition of angular momenta we obtain that the minimum and maximum eigenvalues of $(\hat{\mathbf{S}}_j \cdot \hat{\mathbf{S}}_l)$ are given by $-S(S+1)$ and $S^2$, respectfully. This lack of symmetry between minimum and maximum values of the the eigenvalues indicates that the ground state of spin systems show quantum phenomena emerging from many body systems in a more explicit manner [2].

## 3.3 The Heisenberg Model

The Heisenberg model is a minimal model developed in order to describe magnetism in materials. It is also very helpful, as will be seen, as an approximation to more realistic models that consider magnetism arising from electrons interacting and moving through a lattice, e.g., the Hubbard Model. We shall study the results and properties of this model both in the antiferromagnetic and ferromagnetic limit.

### 3.3.1 Ferromagnetic

Consider a lattice $\Lambda$ as defined in section 3.2.1. The Hamiltonian of the ferromagnetic Heisenberg model on a spin quantum system on $\Lambda$ is given by

$$\hat{H} = -\sum_{\{j,l\}\in\mathcal{B}} \hat{S}_j \cdot \hat{S}_l. \tag{3.14}$$

From the properties of the operator $\hat{S}_j \cdot \hat{S}_l$ we find that

$$[\hat{H}, \hat{S}_{tot}^{(\alpha)}] = 0 \tag{3.15}$$

for $\alpha = x, y, z$, which shows that the Hamiltonian is $SU(2)$ invariant.

A ground state of the system is given by the state

$$\left|\Psi^{\uparrow}\right\rangle = \bigotimes_{j\in\Lambda} |\uparrow\rangle_j, \tag{3.16}$$

in which all the spins are pointing in the positive z-direction. This state satisfies $\hat{\mathbf{S}}_{tot}^2 \left|\Psi^{\uparrow}\right\rangle = S_{max}(S_{max}+1)\left|\Psi^{\uparrow}\right\rangle$ and $\hat{S}_{tot}^{(z)}\left|\Psi^{\uparrow}\right\rangle = S_{max}\left|\Psi^{\uparrow}\right\rangle$, where $S_{max} = |\Lambda|S$ is the largest magnitude

[2] This means that the $\hat{\mathbf{S}}_j \cdot \hat{\mathbf{S}}_l$ is invariant under a global rotation of spins

of the total spin. Note that $\left|\Psi^{\uparrow}\right\rangle$ minimizes each term of the Hamiltonian separately i.e.

$$-\hat{S}_j \cdot \hat{S}_l \left|\Psi^{\uparrow}\right\rangle = -\{\frac{1}{2}(\hat{S}_j^{+}\hat{S}_l^{-} + \hat{S}_j^{-}\hat{S}_l^{+}) + \hat{S}_j^{(z)}\hat{S}_l^{(z)}\}\left|\Psi^{\uparrow}\right\rangle = -\hat{S}_j^{(z)}\hat{S}_l^{(z)}\left|\Psi^{\uparrow}\right\rangle = -S^2\left|\Psi^{\uparrow}\right\rangle \quad (3.17)$$

where we used the fact that $\hat{S}^{+}\left|\psi^{S}\right\rangle = 0$ and $\hat{S}_j^{(z)}\left|\psi^{S}\right\rangle = S\left|\psi^{S}\right\rangle$. Thus we have that $-S^2$ is the minimum eigenvalue of $-\hat{S}_j \cdot \hat{S}_l$. From this it can be shown that $\left|\Psi^{\uparrow}\right\rangle$ is a ground state of the Hamiltonian associated with the ferromagnetic Heisenberg model [2].

We can also find a simple class of excited states on the ferromagnetic Heisenberg model[3]. Consider the set $\mathcal{N}(j)$ defined on a pair $(\Lambda, \mathcal{B})$ whose elements are defined by $\mathcal{N}(j) = \{l \in \Lambda; \{j, l\} \in \mathcal{B}\}$ are the sites directly connected to the site $j$ i.e. the nearest neighbors of $j$. Let $f = (f_j)_{j\in\Lambda}$, $f_j \in \mathbb{C}$, and $\lambda \in \mathbb{R}$ be the solutions to the "Schrödinger equation"

$$-\sum_{l\in\Lambda} \Delta_{j,l} f_l = \lambda f_j \text{ for each } j \in \Lambda, \quad (3.18)$$

where the lattice Laplacian $\Delta$ is a real symmetric $|\Lambda| \times |\Lambda|$ matrix defined by

$$\Delta_{j,l} = \begin{cases} - & |\mathcal{N}(j)|, \text{ if } j = l, \\ & 1, \text{ if } \{j, l\} \in \mathcal{B}, \\ & 0, \text{ otherwise.} \end{cases} \quad (3.19)$$

An important relation involving the Laplacian matrix is given by

$$\sum_{j\in\Lambda} (g_j)^* \Delta_{j,l} g_l = -\sum_{\{j,l\}\in\mathcal{B}} |g_j - g_l|^2 \quad (3.20)$$

where $g_j \in \mathbb{C}$ is an arbitrary complex function and $j \in \Lambda$. If we multiply the Schrödinger equation 3.18 by $f_j^*$ and sum over $j \in \Lambda$, and substitute the result of equation 3.20 we obtain

$$\lambda \sum_{j\in\Lambda} |f_j|^2 = \sum_{\{j,l\}\in\mathcal{B}} |f_j - f_l|^2. \quad (3.21)$$

Thus we see that any eigenvalue satisfies $\lambda \geq 0$. If we rewrite the left hand side of equation 3.21 as $\sum_{l\in\mathcal{N}(j)}(f_j - f_l)$ we can see that a constant $f_j$ is an eigenvector satisfying 3.18 with $\lambda = 0$ and, when the lattice is connected [4] it follows from 3.21 that this eigenvector is unique and the eigenvalues, i.e., energies of the remaining eigenvectors satisfy $\lambda > 0$.

The connection between the eigenvalue problem described above and the spin system discussed in this section is the following. Consider the states:

$$\left|\Psi^{f}\right\rangle := \sum_{j\in\Lambda} f_j \left|\phi_j\right\rangle, \quad (3.22)$$

[3] Usually these states are called spin wave excitations.

[4] A lattice $(\Lambda, \mathcal{B})$ is connected when for any $j, l \in \Lambda$ such that $j \neq l$, there exists a finite sequence $\{z\}_1^n = (z_1 = j, z_2 ..., z_n = l)$ with $\{z_j, z_{j+1}\} \in \mathcal{B}$.

where

$$|\phi_j\rangle = \hat{S}_j^- \, |\uparrow\rangle_j \tag{3.23}$$

is the state obtained by applying the lowering spin operator on site $x$ with a initial "all up" state. It can be shown that

$$\hat{H} \left|\Psi^f\right\rangle = (E + \lambda S) \left|\Psi^f\right\rangle, \tag{3.24}$$

where $E$ is the ground state energy of the Hamiltonian. In this case, when we have $f_\alpha$ constant, i.e. $\lambda = 0$, $\left|\Psi^f\right\rangle$ is a ground state, whereas an eigenstate $\left|\Psi^f\right\rangle$ with an $f$ associated with a nonvanishing $\lambda$ is an exited state.

### 3.3.2 Antiferromagnetic

The antiferromagnetic Hamiltonian for the Heisenberg model takes the form:

$$\hat{H} = \sum_{\{j,l\}\in\mathcal{B}} \hat{S}_j \cdot \hat{S}_l. \tag{3.25}$$

This Hamiltonian is $SU(2)$ invariant as was made clear on the last section. Finding the ground state in this case is a lot harder and a special condition upon the lattice is necessary in order to obtain a characterization of this state, namely the lattice will be assumed to be bipartite - which are lattices that can be decomposed into two sublatices in such a way that any bond connects sites in different sublattices - which facilitates the extraction of the properties of the ground state.

Intuitively we expect that the energy of an antiferromagnetic quantum spin system should be minimized when every spin is pointing in the opposite direction to its neighbors [5](See figure 6). Nevertheless this intuition is wrong since, from the arguments presented in 3.17:

$$\begin{aligned} -\hat{S}_j \cdot \hat{S}_l \left|\psi_j^S\right\rangle \left|\psi_l^{-S}\right\rangle &= -\{\tfrac{1}{2}(\hat{S}_j^+ \hat{S}_l^- + \hat{S}_j^- \hat{S}_l^+) + \hat{S}_j^{(z)} \hat{S}_l^{(z)}\} \left|\psi_j^S\right\rangle \left|\psi_l^{-S}\right\rangle \\ &= -S^2 \left|\psi_j^S\right\rangle \left|\psi_l^{-S}\right\rangle + S \left|\psi_j^S\right\rangle \left|\psi_l^{-S}\right\rangle, \end{aligned} \tag{3.26}$$

since the last term on the right hand site of equation 3.26 does not vanish in this state, we have that this cannot be an eigenstate of the spin system. Moreover, its energy is not the lowest possible energy of the system.

A characterization of the ground state of the antiferromegnetic Hamiltonian was provided in a theorem which was proved by Marshall, Lieb and Mattis [29,30]. A simplified version of the theorem states that for a connected, bipartite lattice in which the sublattices have the same amount of elements, the ground state of the antiferromagnetic Heisenberg

[5] This state is known as the Néel state.

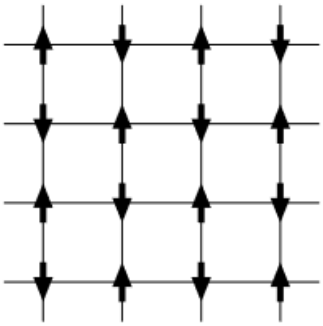

Figure 6 – 2 dimensional lattice with a Néel state configuration.Image extracted from [2]

model is unique and has total spin $S_{tot} = 0$ [2]. The theorem also states that the ground state may be expanded in terms of the total spin system state $|\Psi^{\sigma}\rangle$ in the following way

$$|\gamma_{gs}\rangle = \sum_{\sigma,\bar{\sigma}=0} \{\prod_{j\in\Lambda} (-1)^{\sigma_j - S}\} c_{\sigma} |\Psi^{\sigma}\rangle . \tag{3.27}$$

with coefficients satisfying $c_{\sigma} > 0$.

## 3.4 The Ising Model

The Ising model is one of the simplest model used to describe phase transitions in materials. To that end, the model considers short distance interactions on a $D-$dimensional lattice. Classically, the (spin) variables of the model may be used to describe several types of physical systems, such as magnets, materials composed of two kinds of particles, and materials which present atoms and holes in the lattice [31, 32]. In the quantum regime the model cannot be described by classical statistical mechanics and may give rise to interesting properties and phases.

### 3.4.1 Classical Ising Model

The classical Ising model on a $D-$dimensional lattice is described by the Hamiltonian

$$H(\sigma) := \sum_{\{j,l\}\in\mathcal{B}} \sigma_j \sigma_l \tag{3.28}$$

where $\sigma_j$ is a random variable which has two possible values, e.g., $\pm 1$ on sites $j = 1, 2, ..., N$ of the lattice. Frequently only nearest neighbors interactions are considered and, therefore, the Ising Hamiltonian may be rewritten as

$$H(\sigma) = \sum_{\langle j,l\rangle} \sigma_j \sigma_l \tag{3.29}$$

where the symbol $\langle j, l\rangle$ indicates a sum over the nearest neighbors of a site. This Hamiltonian represents interaction energies capable of producing a ferromagnetic ordered state. The spin variables may be thought of in three different ways:

- As spin components of atoms, which may have an "up" or "down" directions.
- As a material composed of two types of molecules in which each site may be occupied by exactly one of them.
- As the occupation number of a given site, in which the site may be either occupied ($\sigma_\alpha = 1$) or unoccupied ($\sigma_\alpha = -1$).

The equilibrium state of this model is described by the statistical mechanical expectation value

$$\langle \Omega \rangle := \frac{1}{Z(\beta)} \sum_{\sigma} \Omega(\sigma) e^{-\beta H(\sigma)}, \tag{3.30}$$

where $\Omega$ is an arbitrary function of spin configurations $\sigma$, $\beta = (K_B T)^{-1} > 0$ and $Z(\beta) = \sum_\sigma e^{-\beta H(\sigma)}$ is the partition function.

### 3.4.2 Transverse Ising Model

The quantum version of the Ising model is given by the transverse field Ising Model with $S = 1/2$, whose Hamiltonian is given by

$$\hat{H} = -\sum_{\langle j,l \rangle} \hat{S}_j^{(z)} \cdot \hat{S}_l^{(z)} - h \sum_j \hat{S}_j^{(x)}. \tag{3.31}$$

The first term alone is exactly the same as the classical Ising Hamiltonian. The second term, which describes an external magnetic field with magnitude $h \geq 0$ in the 1-direction, is what raises the quantum nature of the problem since the commutator $[\hat{S}^{(z)}, \hat{S}^{(x)}]$ does not vanish for quantum spin angular momentum.

The simplest case where phase transitions may be studied for this model is in the one dimensional regime. Then the Hamiltonian can be written as

$$\hat{H} = -\sum_{j=1}^{L-1} \hat{S}_j^{(z)} \cdot \hat{S}_{j+1}^{(z)} - h \sum_{j=1}^{L} \hat{S}_j^{(x)}. \tag{3.32}$$

From this Hamiltonian we can see that, for $h \ll 1$, the ground state of this system is approximately the same as for the classical Ising model, i.e., either all spins $\uparrow$ or all spins $\downarrow$. On the other hand, for $h \gg 1$, the first term on the righthand side of equation 3.32 becomes negligible and the ground state is unique and described by all spins pointing in the $\hat{S}^{(x)}$ direction. It can be analytically shown that there exists a critical field strength $h_c$ such that the system is in an ordered state for $h < h_c$ (which is a ferromagnetic state) and a disordered state for $h > h_c$ (which characterizes a paramagnetic states). This happens because the transverse field parameter causes fluctuations on the spin directions leading the system to a disordered state.

### 3.4.3 Other Quantum Spin Models

There exists a variety of quantum spin models and modifications of them. Between this models it is worth mentioning the $XX$, $XY$, $XXZ$ models which add anisotropy or variations to the Ising and Heisenberg models (see for example [33] for an introduction to such systems).

## 3.5 The Hubbard model

In light of the models seen so far one element which is often present in various types of materials has not been considered, i.e., particle movement on the lattice. Quantum spin systems were developed as simple models used to understand the emergence of certain properties and behaviors of materials such as magnets, alloys and gases [31].

But it is experimentally known that there exists materials which exhibited ferromagnetic properties and present electron movement between its atoms. A more sophisticated model was introduced by John Hubbard in the early years of the decade of 1960 in order to approximate the behavior of electronic correlations in narrow energy bands [34].

To the present day the Hubbard model (named after Hubbard) is studied for two main reasons, understanding the mechanism of ferromagnetism and electron conductivity in certain kinds of materials. The model is believed to exhibit various phenomena, such as ferromagnetism, antiferromagnetism and superconductivity. Recent works have also explored the idea off analog quantum simulation in order to study high energy physics in systems represented by the model (and variations of it) [35]. The model is also used to describe systems of bosons and Bose Einstein condensation [2]. In order to write the Hamiltonian of the Hubbard model we usually work on the framework of the second quantization (see appendix C.3).

### 3.5.1 Fermi-Hubbard Hamiltonian

The Hamiltonian of the Hubbard model consists of a kinetic part, which dictates how particles move, by the process of annihilation of one particle in one site and creation of the particle on the other (usually this process is assumed to happen between nearest neighboring sites), and normally called a hopping between sites. The second part consider the interactions between particles (in this case, fermions), which are assumed to occur only when two particles occupies the same site. Therefore the Fermi-Hubbard model is written as

$$H_{FH} = -\sum_{\langle j,l\rangle,\sigma=\uparrow,\downarrow} J_{(j,l)} a^{\dagger}_{j\sigma} a_{l\sigma} + \sum_{l} U_l (a^{\dagger}_{l\uparrow} a_{l\uparrow} a^{\dagger}_{l\downarrow} a_{l\downarrow}) \tag{3.33}$$

where $a^\dagger_{j\sigma}$ and $a_{j\sigma}$ are the fermionic creation and annihilation operators, respectively (see appendix C.3). $J_{(j,l)}$ represents the hopping amplitude between sites $j$ and $l$ (which represent the probability a hopping between those specific sites may occur). Finally, $U$ represents the coulomb repulsive interaction magnitude between to particles on the same site.

The Hamiltonan presents $SU(2)$ invariance, since if we define:

$$\hat{\mathbf{S}}^{(\alpha)}_j := \sum_{\sigma,\tau=\uparrow,\downarrow} \hat{a}^\dagger_{j,\sigma} \hat{\mathbf{S}}^{(\alpha)}_{\sigma,\tau} \hat{a}_{j,\sigma} \tag{3.34}$$

as the spin operator on the $\alpha$ direction and site $x$ on the lattice, it is possible to show that the commutation relations

$$[\hat{S}^{(\alpha)}_j, \hat{S}^{(\beta)}_l] = i\delta_{j,l} \sum_{\gamma=x,y,z} \epsilon_{\alpha,\beta,\gamma} \hat{S}^{(\gamma)}_j \tag{3.35}$$

remains valid and, therefore, the operator 3.34 represents a spin operator. Thus, we can define the total spin on the lattice as:

$$\hat{\mathbf{S}}_{tot} := \sum_{j\in\Lambda} \hat{\mathbf{S}}_j. \tag{3.36}$$

Using the same definition of a spin rotation as defined in section 3.2.2 for the total spin of the system, we can show that the Hamiltonian satisfies

$$[\hat{H}_{FH}, U^{(\alpha)}_\theta] = 0 \tag{3.37}$$

and is, thus, invariant under rotations about any of the $\alpha = x, y, z$ directions.

On the case of the Fermi-Hubbard model a site may be occupied with at most two electrons due to the Pauli exclusion principle. The principle states that the total wave function describing the state of any number of electrons must be antisymmetric, which implies that electrons cannot occupy the same energy state. Thus, since electrons have 2 possible spin states $(\uparrow, \downarrow)$ only two electrons are allowed to be on a single site.

A commom form of the Hamiltonian used to study its properties considers that both the hopping amplitude and the interaction magnitude do not change on any site, i.e. they are constants in the whole lattice,

$$H_{FH} = -J \sum_{\langle j,l\rangle,\sigma=\uparrow,\downarrow} a^\dagger_{j\sigma} a_{l\sigma} + U \sum_l a^\dagger_{l\uparrow} a_{l\uparrow} a^\dagger_{l\downarrow} a_{l\downarrow}. \tag{3.38}$$

What occurs in the dynamics of the system after it starts its evolution from an arbitrary state will depend on values of parameters in this state. One possible parameter which is important in this perspective is the electron number. This number has to be on the interval $[0, 2|\Lambda|]$. In the case of the extreme number of electrons (0 or $2|\Lambda|$) the system should remain on its initial state since no hopping should occur. On the other hand, much

interesting physics may happen on half filling, i.e., when there is,initially, one electron on each site, which now depends on $J$ and $U$.

When we neglect the interaction parameter, i.e., make $U \to 0$, particles with opposite spin should move on the lattice without any interactions. If all the spins point in a single direction, then there should be no hopping between sites (because of the Pauli exclusion principle). On the other extreme i.e., when $U \to \infty$, the strong Coulomb repulsion leads to a regime where no site has more then one electron, and electrons can only move if there is a vacant neighboring site. This regime is called a Mott-Insulator.

### 3.5.2 Bose-Hubbard Hamiltonian

The Bose-Hubbard Hamiltonian is used as a good approximation in the context of AMO physics to describe low energy band dynamics in systems composed of ultracold atoms and molecules [6, 8].

Since bosons have a symmetric total wave function in the lattice, they can be on the same total state,having the same spin quantum number quantum number. Thus the Hamiltonian of the (simplified) Bose-Hubbard Model becomes,

$$H_{BH} = -J \sum_{\langle j,l \rangle} a_j^\dagger a_l + \frac{U}{2} \sum_l a_l^\dagger a_l (a_l^\dagger a_l - 1), \tag{3.39}$$

where $a_l$ is the bosonic annihilation operator. The model presents a Bose-Einstein condensate phase as a ground state when we consider the particles are non interacting. On interacting systems the criterion for establishing that a Bose-Einstein condensate is formed becomes more intricate. In this case the system should present off-diagonal long-range order (ODLRO)[6].

## 3.6 AMO Open Quantum Systems and Approximation of its Dynamics by the Hubbard Model

A key starting point to understanding how these descriptions and models can be applied to open many body AMO systems is the level of control achieved in systems composed of ultracold cold gases in optical lattices. Such a control level is possible because magnetic and optical trapping physics from these systems are well understood [36, 37]. This makes it possible to use external magnetic fields and optical traps to obtain precise configurations and effective interactions between particles. Moreover, because of the low energy of the particle collisions in those systems it is possible to make an important

[6] Here we consider a system of hard-core bosons,i.e. $U \to \infty$ and the condition for (ODLRO) considering the system's ground state to be $|\mathbf{\Psi_{GS}}\rangle$ is given by $\langle \mathbf{\Psi_{GS}}| a_x^\dagger a_y |\mathbf{\Psi_{GS}}\rangle \to (constant) > 0$ for large enough $|x - y|$ see [2].

simplifying approximation with regard to the the description of the scattering dynamics of the atoms which,in this regime, can be described by a single parameter called the s-wave scattering $a_{scatt}$ [38].

For cold bosonic particles the Hamiltonian of the systems can then be described in terms of bosonic field operators $\hat{\psi}(\mathbf{r})$ which satisfy the commutation relation:

$$[\hat{\psi}(\mathbf{x}), \hat{\psi}^{\dagger}(\mathbf{y})] = \delta(\mathbf{x} - \mathbf{y}),$$

and it can be written as [9]:

$$H_{uca} \approx \int d^3r\, \hat{\psi}^{\dagger}(\mathbf{r})\Big[ -\frac{\hbar^2}{2m}\nabla^2 + V_0(\mathbf{r})\Big]\hat{\psi}(\mathbf{r}) + \frac{g}{2}\int d^3r\, \hat{\psi}^{\dagger}(\mathbf{r})\hat{\psi}^{\dagger}(\mathbf{r})\hat{\psi}(\mathbf{r})\hat{\psi}(\mathbf{r}) \tag{3.40}$$

where $m$ is the atomic mass, $g = 4\pi\hbar^2 a_{scatt}/m$ characterizes the the strength of the interaction processes upon elestic colisions between particles and $V_0(\mathbf{r})$ is the effective single-particle potential generated by external magnetic fields and optical traps.

The first term on the right handside of equation 3.40 characterizes the action of the Hamiltonian on single particles in the system. The kinetic part accounts for the tunneling between potential wells and the term $V_0(\mathbf{r})$ [36] refers to a controlled potential interaction with the optical lattice. Whereas the second term is related to the interaction between particles once they are in the same potential well.

In addition, since it is possible to achieve energy scales and temperatures much smaller then the band gap in an optical lattice potential [39], simple hamiltoninans for particles in a single band can be engineered in this context, such as the Bose-Hubbard model:

$$H_{BH} = -J\sum_{\langle j,l\rangle} a_j^{\dagger}a_l + \frac{U}{2}\sum_l a_l^{\dagger}a_l(a_l^{\dagger}a_l - 1), \tag{3.41}$$

or the Fermi-Hubbard model:

$$H_{FH} = -J\sum_{\langle j,l\rangle,\sigma} a_{l\sigma}^{\dagger}a_{l\sigma} + U\sum_l a_{l\uparrow}^{\dagger}a_{l\uparrow}a_{l\downarrow}^{\dagger}a_{l\downarrow}. \tag{3.42}$$

### 3.6.1 Special Case: Obtaining the Dissipative Hamiltonian Model for a Gas of Hardcore Bosons

The description of one type of system which can be studied in such a way was done by Garcia-Ripoll et al [40] where a hard-core boson gas description for polar molecules in an optical lattice was done by modeling the system through a Markovian master equation

$$\hbar\frac{d\rho}{dt} = -i[H, \rho] + \mathcal{D}\rho \tag{3.43}$$

where $H$ is the systems Hamiltonian describing unitary evolution and $\mathcal{D}$ is a superoperator acting on the density operator which describes the dissipative processes. In terms of bosonic field operators ($\psi$) they are given by

$$H = \int d^3x \psi^\dagger H' \psi + \frac{Re(g)}{2} \int d^3x \psi^{\dagger 2} \psi^2 \tag{3.44}$$

$$\mathcal{D}\rho = -\frac{Im(g)}{2} \int d^3x (2\psi^2 \rho \psi^{\dagger 2} - \psi^{\dagger 2}\psi^2 \rho - \rho \psi^{\dagger 2}\psi^2) \tag{3.45}$$

where $H'(\mathbf{r}) = -\hbar^2\nabla^2/2m + V_{trap}(\mathbf{r})$ is the single particle Hamiltonian and the strength of particle interactions is given by $g = 4\pi\hbar^2 a_{scatt}/m$, where $m$ is the mass of the particle and $a_{scatt}$ is the s-wave scattering length. The parameter $a_{scatt}$ describes both elastic, $Re(a)$, and inelastic, $Im(a)$, collisions.

It is possible to expand the bosonic field operator using Fock space operators $a_k^\dagger$ which obey the commutation relations

$$[a_j, a_l] = [a_j^\dagger, a_l^\dagger] = 0 \tag{3.46}$$

$$[a_j, a_l^\dagger] = \delta_{j,l} \tag{3.47}$$

$\psi^\dagger$ may then be expanded as:

$$\psi^\dagger(\mathbf{r}) = \sum_j a_j^\dagger w(\mathbf{r} - \mathbf{r_j}) \tag{3.48}$$

where $w(\mathbf{r})$ are Wannier wavefunctions associated with states on each site[7]

It is, then, possible to make a tight binding aproximation where the overlap in between Wannier functions is neglected. The system is, thus, approximately described by a Bose-Hubbard model and the terms in the master equation 3.43 are given by [40]:

$$H_{BH} = -J \sum_{\langle j,l \rangle} a_j^\dagger a_l + \frac{U}{2} \sum_l a_l^\dagger a_l (a_l^\dagger a_l - 1) \tag{3.49}$$

$$\mathcal{D}\rho = \frac{\hbar\Gamma}{4} \sum_k (2a_k^2 \rho a_k^{\dagger 2} - a_k^{\dagger 2} a_k^2 \rho - \rho a_k^{\dagger 2} a_k^2) \tag{3.50}$$

The master equation can be rewritten in terms of an effective Hamiltonian

$$\frac{d\rho}{dt} = -i(H_{eff}\rho - \rho H_{eff}^\dagger) + \Gamma \sum_k a_k^2 \rho a_k^{\dagger 2} \tag{3.51}$$

[7] Wannier wavefunctions are localized funtions defined on a lattice. They can be defined in terms of Bloch states and form a complete set of orthonomal states for a single band on a lattice. See [41, 42] For quantitative definitions of these functions.

where

$$H_{eff} = H_{BH} - i\frac{\Gamma}{2}\sum_k a_k^{\dagger^2} a_k^2. \tag{3.52}$$

In the next chapter, a more in depth study of the consequences of this master equation will be given . In particular, the continuous quantum Zeno effect on many body systems which undergo particle losses shall be our main focus in this regard.

# 4 Quantum Trajectories Technique Applied to Open Many Body Quantum Systems

## 4.1 Open Many Body Quantum Systems

So far the many body models and Hamiltonians studied have neglected interactions with the system's environment, i.e., the systems were considered to be closed. The dynamics of many body systems, as in the case of few body systems, may change drastically when we take these interactions into consideration. In order to understand a special class of open many body quantum systems (namely systems whose evolution can be described by a master equation in Lindblad form such as described in Chapter 2.2), we shall focus on AMO quantum systems whose Hamiltonians are well approximated by the Hubbard model. The research of these systems have become of great importance in many fields of physics and have implications on understanding analog quantum simulations [43], quantum computers [44], production of specific states in condensed matter physics [6] suppression of body losses in the system due to continuous quantum Zeno effect [4, 40, 45–47], changing magnetic states on Mott insulators [3] to name a few.

The fact that these systems may be approximately described by a master equation in Lindblad form (meaning the approximations discussed in 2.2 are still valid) makes it possible to immediately apply widely known numerical techniques to solve them in the context of many body systems. In particular, the quantum trajectories approach has been successfully implemented in open many body AMO systems in order to understand the dynamics and obtain important results, making it possible to extend the sizes of the systems simulated by exploiting other methods which are commonly used in the study of many body systems, such as t-DMRG, tensor networks and exact diagonalization [6, 7, 9]. In this thesis we shall focus on these applications to continuous quantum Zeno effect and state preparation.

## 4.2 Particle-Loss Dissipative Processes

The quantum trajectories technique can be used to study and understand various properties of open many body quantum systems described by a master equation. One interesting application is seen when particle loss type dissipation is involved in the evolution of the system.

Systems which undergo particle losses have been observed in a variety of different setups, including lattices comprised of polar molecules [4] and trapped ions [3]. Those

configurations may lead to interesting physics and even some counter intuitive results, as will be seen in the next sections.

### 4.2.1 Reversal of Magnetic Order by Particle Losses

We first turn our attention to an interesting example given by Nakagawa et al. [3] where the study of the evolution of a chain of trapped ions which undergo particle loss leads to the sign reversal of the magnetism of a Mott insulator. A 1-dimensional Mott insulator composed of spin-$\frac{1}{2}$ particles (electrons) can be described by a Fermi-Hubbard model whose lattice is half filled, i.e., there is one particle in each site[1], and the system is in the regime of strong interaction.

More specifically, the Hamiltonian that describes a Mott insulator is given by

$$H_{FH} = -J \sum_{l\sigma=\uparrow\downarrow} (a^\dagger_{l\sigma} a_{l+1\sigma} + a_{l\sigma} a^\dagger_{l+1\sigma}) + U \sum_l n_{l\uparrow} n_{l\downarrow}, \tag{4.1}$$

where $n_{l\sigma}$ is the number operator on site $l$, and $U \gg J$. In this regime double occupation becomes unlikely due to strong repulsion and particles are essentially frozen, leading to a configuration where there is a single spin on each lattice site.

Even though hopping is strongly suppressed in the model, quantum mechanics tells us there can be virtual jumps of the particles in the lattice. A second order process which involves a virtual exchange of particles lead to an effective spin exchange interaction, which offers an explanation towards the fundamental origin of magnetism [2, 48](see 7). Indeed, assuming the system is at half filling and has $SU(2)$ invariance, we can approximate the Hamiltonian 4.1 through second order perturbation theory to the Heisenberg model:

$$H_{spin} = t \sum_{\langle j,l \rangle} (\mathbf{S}_j \cdot \mathbf{S}_l - \frac{1}{4}) \tag{4.2}$$

as explained in A. Here, $t = 2|J|^2/U$.

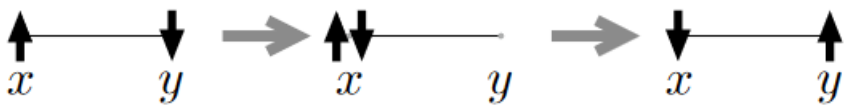


Figure 7 – Schematic ilustration of a second-order process mediating the spin-exchange interaction. This process lead to the origin of antiferromagnetic order on Mott insulators. Image extracted from [2].

[1] As a consequence of Pauli exclusion principle, a fermionic particle with spin 1/2 cannot occupy the same state as another spin 1/2 particle, i.e., the same site may only be doubly occupied if the particles spinors in the site are $|\uparrow\rangle$ and $|\downarrow\rangle$, respectfully. This means that a lattice $\Lambda$ composed of electrons may have at most $2|\Lambda|$ electrons. Thus, the lattice is half filled when only one electron occupy each of its sites.

When we consider particle loss dissipative processes on Mott insulators, the mechanism responsible for the quantum magnetism achieved in the system has a different explanation. As will be seen, particle loss induced by inelastic collisions in the lattice makes the system stabilize at high energies states(ferromagnetic order), as opposed to the expected relaxation to low energy states(antiferromagnetic order). In Fig. 8 a schematic illustration of the second order process which leads to spin exchange or particle loss is shown. Since the second step in the process involves a doubly occupied site with opposite spins, it will have a finite life time due to the dissipative effect. However, spins pointing in the same direction are not allowed on the same site due to the pauli exclution principle and, thus, do not decay (no dissipation occurs if the particles cannot occupy the same site). This mechanism leads ferromagnetic states (spins pointing in the same direction), to survive longer then anti-ferromegnetic (alternate spin direction configuration) ones.

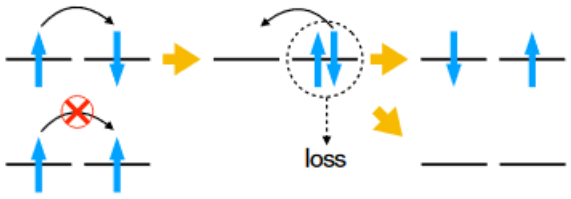


Figure 8 – Schematic ilustration of a second-order process mediating the spin-exchange interaction in the dissipative Hubbard system. On the first part we have two possible configurations, i.e, spins pointing in the same direction and spins pointing on opposite directions. Due to the pauli exclusion principle, only the latter can go through the second order process that leads to spin exchange (second part). Since the particles have to occupy the same site for the interaction to occur they can also go through innelestic collisions and therefore be ejected from the system to the environment (second process on the third part). Since spins which point in the same direction cannot occupy the same site these (ferromagnetic) states survive longer, leading to ferromagnetic order. Image extracted from [3].

To see this more concretely, we can consider a dissipative Hubbard model whose unitary part of the dynamics satisfy Eq. (4.1). The master equation can then be derived for the system which takes the form:

$$\frac{d\rho}{dt} = -\frac{i}{\hbar}[\rho, H_{FH}] + \sum_{j,\sigma'\sigma} (L_{j,\sigma'\sigma}\rho L^{\dagger}_{j,\sigma'\sigma} - \frac{1}{2}\{L^{\dagger}_{j,\sigma'^{\dagger}\sigma} L_{j,\sigma'\sigma}, \rho\}) \tag{4.3}$$

where $L_{j,\sigma'\sigma} = \sqrt{2\gamma} c_{j\sigma} c_{j\sigma'} \delta_{\sigma,\uparrow}\delta_{\sigma',\downarrow}$. The $c_{j\sigma}$ are annihilation operators at site $j$ with spin $\sigma$ and the Kronecker deltas are used to ensure the dissipation interaction occurs only between particles with opposite spins.

It is also possible to derive an effective Heisenberg Hamiltonian through second order perturbation theory substituting $U$ for $U - i\gamma$ in 4.1 [3]. This leads to the following effective Hamiltonian:

$$H_{eff} = (J_{eff} + i\Gamma) \sum_{\langle j,l \rangle} (\mathbf{S}_j \cdot \mathbf{S}_l - \frac{1}{4}) \tag{4.4}$$

where $J_{eff} = 4Ut^2/(U^2 + \gamma^2)$ and $\Gamma = 4\gamma t^2/(U^2 + \gamma^2)$. From $H_{eff}$, we can see that the spin-spin interactions will be affected by dissipation even in the strong repulsive regime. The eigenvalues of the effective Hamiltonian will be given by $E_n = \frac{(J_{eff}+i\Gamma)E_n^{(0)}}{J}$, where $E_n^{(0)}$ are the eigenvalues of the hermitian Hamiltonian 4.2. In this case the decaying rate, $\eta_n$, of the $n$-th eigenstate will be given by the imaginary part of $E_n$,i.e. $\eta_n = -(\Gamma/J)E_n^{(0)}$. Since $E_n^{(0)} < 0$, we get that the smaller the energy $E_n^{(0)}$ the higher the decay rate, which leads to the conclusion that higher energy states will survive longer in this regime. Moreover, this implies that after sufficient long times the Hamiltonian 4.4 will develop ferromagnetic correlations.

Using the quantum trajectories technique it is possible to study the evolution of the spin correlation functions on the system. Let us consider the case where the system has,initially, 8 sites and 8 particles in which no particle loss happens, i.e., the avarages are made only over the trajectories which, after a certain span of time, have had no quantum jumps. It is clear from Fig. 9 that the correlation functions $C^{(0)}(i,j,\tau) = \frac{\langle\psi(\tau)|\mathbf{S}_i\cdot\mathbf{S}_j|\psi(\tau)\rangle}{\langle\psi(\tau)|\psi(\tau)\rangle}$ [2] turn from a negative value (indicating antiferromagnetism) to a positive value (indicating ferromagnetism) saturating at 0.25.

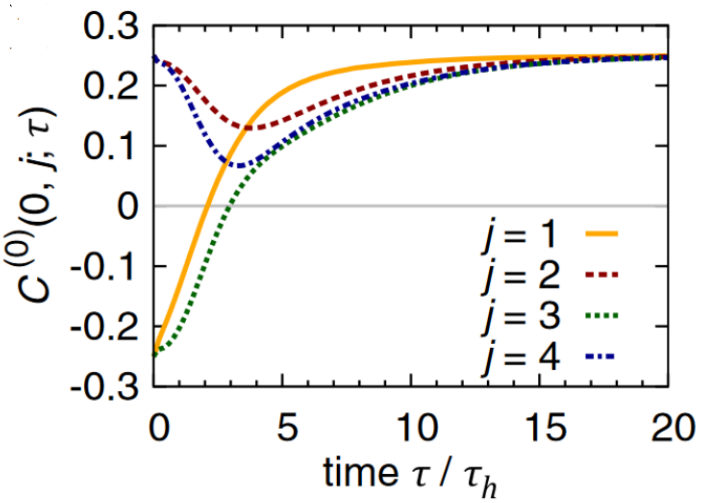


Figure 9 – Dynamics of the spin correlations $C^{(0)}(0,j,\tau)$ for a dissipative 8-site Fermi-Hubbard system in the absence of quantum-jumps.The initial state of the system is chosen to be a Néel state $|\uparrow\downarrow\uparrow\downarrow\uparrow\downarrow\uparrow\downarrow\rangle$. The parameters are set to $U/J = 10$ and $\gamma/J = 10$. The unit of time is the inverse hopping rate $\tau_h = 1/J$. Image extracted from [3]

[2] the upper symbol $C^{(\alpha)}$ indicate the number of quantum jumps in the evolution and $i,j$ indicate the sites on which the function is being calculated. In the figure the correlation functions are taken with respect to the first site

Including quantum jumps in the evolution of single trajectories, i.e., evolving the full master equation, also leads sign reversal of the spin correlation functions. To see that, the dynamics of spin correlations for the first and second spin in the chain were studied considering that only a specific number of quantum jumps happened in the process. The results (shown in fig. 10) show that the formation of holes in the lattice have considerable influence on the magnitude of the correlation function. Analysis of the results also show that, despite the smaller magnitude of $C^{(n)}(0,1,\tau)$ (compared to the case where no quantum jumps ocuur) the sign reversal still happens.

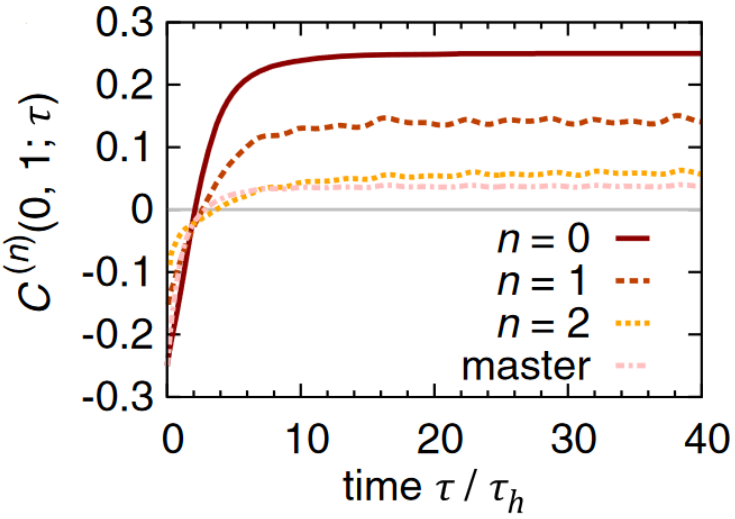


Figure 10 – Dynamics of spin correlations $C^{(n)}(0,1,\tau)$ average over quantum trajectories which involve $n$ quantum jumps for the dissipative Fermi-Hubbard model. The label "master" indicates the average over all possible numbers $n$, i.e. the solution to the master equation. The sign reversal of the spin correlations happens for all cases. The initial state of the system is chosen to be a Néel state $|\uparrow\downarrow\uparrow\downarrow\uparrow\downarrow\uparrow\downarrow\rangle$. The parameters are set to $U/J = 10$ and $\gamma/J = 10$. The unit of time is the inverse hopping rate $\tau_h = 1/J$. Image extracted from [3]

### 4.2.2 Particle loss Continuous Quantum Zeno Effect

The quantum Zeno effect was first brought to light by Misra and Sudarshan [49] and can be described as a phenomenon where frequent measurements in quantum systems inhibit state changes. It is well illustrated by an example given by Daley [9] of the case of a two-level atom coupled to a laser. Suppose the atom is initially in its ground state $|g\rangle$ and is coupled resonantly to the excited state $|e\rangle$ with Rabi frequency $\Omega$. Under this conditions, the atom periodically oscilates between the excited and the ground state. After a measurement to find weather the state of the system is $|e\rangle$ when an interval of time $\Delta t$ has passed, the probability of the atom being in the excited state takes the form $P_e \approx \frac{\Omega \Delta t}{4}$ which is proportional to $\Delta t$. If we reduce the interval in which the measurements occur

such that $\Delta t \to 0$ the probability the state of the system is $|e\rangle$ reduces monotonically to zero, that is, if the measurements are done frequently enough, the state of the atom is frozen in the ground state. This effect has been seen on experiments with trapped ions [50].

#### 4.2.2.1 Continuous Zeno Effect

When dealing with open quantum systems a generalization of the quantum Zeno effect in the context of continuous measurements can be realized, i.e., the continuous quantum Zeno effect [50, 51]. In this case, the system is considered to be measured continuously by the environment and strong dissipative processes can suppress coherent dynamics. The simplest example of this phenomenon is again given by a two level atom coupled to a laser. As was seen in Chapter 2, this system can be described by the master equation

$$\frac{d\rho}{dt} = -\frac{i}{\hbar}(H_{eff}\rho - \rho H_{eff}) + \Gamma\sigma_-\rho\sigma_+, \tag{4.5}$$

where

$$H_{eff} = -\frac{\Omega}{2}\sigma_x - \Delta\sigma_+\sigma_- - i\frac{\Gamma}{2}\sigma_+\sigma_-, \tag{4.6}$$

$\Omega$ is the Rabi frequency, $\Delta$ is the detuning and $\Gamma$ the Dissipation rate. In the case the system has a strong dissipation $\Gamma \gg \Omega$ the probability of a transition from the ground state $|g\rangle$ to the excited state $|e\rangle$ (considering that the atom starts on the state $|g\rangle$) becomes increasingly lower as $\Gamma$ grows. Figure 11 shows the value for the probability of the state to be $|g\rangle$ for several values of $\Gamma$. As is expected, when the system has no dissipative processes ($\Gamma = 0$), it undergoes Rabi oscillations. As the value of $\Gamma$ increases, $\rho_{gg}$ also grows, making jumps to the excited state $|e\rangle$ less likely. In the limit of $\Gamma \gg \Omega$ the system will continue in the state $|g\rangle$ indefinitely.

In this case it is also interesting to see the effects of the dissipation strength on single trajectories. As is shown in figure 12, the quantum zeno effect is already explicit on the evolution of pure states when the dissipation strength increases.

An interesting example of this effect in the field of open many body AMO quantum systems have been seen to occur experimentally on an optical lattice whose component particles were polar molecules and were subjected to particle losses [4]. In this setup, the polar KRb molecules are loaded into an optical lattice formed by three mutually orthogonal standing waves, and their interaction is controlled in such a way as to be described by an XY model Hamiltonian:

$$H = \frac{J_\perp}{2}\sum_{j\geq l} V_{dd}(S_j^+ S_l^- + S_j^- S_l^+), \tag{4.7}$$

where $J_\perp$ characterizes the spin-exchange interaction energy. The interaction between any two molecules depends on their relative position and is also characterized by the geometrical factor $V_{dd}$.

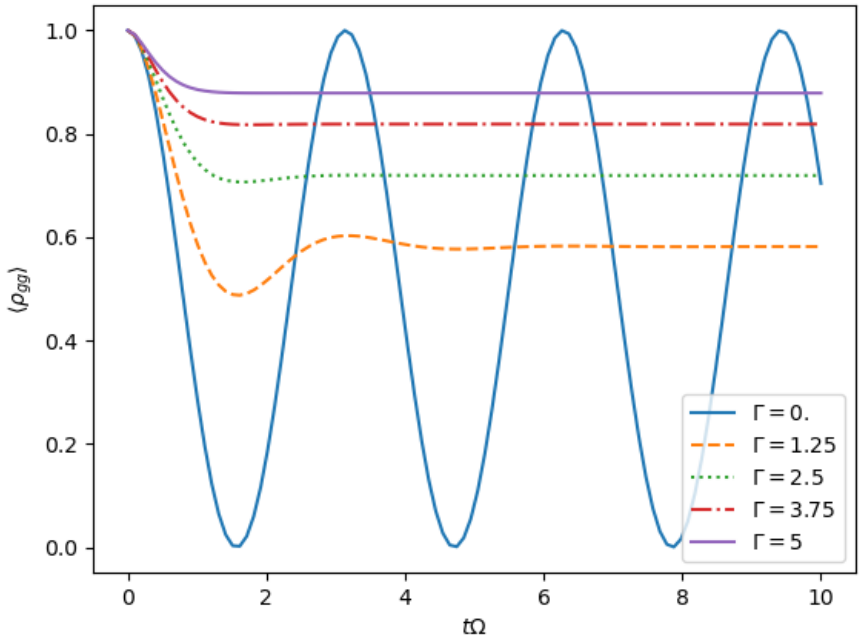


Figure 11 – Evolution of the probability of a two level atom to be found in the ground state $|g\rangle$ as a function of time for several $\Gamma$.

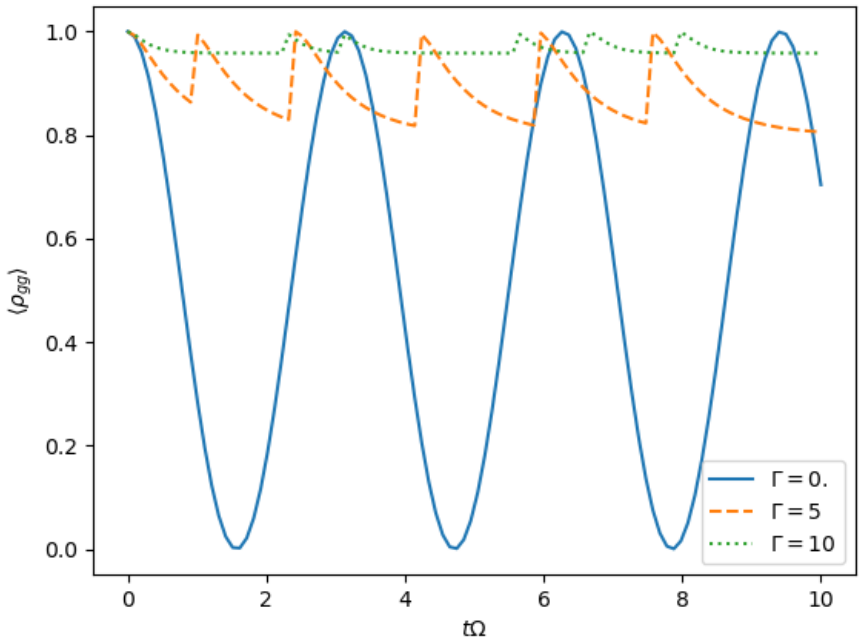


Figure 12 – Evolution of the probability of a two level atom to be found in the ground state $|g\rangle$ as a function of time for several $\Gamma$ on three separate trajectories.

In the experiment, the lattice molecules were initially prepared in such a way that the lattice had a 50:50 proportion of the particles with spins $|\uparrow\rangle$ and $|\downarrow\rangle$ in order for on site interactions to occur. This is because the lattice is approximated by a spin 1/2 system and, thus, Pauli blocking strongly suppresses particles with the same spin state on a single site. The potential wells of the lattice started at the same depth in all three orthogonal directions and the trap potential along one direction was then reduced to favor the interaction (collisions) between molecules and subsequent particle loss as is shown in Fig 13- **a**. Fig 13-**b** shows the number of lost particles versus time for two different $\hat{y}$ direction potential depths.

The on site loss rate $\Gamma_0$ is proportional to the rate of chemical reactions between two molecules on the same site and results in a particle loss process (the chemical reaction energy is much higher than the lattice potential, so the resulting particles are ejected from the lattice). It was observed that $\Gamma_0$ is much larger when molecules have distinguishable spin states [4]. This is a desired effect in this context, since it is important that the system is in the strong interacting regime, i.e. $\Gamma_0 \gg J_t/\hbar$ where $J_t$ is the tunneling amplitude, for the observation of the quantum Zeno effect. The effect is indeed observed, since increasing the on site dissipative process actually *decreases* the effective two-body loss rate between neighbouring molecules. In terms of $J$ and $\Gamma_0$, an effective dissipative rate parameter for the process may be written as [52]

$$\Gamma_{eff} = \frac{2(J_t/\hbar)^2}{\Gamma_0}, \tag{4.8}$$

and the time evolution of the number of molecules in state $|\downarrow\rangle$, i.e., $N_\downarrow(t)$ is described through a two-body loss equation [52]

$$\frac{dN_\downarrow}{dt} = -\frac{\kappa}{N_{\downarrow,0}} N_\downarrow^2, \tag{4.9}$$

where $N_{\downarrow,0}$ is the initial number of molecules on state $|\downarrow\rangle$ and $\kappa$ is the loss rate coefficient (which is proportional to $\Gamma_{eff}$).

The continuous quantum Zeno effect has been verified by measuring the dependency of the loss rate, $\kappa$, on $\Gamma_0$ and $J_t$ as can be seen in figure 13 $\mathbf{b} - \mathbf{c}$, respectively. It is clear from the graphs that $\kappa$ scales with $1/\Gamma_0$ 13 **c** and obeys a square power law for the Tunneling rate $J_t/\hbar$ as expected from Eq. 4.8.

#### 4.2.2.2 Continuous Quantum Zeno Effect and Quantum Trajectories

As was seen in the last section, the level of control reached in experiments with cold molecules in optical lattices has opened opportunities to study dissipative effects and see how systems experimentally evolve through simple Hamiltonians, such as the transverse Ising, Heisenberg and XY models. Nevertheless, the possibility of describing these systems

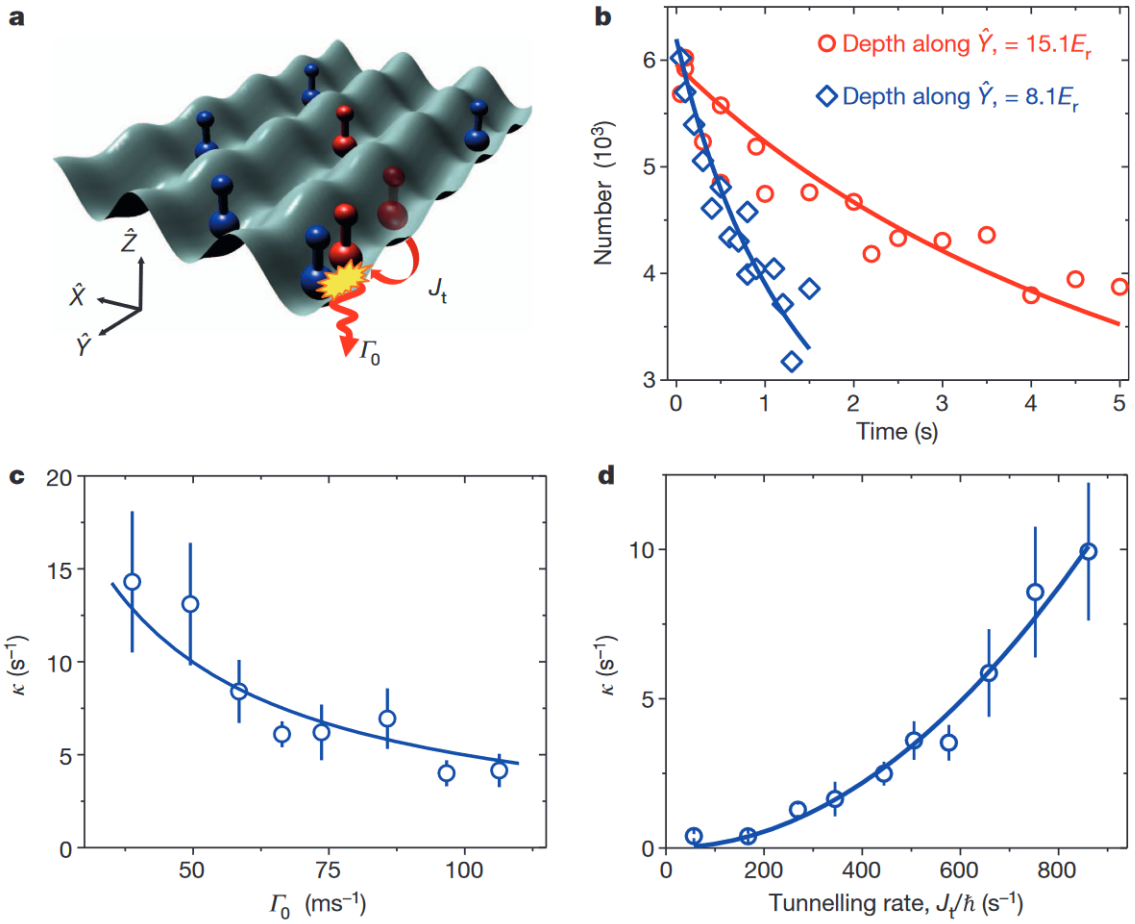


Figure 13 – Quantum Zeno effect for polar molecules in a 3D lattice.**a** The lattice depths along $\hat{x}$ and $\hat{z}$ are kept at $40E_r$ and the depth along $\hat{y}$ is decreased to allow tunnelling along the $\hat{y}$ directionat a rate $J_t/\hbar$.**b** Number of $|\downarrow\rangle$ molecules versus time is shown for lattice depths along $\hat{y}$ for two different potential depths.**c** The number loss rate,$\kappa$, has a $1/\Gamma_0$ dependence, which is consistent with the quantum Zeno effect. **d** The number loss rate, $\kappa$, has a $J_t^2$ dependence, as predicted from the quantum Zeno effect. Image extracted from [4]

dynamics using a master equation in Lindblad form open new oportunities to study them by well known numerical methods.

One of those methods is the quantum trajectories approach described in Chapter 2, which may be transferred to the context of many body quantum systems in a straightforward manner. As an example, we numerically studied the continuous quantum zeno effect on systems which undergo 2-particle loss making use of both exact integration and the quantum trajectories approach. Our study on the subject was separated into three main parts. Firstly, we simulated how the behavior of local densities may vary as a function of the dissipation strength, $\Gamma$, on one-dimensional systems. Secondly, we have sought to understand the mechanisms behind quantum Zeno effect by making use of the relationship between important variables in a simple, intuitive model. Lastly we provided numerical

data on the particle density of minimal systems in order to find evidence that support the viewpoint previously presented.

- **Particle Density and Decaying Rates**

  We used the quantum trajectories technique to obtain the behavior of local densities in the one-dimensional Bose-Hubbard model as a function of time for different dissipative strengths. The dissipative process was set to be a two particle loss dissipation, for which the master equation is given by

  $$\frac{d\rho}{dt} = -\frac{i}{\hbar}(H_{eff}\rho - \rho H_{eff}^{\dagger}) + \Gamma \sum_k a_k^2 \rho a_k^{\dagger 2}, \tag{4.10}$$

  where

  $$H_{eff} = H_{BH} - i\frac{\Gamma}{2}\sum_k a_k^{\dagger 2} a_k^2 \tag{4.11}$$

  and the Hubbard Hamiltonian $H_{BH}$ is given by Eq. 3.41.

  The results are shown in figure 14, where the parameters were set to $J = 1$ and $U = 10J$ and the system started with one boson in each site. From results we can infer that the average density on a single site reduces more slowly with time when the strength of the dissipation, i.e. $\Gamma$, is increased. In E we show that the same behavior is seen for the other sites. This effect is attributed to the continuous quantum Zeno effect.

  In order to better understand how loss of particles is affected by the dissipation strength, $\Gamma$, we obtained the time average of the density of particles on a single site as a function of $\Gamma$. The results (see Figure 15) show that, as dissipation strength increases from zero, at first we get the intuitively expected result, i.e. the average density is reduced when $\Gamma$ is increased. On the other hand after $\Gamma$ reaches the value $\Gamma = U$ this decrease stops and an increase of the average density starts. Our data shows that for a sufficiently large $\Gamma$ the density gets arbitrarily close to unit (Inset figure 15).

- **Intuition Behind the Quantum Zeno Effect**

  To understand the mechanisms of *particle loss vs dissipation strength* dynamics we started by considering a minimal model composed of a three level system. As shown in figure 16. In this model the two upper energy levels ($|1\rangle, |2\rangle$) are coupled to a laser and the resonance frequency between those levels is given by $\omega_0$. We further make the assumption that a particle on energy state $|1\rangle$ decays into a much less energetic level $|0\rangle$ (which would correspond to particle loss as presented in the previous sections). The particle is set to oscillate between the energy states $|1\rangle$ and $|2\rangle$ with Rabi frequency $J$ and the dissipative parameter for the decay into the energy state $|0\rangle$ is

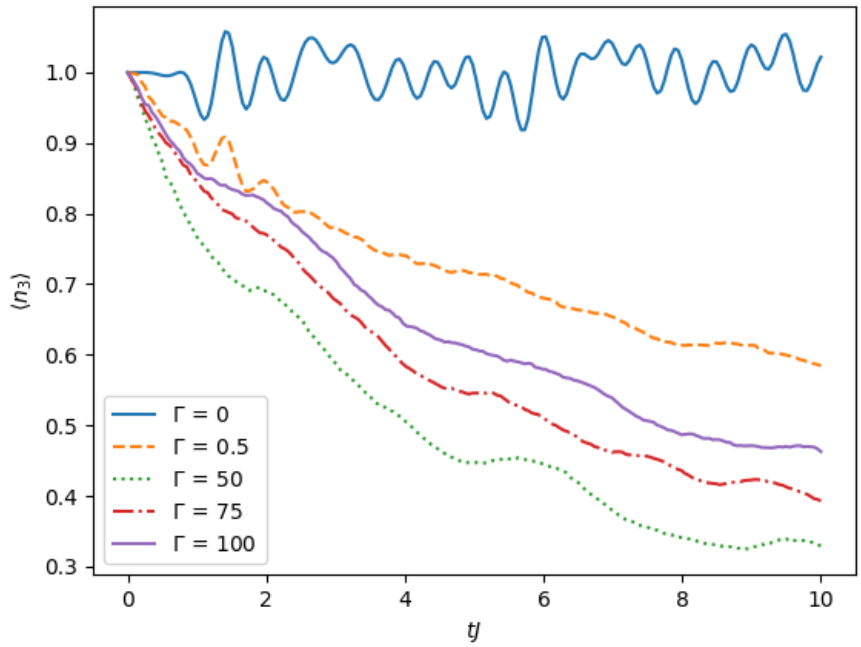


Figure 14 – Time evolution of particle density on site 3 on a lattice with 6 bosons and 6 sites for 5 different values of dissipation strength Γ. It is qualitatively seen that stronger dissipation reduces density loss over time

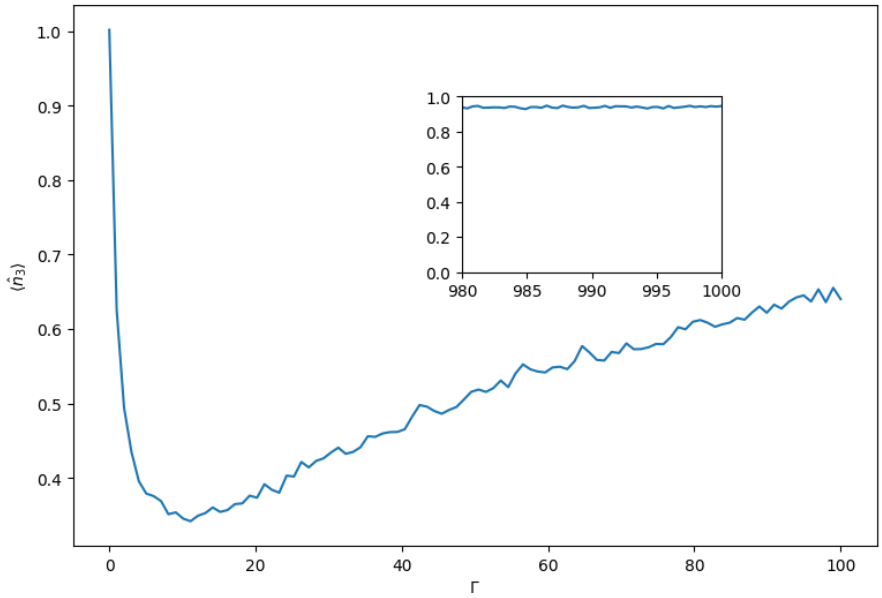


Figure 15 – Time average of the particle density as a function of Γ. The lattice comprises of 5 sites and (at the begining of the evolution) five bosons. From the results we are able to see how Γ affects particle loss in the lattice showing an expected decay in the interval $[0, U]$ and the counter intuitive increase after that. In the inset we show the same results for $\Gamma \in [980, 1000]$

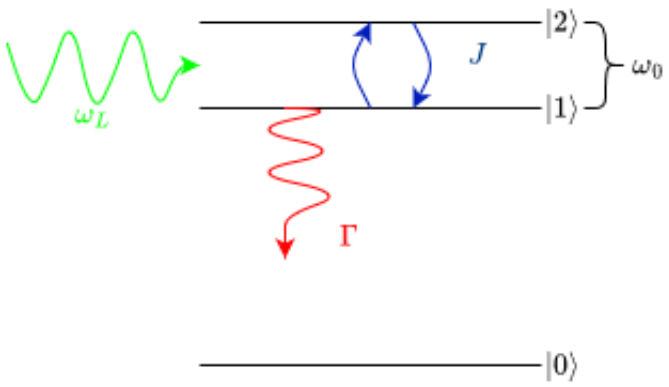


Figure 16 – Ilustrative diagram of the minimal model used as an example to describe the intuition behind the Continuous quantum Zeno effect

given by $\Gamma$. In order to get more intuitive results we further assume the system is in one of two regimes i.e., either $\frac{J}{\Gamma} \ll 1$. or $\frac{J}{\Gamma} \gg 1$ We then ask how long would it take for the population of state $|2\rangle$ to decay into the zero state once we increase/decrease $\Gamma$?

- In the limiting case where $\frac{J}{\Gamma} \ll 1$ we start by evaluating how the system would behave if $J \ll 1$. In this case, since the change of states between $|1\rangle$ and $|2\rangle$ is negligible, the period of time $\tau$, it would take for the populations of state $|2\rangle$ to decay into the state $|0\rangle$ would grow indefinitely as $J$ approaches zero i.e., $J \to 0 \implies \tau \to \infty$ (there would essentially be no oscillation between states $|1\rangle$ and $|2\rangle$ and therefore the population of $|2\rangle$ would not decrease). Moreover, since $\frac{J}{\Gamma} \ll 1$ is the same as $\Gamma \gg 1$ and $J > 0$ (constant) or $J \ll 1$ and $\Gamma > 0$ (constant), we can conclude that, in this regime, increasing $\Gamma$ is the same as decreasing $J$ and the time the population on $|2\rangle$ survives will grow indefinitely as $\Gamma$ grows.
- Following analogous arguments, the regime where $\frac{J}{\Gamma} \gg 1$ is the same whether $J \gg 1$ and $\Gamma > 0$ (constant) and or $\Gamma \ll 1$ and $J > 0$ (constant). Thus, we see that this limit is the same as $\Gamma \to 0$ and, since if there is essentially no dissipation then no decay into the $|0\rangle$ state would occur, the time interval, $\tau$ would also grow indefinitely.

Therefore, since in both limiting cases $\tau$ will grow indefinitely, there must be a minimum value $\tau_0$ in the interval $0 < \tau < \infty$ with $J/\Gamma \in (0, \infty)$ in which dissipation is maximum.

- **Numerical Data on $\tau$**

We explored the idea presented on the last section numerically in order to find evidence that the quantum Zeno effect may be intuitively seen in an analogous

manner for many body systems. In this case we chose a simple minimal system that could reproduce the results above. The model is composed of a two site lattice and a single particle. The dissipative process considered in this case is that of single particle loss in only one site and the effective Hamiltonian (still cosidered to be that of the Bose-Hubbard model) may be written as

$$H_{eff} = -J(a_1^\dagger a_2 + a_2^\dagger a_1) - i\frac{\Gamma}{2}(a_1^\dagger a_1), \tag{4.12}$$

where we consider the dissipation to happen on site 1, and we do not have to consider the interaction term since there is only one particle in the system.

Since the system considered is small it is more efficient to solve the master equation exactly to obtain the expected value of the total particle number operator as a function of time $\langle \hat{N}(t) \rangle = \hat{n}_1(t) + \hat{n}_2(t)$. In figure 17 we show the results of the time span, $\tau$, for dissipation as a function of $\Gamma/J$. We define $\tau$ as the time it takes for $\hat{N}(t)$ to reach a certain value $\alpha$, i.e., $\langle \hat{N}(\tau) \rangle \leq \alpha$; In the case of 17 $\alpha = 0.6$.

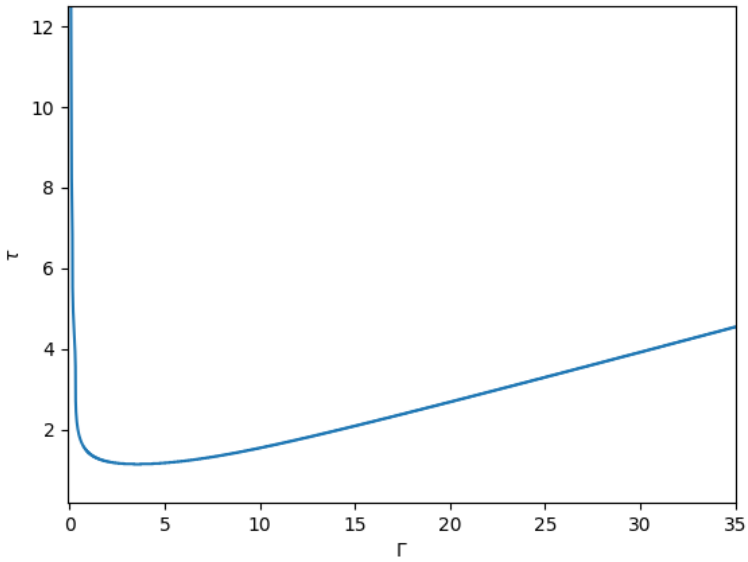


Figure 17 – Exact integration results for the Lindblad master equation with effective Hamiltonian(4.12. Here $\tau$ is the time it takes for the total occupation number to satisfy $\langle \hat{N}(\tau) \rangle \leq 0.6$. We can see that for small $\Gamma$, $\tau$ decreases fast with small variations of $\Gamma$. On the other hand after a certain minimum point, $\tau$ grows monotonicaly, albeit slowly when compared with the decrease rate for $\Gamma \ll 1$.

The results show that the total occupation number has the behavior deduced in the last section, i.e., $\tau \gg 1$ when $\Gamma \ll 1$ and $\tau \gg 1$ when $\Gamma \gg 1$, supporting the idea that the factor $\frac{J}{\Gamma}$ is strongly related to the occurrence of the continuous quantum Zeno effect.

To see that this characteristic behavior may be extended to systems with higher number of particles we have simulated the total occupation number of a system with 2 particles in 2 sites, whose dissipative processes is of two particle loss type, as a function of time and dissipation strength. The results, shown in figure 18, stresses that with stronger dissipative effects the two particles survive longer (as for very weak $\Gamma$ also).

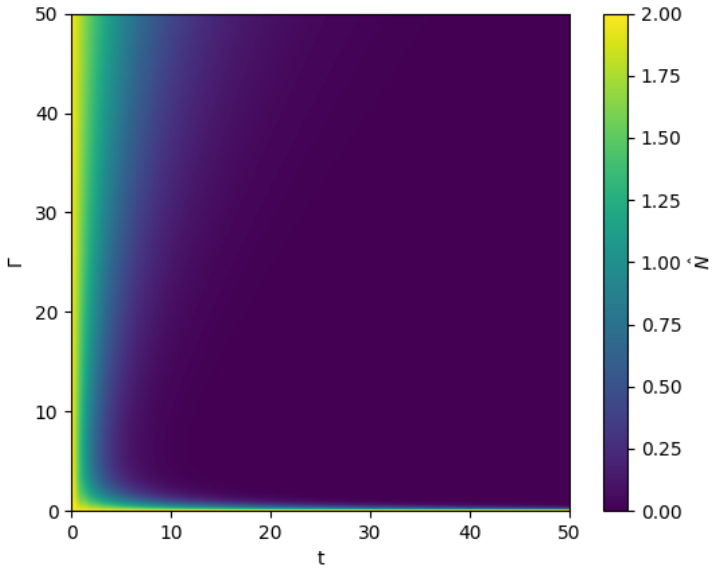


Figure 18 – Results for exact integration of the the expected value of total occupation number as a function of time and dissipation strength supporting the ideas discussed in the text. The system is composed of 2 sites and 2 bosons and the effective Hamiltonian is given by 4.11

Similar consequences of particle loss dissipative effects may be seen for systems which undergo both three and single body loss. More details on the consequences of such dissipative effects may be seen on appendix D.

## 4.3 State Preparation

As was previously said, the control over AMO systems has reached the precision of a single atom, ion or molecule [5,53]. This, in return, allowed specific Hamiltonians, such as the ones for the Fermi or Bose-Hubbard models, to be engineered in order to evolve those systems [5] and paved the way for realizing analog quantum simulations, which can be largely advantageous to study such models than using classical computing. This is because the level of complexity of these systems scales exponentially with system size - which make large size systems classically intractable. The preparation of those systems has been possible mostly thanks to the use of dissipative processes to control the coherent evolution of AMO systems, a technique well understood and utilized in quantum optics [1, 26].

In the context of quantum optics, the idea behind state preparation is to find a dissipator $\mathcal{D}$ for the master equation such that the dynamics of the system will lead its state asymptotically to a desired state. An interesting example is the optical pumping of a three level atom into a stable pure state, which shall be discussed below 4.3.1. Moreover, in the next sections, extensions of this quantum optics protocol for obtaining specific many body states, such as Bose-Einstein condensates and superconducting, BCS-type, states are discussed.

### 4.3.1 Optical Lattices Immersed in Ultra-Cold Gasses

One of the simplest examples of an open many body system which can be used to drive an arbitrary initial state into a pure state in a long time evolution may be described by an optical lattice composed of bosons which is subjected to driving fields that can lead the system to a lower energy state [5]. In this scenario the lattice is immersed in a superfluid as is shown in Figure 19. The BEC works as a bath of Bogoliubov excitations and provides an efficient way as to lead particles to decay into the lowest energy bands. Moreover, the Bloch band energies[3] $\epsilon$ are larger than both the possible kinetic energy of the particles and the energy produced from collisions of lattice bosons with the BEC particles. This allows for the necessary approximations as to describe the system through the extended Bose-Hubbard model:

$$H = -J\sum_j (a_j^\dagger a_{j+1} + a_j a_{j+1}^\dagger) - \mu\sum_j n_j + \frac{U}{2}\sum_j n_j(n_j - 1). \tag{4.13}$$

In order to realise the decay of the system into a specific state (A BEC in this context) it is possible to drive the system into dark states with the help of external fields provided by lasers in specific frequencies. This is done by extending the concept of state preparation via optical pumping from quantum optics.

To this end, consider a three level system in a $\Lambda$ configuration. The lower energy states, are coupled to the most excited state, by two fields of antisymmetric Rabi frequencies $\Omega_+$ and $\Omega-$[4] as illustrated in figure 20$(a)$.Consider that dissipation $\Gamma$ leads to decay into one of the lower energy states via spontaneous emission. For suficient detuning between excited and ground states the state of the system will evolve in such a way that the stationary solution of the master equation governing the system is a pure state, which is composed of the linear combination of the lower energy states. This linear combination is

[3] Bands formed from close energy states that emerge from Bloch theorem for periodic potentials.

[4] The term "antisymmetric Rabi frequencies" refer to two frequencies which will couple separately to the degenerate ground states in this case. From this coupling, spontaneous emission leading back to the ground states occur symmetrically

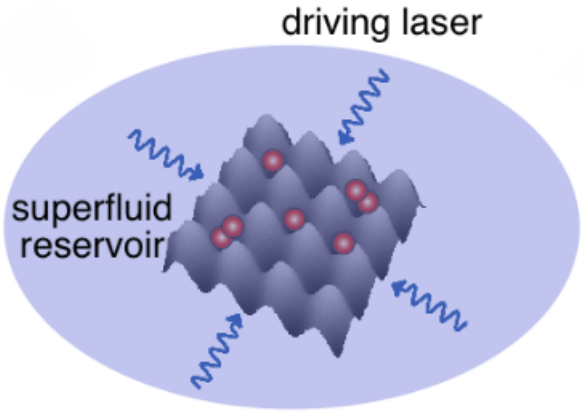


Figure 19 – Illustrative representation of the system setup for obtaining a many body state driven by dissipative dynamics. The optical lattice is immersed in a BEC and driving fields are used to lead the system to a low energy state. Image extracted from [5].

called a dark state and in the long time limit will be occupied by the entire population of the system (Fig 20a).

This idea can be extended to a optical lattice when the external fields are applied to the entire system and in the long time limit the system should eventually relax to a completely symmetric state which is a BEC (Fig 20b,c),

$$|BEC\rangle = \frac{1}{N!}\left(\frac{1}{\sqrt{M}}\sum_j a_j^\dagger\right)^N |VAC\rangle\,, \tag{4.14}$$

where $N$ is the particle number and $M$ is the number of sites.

The dissipative processes can be described in terms of the operators:

$$c_\beta = (a_j^\dagger + a_l^\dagger)(a_j - a_l) \tag{4.15}$$

acting on each pair of adjacent lattice sites $\beta = \langle j, l\rangle$. These operators describe the annihilation of an anti-symmetric state and the creation of a symmetric one. It is then possible to write a master equation for the evolution of the optical lattice state under these conditions:

$$\dot{\rho} = \frac{-i}{\hbar}[H,\rho] + \Gamma(\sum_j c_j \rho c_j^\dagger - \frac{1}{2}\{c_j^\dagger c_j, \rho\}) \tag{4.16}$$

Where the anti-commutator $\{A, B\}$ is defined as $\{A, B\} = AB + BA$.

This master equation was studied by *Diehl et al* [6] where the authors found evidence that, under the appropriate conditions, the system should decay into a pure state (BEC) and have long range order as is shown in figure 21. This allowed the study of the

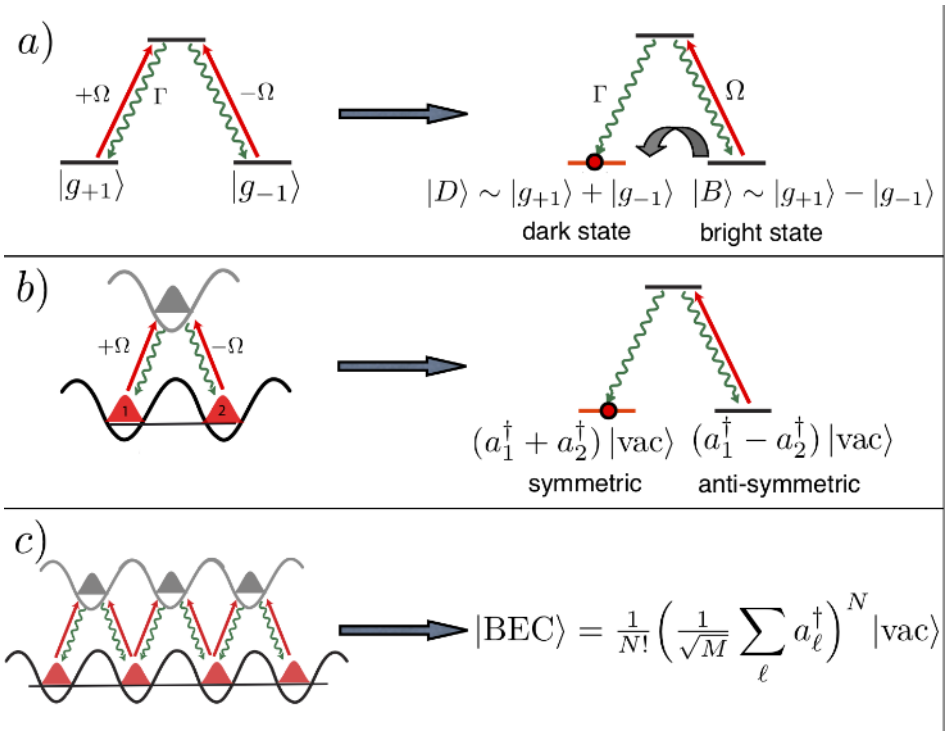


Figure 20 – Qualitative picture of state preparation in many body systems in analogy with optical pumping. a) Two degenerate low energy levels are coherently coupled to a higher energy level with anti-symmetric Rabi frequencies, this leads the system to populate a dark state entirely (symmetric linear combination of the two low energy states in this case), the anti- symmetric linear combination is still coupled to the higher energy state. b) implementation for a two particle optical lattice of the configuration that leads to the dark state occupation c) extension of the case in b for a many-particle system (which leads to a BEC state in the long time limit). Image extracted from [5]

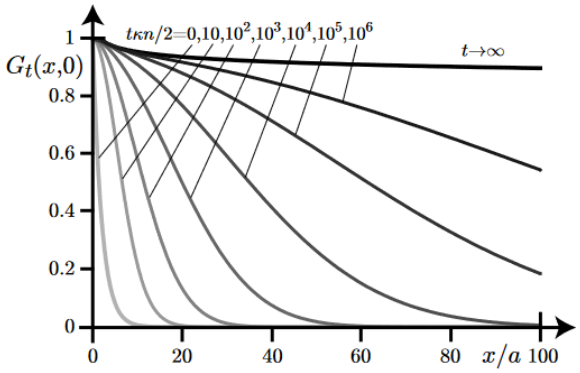


Figure 21 – Appearance of quasi long-range order during the time evolution: the correlation function $G_t(x,0) = \langle a_\alpha(t_1)a_\beta^\dagger(t_0)\rangle$ (where $\alpha$ and $\beta$ are the considered sites) is shown for various times $t\kappa n/2 = 0{,}10{,}10^2, 10^3, 10^4, 10^5, 10^6, \infty$. The initial disordered state has a correlation length $= xi = 2a$, and the system parameters are chosen at $T_{eff}/(4T_{KT}) = 1/18$ and $x_0 = 0.55a$. Figure extracted from [6]

evolution of the dissipative systems at long times using quantum trajectories and analyse if the system decays into a BEC state under the dissipative processes.

### 4.3.2 Dissipative Ferminonic System Driven into Dark State

The logic applied to bosons in the last section has also been applied to fermions on 2D systems by *Yi et al* [7] where they focused on the preparation of paring states, this time using quantum trajectories to study the driven dissipative dynamics of the system whose dark state is of a BCS type (a state which is not altered by quantum jumps).

A key mechanism for obtaining a dissipation into a dark state in these kind of systems is the Pauli blocking, which is a property of such systems of fermions where spontaneous emission to an already occupied state is inhibited due to Pauli exclusion principle as is shown in figure 22. This phenomenon leads to a different non-equilibrium paring mechanism which does not rely on attractive forces.

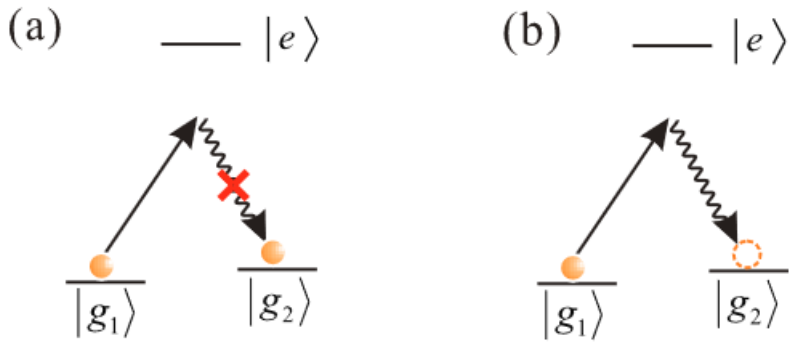


Figure 22 – a) When two low energy states are occupied there cannot be a decay from an excited to an the already occupied state due to the Pauli exclusion principle.b) When the state $|g2\rangle$ is free the decay can happen. Image extracted from [7]

The states involved in the research were the ones that could be described through a homogeneous product of $N$ identical fermion pairs such as:

$$|\psi\rangle = \eta^{\dagger N} |VAC\rangle \tag{4.17}$$

where $\eta^\dagger = \sum_{a,b} \eta_{a,b} c_a^\dagger c_b^\dagger$ with a and b being pairs of values $(\sigma, q)$ that represent spin and position on the 2D lattice, respectively. For large enough systems (in the thermodynamic limit) the states represented in equation 4.17 can be described with the grand canonical ensemble and Fourier transformed so it can be evaluated in the momentum representation, for states of paired Fermions they will be described by BCS-type states:

$$|\psi\rangle = \mathcal{F} \exp\left\{ \sum_{A,B} f_{A,B} c_A^\dagger c_B^\dagger \right\} |VAC\rangle = \mathcal{F} \prod_{A,B} (1 + f_{A,B} c_A^\dagger c_B^\dagger) |VAC\rangle \tag{4.18}$$

where $f_{A,B} = \sum_{i,j} \eta_{a,b} e^{(q\mathbf{k}\mathbf{r_i} + q\mathbf{k'}\mathbf{r_j})}$, A,B are the pairs of values $(\sigma, \mathbf{k})$ which respectively represent the spin and momentum and $\mathcal{F}$ is a normalization factor.

According to Yi *et al* [7], in general the evolution of such a fermionic system into a pairing state as in 4.18 involves multiple particle dissipative processes. In the case of two particle processes the dissipative dynamics can be viewed as phase locking between pairs of Fermions [7] and jump operators in 1D systems may be written as

$$J_q = C^\dagger M c_{q\uparrow} \tag{4.19}$$

where $M = (c_{q+1\downarrow} + c_{q-1\downarrow})(c_{q+1\downarrow} - c_{q-1\downarrow})$ and $C^\dagger$ is an arbitrary superposition of single-fermion creation operator with spin up. It can be shown from symmetry arguments that the dark state reached after sufficiently long times is unique for all initial states [7]. Another important condition necessary for state preparation after dissipative dynamics is that there should not be any other stationary state, i.e. only the dark state can be a stationary solution of the master equation. In that regard, numerical simulations can be used to find evidence that the system relaxes to the dark state no matter the initial state. The results obtained by Yi *et al* are shown in figures 23 and 24. On figure 23 the fidelity and entropy obtained from the evolution of the master equation have been evaluated for 1D systems whose initial states were chosen to be the antiferromagnetic Neél (figure 24-a) and spin-singlet (figure 24-b) states. The results show that both the fidelity and entropy of the system point to the conclusion that the state of the system relaxes to the desired dark state on both systems. The the evolution systems for 2D is shown in in figure 23 and was done using quantum trajectories to solve the master equation. The results show evidence that there is an exponential decay to a steady state, and, from that, the existence of a dissipative gap can be inferred (analogous to the energy gap for the ground state of the BCS-paring state).

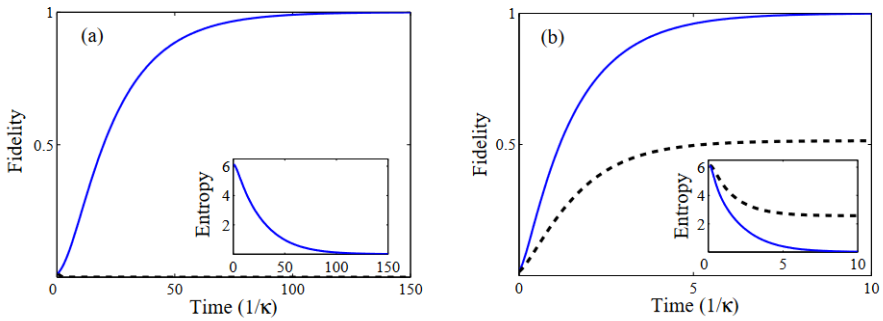


Figure 23 – Fidelity and entropy evolution for 4 atoms on a 1D chain with 4 sites. (a) The fidelity is with respect to an antiferromagnetic Néel state. The dashed curve represents the evolution of the fidelity with respect to the other antiferromagnetic state of the system with a total spin flip; (b) The fidelity is with respect to a 1-D singlet pairing state. The dashed curve shows the evolution without $\{J_q^z\}$ jump operators. Image extracted from [7].

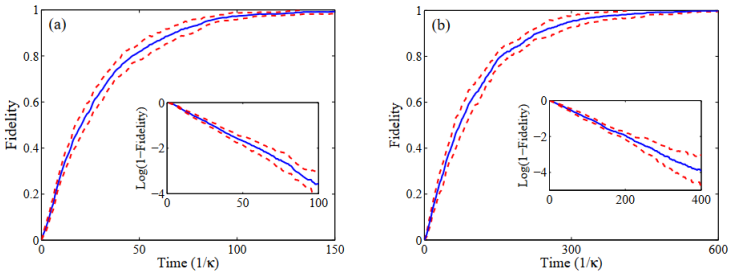


Figure 24 – Quantum trajectory evolution of the master equations for d-wave and p- wave states in 2 dimensions. (a) Evolution with d-wave jump operators on a 2×6 ladder with 4 atoms; (b) evolution with p-wave jump operators on a 4×4 plaquette with 4 atoms. The insets indicate the existence of dissipative gaps in both cases, which render the convergence to the steady states exponentially fast. This result is robust in the thermodynamic limit as revealed by mean-field theory in [7]. The fidelity (solid) is calculated by averaging over 1000 trajectories. These trajectories are then bunched into 100-trajectory groups, whose standard deviations are then calculated to show the sampling errors (dashed). Image extracted from [7]

# 5 Conlcusions

We have done a review on open many body AMO systems, exploring the consequences of dissipative dynamics on them. These dynamics are proving to have promising effects which can lead towards having better control over systems and a better understanding of phenomena in many areas of physics, including quantum simulation, quantum information and quantum magnetism.

Our focus was concentrated on particle loss dissipative processes and the mechanisms behind the continuous quantum Zeno effect on systems which could be approximated by the Hubbard model. In this perspective, we found numerical evidence that suggests the relationship between hopping amplitude and dissipative strength is essential for the process to occur on one dimensional bosonic systems, meaning the effect will occur once we are in the regime $\Gamma \gg J$. This was also seen experimentally, as was shown in chapter 4.1. The continuous quantum Zeno effect may be a promising process in many body problems, leading to a greater experimental control over time of system properties such as magnetism and particle density.

We were also able to use the quantum trajectories method to study state (and observable) evolution on dissipative many body systems, which proved to be an efficient method to obtain expected values and states of global observables as well as a class of local ones. However, although the method shows an improvement on memory cost in comparison with direct integration of the master equation, it may take extensive time periods to be performed in many body problems depending on the degree of accuracy (number of trajectories) needed for the results. In this context, possible improvements on the method were found in the literature. Those improvements rely on the use of other numerical methods for state evolution in between quantum jumps, such as exact diagonalization, t-DMRG and Tensor Networks, and may considerably improve the size of systems simulated.

# Bibliography

[1] Gleyzes, Sebastien, Stefan Kuhr, Christine Guerlin, Julien Bernu, Samuel Deleglise, Ulrich Busk Hoff, Michel Brune, Jean Michel Raimond, and Serge Haroche: *Quantum jumps of light recording the birth and death of a photon in a cavity.* Nature, 446(7133):297–300, 2007. Cited 4 times on pages 9, 16, 32, and 62.

[2] Tasaki, Hal: *Physics and mathematics of quantum many-body systems*, volume 62. Springer, 2020. Cited 13 times on pages 9, 34, 35, 37, 38, 39, 41, 43, 45, 50, 76, 77, and 81.

[3] Nakagawa, Masaya, Naoto Tsuji, Norio Kawakami, and Masahito Ueda: *Dynamical sign reversal of magnetic correlations in dissipative Hubbard models.* Physical Review Letters, 124(14):147203, 2020. Cited 7 times on pages 9, 10, 49, 50, 51, 52, and 53.

[4] Yan, Bo, Steven A Moses, Bryce Gadway, Jacob P Covey, Kaden RA Hazzard, Ana Maria Rey, Deborah S Jin, and Jun Ye: *Observation of dipolar spin-exchange interactions with lattice-confined polar molecules.* Nature, 501(7468):521–525, 2013. Cited 6 times on pages 10, 49, 54, 56, 57, and 84.

[5] Müller, Markus, Sebastian Diehl, Guido Pupillo, and Peter Zoller: *Engineered open systems and quantum simulations with atoms and ions.* In *Advances in Atomic, Molecular, and Optical Physics*, volume 61, pages 1–80. Elsevier, 2012. Cited 6 times on pages 11, 16, 62, 63, 64, and 65.

[6] Diehl, Sebastian, A Micheli, Adrian Kantian, B Kraus, HP Büchler, and Peter Zoller: *Quantum states and phases in driven open quantum systems with cold atoms.* Nature Physics, 4(11):878–883, 2008. Cited 5 times on pages 11, 45, 49, 64, and 65.

[7] Yi, Wei, S Diehl, AJ Daley, and P Zoller: *Driven-dissipative many-body pairing states for cold fermionic atoms in an optical lattice.* New Journal of Physics, 14(5):055002, 2012. Cited 6 times on pages 11, 12, 49, 66, 67, and 68.

[8] Daley, AJ, JM Taylor, S Diehl, M Baranov, and P Zoller: *Atomic three-body loss as a dynamical three-body interaction.* Physical review letters, 102(4):040402, 2009. Cited 7 times on pages 12, 45, 83, 84, 85, 86, and 87.

[9] Daley, Andrew J: *Quantum trajectories and open many-body quantum systems.* Advances in Physics, 63(2):77–149, 2014. Cited 8 times on pages 12, 18, 23, 25, 46, 49, 53, and 88.

[10] Barmettler, Peter and Corinna Kollath: *Controllable manipulation and detection of local densities and bipartite entanglement in a quantum gas by a dissipative defect.* Physical Review A, 84(4):041606, 2011. Cited 5 times on pages 13, 87, 88, 89, and 90.

[11] Breuer, Heinz Peter, Francesco Petruccione, *et al.*: *The theory of open quantum systems.* Oxford University Press on Demand, 2002. Cited 4 times on pages 16, 18, 20, and 78.

[12] Bloch, Immanuel, Jean Dalibard, and Sylvain Nascimbene: *Quantum simulations with ultracold quantum gases.* Nature Physics, 8(4):267–276, 2012. Cited on page 16.

[13] Verstraete, Frank, Michael M Wolf, and J Ignacio Cirac: *Quantum computation and quantum-state engineering driven by dissipation.* Nature physics, 5(9):633–636, 2009. Cited on page 16.

[14] García-Ripoll, Juan J, Peter Zoller, and J Ignacio Cirac: *Quantum information processing with cold atoms and trapped ions.* Journal of Physics B: Atomic, Molecular and Optical Physics, 38(9):S567, 2005. Cited on page 16.

[15] Müller, Markus, A Rivas, EA Martínez, D Nigg, P Schindler, T Monz, R Blatt, and MA Martin-Delgado: *Iterative phase optimization of elementary quantum error correcting codes.* Physical Review X, 6(3):031030, 2016. Cited on page 16.

[16] Nielsen, Michael A. and Isaac L. Chuang: *Quantum Computation and Quantum Information.* Cambridge University Press, 2000. Cited 3 times on pages 18, 19, and 34.

[17] Bergou, János A and Mark Hillery: *Introduction to the theory of quantum information processing.* Springer Science & Business Media, 2013. Cited on page 19.

[18] Jacobs, Kurt and Daniel A Steck: *A straightforward introduction to continuous quantum measurement.* Contemporary Physics, 47(5):279–303, 2006. Cited 2 times on pages 19 and 26.

[19] Gardiner, Crispin W and Matthew J Collett: *Input and output in damped quantum systems: Quantum stochastic differential equations and the master equation.* Physical Review A, 31(6):3761, 1985. Cited on page 20.

[20] Gardiner, Crispin, Peter Zoller, and Peter Zoller: *Quantum noise: a handbook of Markovian and non-Markovian quantum stochastic methods with applications to quantum optics.* Springer Science & Business Media, 2004. Cited on page 20.

[21] Carmichael, Howard: *An open systems approach to quantum optics: lectures presented at the Université Libre de Bruxelles, October 28 to November 4, 1991*, volume 18. Springer Science & Business Media, 2009. Cited on page 21.

[22] Mølmer, Klaus, Yvan Castin, and Jean Dalibard: *Monte Carlo wave-function method in quantum optics.* JOSA B, 10(3):524–538, 1993. Cited 4 times on pages 21, 23, 25, and 26.

[23] Dalibard, Jean, Yvan Castin, and Klaus Mølmer: *Wave-function approach to dissipative processes in quantum optics.* Physical review letters, 68(5):580, 1992. Cited on page 21.

[24] Dum, R, P Zoller, and H Ritsch: *Monte Carlo simulation of the atomic master equation for spontaneous emission.* Physical Review A, 45(7):4879, 1992. Cited 2 times on pages 21 and 26.

[25] Teukolsky, Saul A, Brian P Flannery, WH Press, and WT Vetterling: *Numerical recipes in C.* SMR, 693(1):59–70, 1992. Cited on page 25.

[26] Cohen-Tannoudji, Claude, Jacques Dupont-Roc, and Gilbert Grynberg: *Atom-photon interactions: basic processes and applications.* John Wiley & Sons, 1998. Cited 2 times on pages 27 and 62.

[27] Szabo, Attila and Neil S Ostlund: *Modern quantum chemistry: introduction to advanced electronic structure theory.* Courier Corporation, 2012. Cited on page 34.

[28] Artin, Michael: *Algebra. 2nd*, 2011. Cited on page 37.

[29] Marshall, W: *Antiferromagnetism.* Proceedings of the Royal Society of London. Series A. Mathematical and Physical Sciences, 232(1188):48–68, 1955. Cited on page 40.

[30] Mattis, Daniel C: *Ground-state symmetry in XY model of magnetism.* Physical Review Letters, 42(23):1503, 1979. Cited on page 40.

[31] Salinas, Sílvio RA: *Introdução a física estatística vol. 09.* Edusp, 1997. Cited 2 times on pages 41 and 43.

[32] Brush, Stephen G: *History of the Lenz-Ising model.* Reviews of modern physics, 39(4):883, 1967. Cited on page 41.

[33] Parkinson, John B and Damian JJ Farnell: *An introduction to quantum spin systems*, volume 816. Springer, 2010. Cited on page 43.

[34] Hubbard, John: *Electron correlations in narrow energy bands III. An improved solution.* Proceedings of the Royal Society of London. Series A. Mathematical and Physical Sciences, 281(1386):401–419, 1964. Cited on page 43.

[35] Dalmonte, Marcello and Simone Montangero: *Lattice gauge theory simulations in the quantum information era.* Contemporary Physics, 57(3):388–412, 2016. Cited on page 43.

[36] Metcalf, Harold J and Peter Van der Straten: *Laser cooling and trapping*. Springer Science & Business Media, 1999. Cited 2 times on pages 45 and 46.

[37] Morgado, M and S Whitlock: *Quantum simulation and computing with Rydberg-interacting qubits*. AVS Quantum Science, 3(2), 2021. Cited on page 45.

[38] Dalibard, Jean: *Collisional dynamics of ultra-cold atomic gases*. In *Bose-Einstein Condensation in Atomic Gases*, pages 321–349. IOS Press, 1999. Cited on page 46.

[39] Jaksch, Dieter, Christoph Bruder, Juan Ignacio Cirac, Crispin W Gardiner, and Peter Zoller: *Cold bosonic atoms in optical lattices*. Physical Review Letters, 81(15):3108, 1998. Cited on page 46.

[40] García-Ripoll, Juan José, Stephan Dürr, Niels Syassen, Dominik M Bauer, Matthias Lettner, Gerhard Rempe, and J Ignacio Cirac: *Dissipation-induced hard-core boson gas in an optical lattice*. New Journal of Physics, 11(1):013053, 2009. Cited 4 times on pages 46, 47, 49, and 84.

[41] Lihm, Jae Mo and Cheol Hwan Park: *Wannier function perturbation theory: localized representation and interpolation of wave function perturbation*. Physical Review X, 11(4):041053, 2021. Cited on page 47.

[42] Gontier, David, Antoine Levitt, and Sami Siraj-Dine: *Numerical construction of Wannier functions through homotopy*. Journal of Mathematical Physics, 60(3), 2019. Cited on page 47.

[43] Cirac, J Ignacio and Peter Zoller: *Goals and opportunities in quantum simulation*. Nature physics, 8(4):264–266, 2012. Cited on page 49.

[44] Asenjo-Garcia, Ana, M Moreno-Cardoner, Andreas Albrecht, HJ Kimble, and Darrick E Chang: *Exponential improvement in photon storage fidelities using subradiance and "selective radiance" in atomic arrays*. Physical Review X, 7(3):031024, 2017. Cited on page 49.

[45] Radzihovsky, Leo, Peter B Weichman, and Jae I Park: *Superfluidity and phase transitions in a resonant Bose gas*. Annals of Physics, 323(10):2376–2451, 2008. Cited 2 times on pages 49 and 84.

[46] Gericke, Tatjana, Peter Würtz, Daniel Reitz, Tim Langen, and Herwig Ott: *High-resolution scanning electron microscopy of an ultracold quantum gas*. Nature Physics, 4(12):949–953, 2008. Cited 2 times on pages 49 and 86.

[47] Barontini, Giovanni, R Labouvie, F Stubenrauch, A Vogler, V Guarrera, and H Ott: *Controlling the dynamics of an open many-body quantum system with localized*

*dissipation*. Physical review letters, 110(3):035302, 2013. Cited 2 times on pages 49 and 86.

[48] Auerbach, Assa: *Interacting electrons and quantum magnetism*. Springer Science & Business Media, 1998. Cited on page 50.

[49] Misra, Baidyanath and EC George Sudarshan: *The Zeno's paradox in quantum theory*. Journal of Mathematical Physics, 18(4):756–763, 1977. Cited on page 53.

[50] Itano, Wayne M, Daniel J Heinzen, John J Bollinger, and David J Wineland: *Quantum zeno effect*. Physical Review A, 41(5):2295, 1990. Cited on page 54.

[51] Gagen, MJ, HM Wiseman, and GJ Milburn: *Continuous position measurements and the quantum Zeno effect*. Physical Review A, 48(1):132, 1993. Cited on page 54.

[52] Syassen, Niels, Dominik M Bauer, Matthias Lettner, Thomas Volz, Daniel Dietze, Juan J Garcia-Ripoll, J Ignacio Cirac, Gerhard Rempe, and S Durr: *Strong dissipation inhibits losses and induces correlations in cold molecular gases*. Science, 320(5881):1329–1331, 2008. Cited on page 56.

[53] Neyenhuis, Brian, Jiehang Zhang, Paul W Hess, Jacob Smith, Aaron C Lee, Phil Richerme, Zhe Xuan Gong, Alexey V Gorshkov, and Christopher Monroe: *Observation of prethermalization in long-range interacting spin chains*. Science advances, 3(8):e1700672, 2017. Cited on page 62.

[54] Vega, Inés de, Diego Porras, and J Ignacio Cirac: *Matter-wave emission in optical lattices: Single particle and collective effects*. Physical review letters, 101(26):260404, 2008. Cited on page 86.

[55] Navarrete-Benlloch, Carlos, Inés de Vega, Diego Porras, and J Ignacio Cirac: *Simulating quantum-optical phenomena with cold atoms in optical lattices*. New Journal of Physics, 13(2):023024, 2011. Cited on page 86.

# Appendices

# APPENDIX A – Derivation of Heisenberg Hamiltonian from Second Order Perturbative Theory on the Hubbard Hamiltonian

We follow the arguments given by Tasaki [2]. Considering the Hubbard Hamiltonian given by

$$H = H_{hop} + H_{int} \tag{A.1}$$

we assume the unperturbed Hamiltonian as being formed by the term $H_{int}$ which is defined as:

$$H_{int} = \sum_j U(n_{j\uparrow} + n_{j\downarrow}) \tag{A.2}$$

we also assume the system is at half-filing, i.e. the total number of electrons in the lattice is equal to the number of sites and $U \gg 1$.

Let $\Gamma_\downarrow \in \Lambda$ be the set of sites where the spin state of the electrons are $\downarrow$ and $\Gamma_\uparrow \in \Lambda$ where their spin states are $\uparrow$. A ground state with zero energy of the interaction Hamiltonian is relized when $\Gamma_\uparrow, \Gamma_\downarrow$ satisfy $\Gamma_\downarrow \cap \Gamma_\uparrow = \emptyset$. These ground states can be represented as

$$|\Psi^\sigma\rangle = (\prod_{j\in\Lambda} c^\dagger_{j,\sigma_j}) \, |\psi_{vac}\rangle \tag{A.3}$$

here $\sigma = (\sigma_j)_{j\in\Lambda}$ with $\sigma_j = \uparrow, \downarrow$ is a spin configuration. Since any spin configuration is allowed, the ground states are $2^{|\Lambda|}$ fold degenerate.

We find that there is no effect of the perturbation $H_{hop}$ to first order. This is because by operating $H_hop$ once onto $|\Psi^\sigma\rangle$ we inevitably and up with an empty site and a doubly occupied one. This new state is no longer a ground state of $H_{int}$ and, therefore, the lowest order contribution from this perturbation theory comes from the second order. This second order contribution generates spin exchange as is illustrated in figure 25.

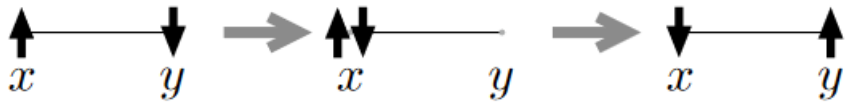


Figure 25 – Illustration of the second order process which is the lowest contribution from perturbation theory on this model (x and y represent sites in the figure)

Let $\mathcal{H}$, be the Hilbert space spanned by all possible spin configurations of the ground state $|\Psi^\sigma\rangle$, and $\mathcal{H}_\perp$ the orthogonal space to $\mathcal{H}$, . Let $P_0$ be the orthogonal projection

onto $\mathcal{H}_{\prime}$. Consider the perturbation Hamiltonian

$$H(\lambda) = H_{int} + \lambda H_{hop}. \tag{A.4}$$

Then, the exact Schrödinger equation for $H(\lambda)$ can be written as

$$(H_{int} + \lambda H_{hop})(|\psi\rangle + |\Gamma\rangle) = E(|\psi\rangle + |\Gamma\rangle\,, \tag{A.5}$$

where $|\psi\rangle \in \mathcal{H}_{\prime}$ and $|\Gamma\rangle \in \mathcal{H}_{\perp}$. Operating $P_0$ to this equation we get

$$\lambda P_0 H_{hop}\,|\Gamma\rangle = E\,|\psi\rangle \tag{A.6}$$

where we we used the fact that $H_{int}\,|\psi\rangle = 0$ and $H_{int}\,|\Gamma\rangle \in \mathcal{H}_{\perp}$. If we now apply $(1 - P_0)$ to equation A.5 we get

$$\lambda H_{hop}\,|\psi\rangle + H_{int}\,|\Gamma\rangle + \lambda(1 - P_0)H_{hop}\,|\Gamma\rangle = E\,|\Gamma\rangle \tag{A.7}$$

which implies

$$\lambda H_{hop}\,|psi\rangle = \{-H_{int} + E + \lambda(1 - P_0)H_{hop}\}\,|\Gamma\rangle \approx -H_{int}\,|\Gamma\rangle \tag{A.8}$$

where we assumed that $E$ and $\lambda H_{hop}$ is much smaller than the energy difference between eigenstates of $H_{int}$. We then find

$$|\Gamma\rangle \approx -\lambda H_{int}^{-1} H_{hop}\,|\psi\rangle \tag{A.9}$$

where $H_{int}^{-1}$ is well defined in the space $\mathcal{H}_{\perp}$. Inserting A.9 into A.6 we get

$$-\lambda^2 P_0 H_{hop} H_{int}^{-1} H_{hop}\,|\psi\rangle \approx E\,|\psi\rangle \tag{A.10}$$

which means that by second order perturbation theory, low-energy eigenstates of $H(\lambda)$ are determined by the effective Hamiltonian

$$H_{eff} = -P_0 H_{hop} H_{int}^{-1} H_{hop} P_0 \tag{A.11}$$

substituting $H_{hop} = J\sum_{j,l\in\Lambda} c_{j,\sigma}^{\dagger} c_{l,\sigma}$ and $H_{int} = \frac{1}{U}$(since there is only one particle on each site) we find

$$-P_0 H_{hop} H_{int}^{-1} H_{hop} P_0 = \sum_{j,l\in\Lambda\sigma,\tau=\uparrow,\downarrow} \frac{J^2}{U} c_{j,\tau}^{\dagger} c_{l,\tau} c_{j,\sigma}^{\dagger} c_{l,\sigma} P_0. \tag{A.12}$$

This can be rewritten in a spin operator form by using the relations

$$\sum_{\sigma,\tau=\uparrow,\downarrow} c_{j,\tau}^{\dagger} c_{l,\tau} c_{j,\sigma}^{\dagger} c_{l,\sigma} = \sum_{\sigma=\uparrow,\downarrow} c_{j,\sigma}^{\dagger} c_{j,\sigma} - \sum_{\sigma,\tau=\uparrow,\downarrow} c_{j,\tau}^{\dagger} c_{j,\sigma} c_{l,\tau}^{\dagger} c_{l,\sigma} \tag{A.13}$$

which implies [2]

$$\sum_{\sigma,\tau=\uparrow,\downarrow} c_{j,\tau}^{\dagger} c_{l,\tau} c_{j,\sigma}^{\dagger} c_{l,\sigma} = n_l - (S_l^{+} S_j^{-} + S_l^{-} S_j^{+}) - \sum_{\sigma=\uparrow,\downarrow} n_{j,\sigma} n_{l,\sigma} \tag{A.14}$$

also, $\sum_{\sigma=\uparrow,\downarrow} n_{j,\sigma} n_{l,\sigma} = 2(S_j^{(z)} S_l^{(z)} + \frac{1}{4} n_j n_l)$ and $(S_l^{+} S_j^{-} + S_l^{-} S_j^{+}) = 2(S_j^{(x)} S_l^{(x)} + S_j^{(y)} S_l^{(y)})$. Which leads to the desired effective Hamiltonian

$$\sum_{j,l\in\Lambda} \frac{2|J|^2}{U}(\mathbf{S_j} \cdot \mathbf{S_l} - \frac{1}{4}) \tag{A.15}$$

# APPENDIX B – Derivation of the Master Equation

We follow the derivation given by Breuer *et al* [11]. Consider the hamiltonian of the total sistem given by:

$$H = H_s + H_B + H_I \tag{B.1}$$

where $H_s$, $H_B$ are the isolated system and bath hamiltonians, respectfully, and $H_I$ is the interaction hamiltonian. We assume that we are working on the weak coupling limit. The Markovian quantum master equation is more conveniently derived on the interaction picture. We shall denote the interaction picture Hamiltonian simply by $H_I(t)$. The Von Neunmann equation in the interaction picture is written as:

$$\frac{d}{dt}\rho(t) = -i[H_I(t), \rho(t)] \tag{B.2}$$

which can be rewritten in its integral form

$$\rho(t) = \rho(0) - i\int_0^t ds[H_I(s), \rho(s)] \tag{B.3}$$

substituting $\rho(t)$ on equation B.2 and tracing over the environment we get

$$\frac{d}{dt}\rho_s(t) = -\int_0^t dstr_B[H_I(t), [H_I(s), \rho(s)]] \tag{B.4}$$

where we assumed that

$$tr_B[H_I(t), \rho(0)] = 0 \tag{B.5}$$

We see from equation B.4 that the differential equation is still in terms of the total density operator $\rho(t)$. To discard this term we first perform a Born approximation, which assumes that, since coupling between system and environment is weak, we can consider the bath state does not change in the evolution, i.e.

$$\rho(t) \approx \rho_s \otimes \rho_B \tag{B.6}$$

inserting B.6 in equation B.4 we get

$$\frac{d}{dt}\rho_s(t) = -\int_0^t dstr_B[H_I(t), [H_I(s), \rho_s(s) \otimes \rho_B]] \tag{B.7}$$

In order to make this equation simpler we perform the second approximation,i.e. We consider the state evolution of the system depends only on the present state. This is called the Markovian approximation and results in the equation

$$\frac{d}{dt}\rho_s(t) = -\int_0^t dstr_B[H_I(t), [H_I(s), \rho_s(t) \otimes \rho_B]] \tag{B.8}$$

where we made the substitution $\rho_s(s) \to \rho_s(t)$. The equation cannot yet be considered a markovian master equation, since it stil depends on the explicit choise for the initial stat at time $t = 0$. In order to obtain a markovian master equation we make the substitution $s \to t - s$ and let the upper limit go to infinity (which is permissible if the integrand disapears suffitiently fast for $s \gg \tau_B$, where $\tau_B$ is the characteristic time scale for the correlation functions of the bath to decay). Thus, we obtain the markovian master equation

$$\frac{d}{dt}\rho_s(t) = -\int_0^\infty dstr_B[H_I(t-s), [H_I(s), \rho_s(t) \otimes \rho_B]] \tag{B.9}$$

In order to obtain the final Lindblad equation we perform a third approximation, which is known as the rotating wave (or secular) approximation. This approximation involves averaging over rapidly oscillating terms in the master equation. To understand it, consider the Schrödinger picture hamilnonian:

$$H_I = \sum_k A_k \otimes B_k \tag{B.10}$$

Where both $A_k$ and $B_k$ are Hermitian operators. The secular approximation is easily obtained if we decompose the hamiltonian B.10 into eigenoperators of the system Hamitonan $H_S$. Assuming the spectrum of $H_S$ is discrete, let the eigenvalues of the system hamiltnonian be represented by the values $\epsilon$ and the projection onto the eigenspace belonging to the eigenvalue $\epsilon$ by $\prod(\epsilon)$. We can, then, define the operators

$$A_k(\omega) := \sum_{\epsilon' - \epsilon = \omega} \prod(\epsilon) A_k \prod(\epsilon'). \tag{B.11}$$

where the sum is over the energy eigenvalues with fixed energy difference $\omega$. From the definition we get:

$$\begin{aligned} [H_S, A_k(\omega)] &= -\omega A_k(\omega), \\ [H_S, A_k(\omega)^\dagger] &= +\omega A_k(\omega)^\dagger. \end{aligned} \tag{B.12}$$

where the operators $A_k$ and $A_k^\dagger$ are said to be eigendoperators of $H_S$ belonging the frequencies $\mp\omega$,respectfully. The corresponding interaction picture operators are given by

$$\begin{aligned} \exp(iH_s t) A_k(\omega) \exp(-iH_s t) &= \exp(-i\omega t) A_k(\omega), \\ \exp(iH_s t) A_k(\omega)^\dagger \exp(-iH_s t) &= \exp(i\omega t) A_k(\omega)^\dagger \end{aligned} \tag{B.13}$$

Summing B.11 over all energy differences and invoking the completeness relation we get:

$$\sum_\omega A_k(\omega) = \sum_\omega A_k^\dagger = A_k. \tag{B.14}$$

Thus, we can cast the interaction Hamiltonian in the following form:

$$H_I = \sum_{k,\omega} A_k(\omega) \otimes B_k = \sum_{k,\omega} A_k(\omega)^\dagger \otimes B_k^\dagger, \tag{B.15}$$

which in the interaction picture is written as

$$H_I = \sum_{k,\omega} e^{-i\omega t} A_k(\omega) \otimes B_k(t) = \sum_{k,\omega} e^{i\omega t} A_k(\omega)^\dagger \otimes B_k^\dagger, \tag{B.16}$$

where $B_k(t) = e^{iH_B t} B_k e^{-iH_B t}$. Inserting the interaction picture operator into the master equation we obtain

$$\frac{d}{dt}\rho_s(t) = \int_0^\infty ds tr_B\{H_I(t-s)\rho_s(t)\rho_B H_I(t) - H_I(t)H_I(t-s)\rho_s(t)\rho_B\} + h.c. \tag{B.17}$$

which leads to

$$\frac{d}{dt}\rho_s(t) = \sum_{\omega,\omega'}\sum_{k,l} e^{i(\omega'-\omega)t}\Gamma_{kl}(A_l(\omega)\rho_S(t)A_k^\dagger(\omega') - A_k^\dagger(\omega')A_l(\omega)\rho_s(t)) + h.c. \tag{B.18}$$

where

$$\Gamma_{kl} = \int_0^\infty ds e^{i\omega s}\langle B_k^\dagger(t)B_l(t-s)\rangle, \tag{B.19}$$

and

$$\langle B_k^\dagger(t)B_l(t-s)\rangle := tr_B\{B_k^\dagger(t)B_l(t-s)\rho_B\}. \tag{B.20}$$

Let us denote $\tau_s$ as the time scale of the intrinsic evolution of the system, which is defined by a typical value fo $|\omega' - \omega|$, $\omega' \neq \omega$. If $\tau_s$ is large compared to the open system relaxation time $\tau_R$ the terms for which $\omega' \neq \omega$ may be neglected. This condition is known as rotating wave approximation, and, from this approximation, we get

$$\frac{d}{dt}\rho_s(t) = \sum_{\omega}\sum_{k,l} \Gamma_{kl}(A_l(\omega)\rho_S(t)A_k^\dagger(\omega) - A_k^\dagger(\omega)A_l(\omega)\rho_s(t)) + h.c. \tag{B.21}$$

We can also decompose the Fourier transformation of the reservoir correlation functions as follows

$$\Gamma_{kl}(\omega) = \frac{1}{2}\gamma_{kl}(\omega) + iS_{kl}(\omega) \tag{B.22}$$

where for fixed $\omega$ coefficients

$$S_{kl}(\omega) = \frac{1}{2i}(\Gamma_{kl}(\omega) - \Gamma_{kl}^*(\omega)) \tag{B.23}$$

form a Hermitian matrix and the matrix defined by

$$\gamma_{kl} = \Gamma_{kl}(\omega) + \Gamma_{kl}^*(\omega) \tag{B.24}$$

is positive. This leads to the interaction picture master equation

$$\frac{d}{dt}\rho_s(t) = -i[H_{LS}, \rho_s(t)] + \sum_{\omega}\sum_{kl}\gamma_{kl}(\omega)\left(A_l(\omega)\rho_s A_k^\dagger(\omega) - \frac{1}{2}\{A_k^\dagger(\omega)A_l(\omega), \rho_s\}\right) \tag{B.25}$$

where

$$H_{LS} = \sum_{\omega}\sum_{kl} S_{kl}(\omega)A_k^\dagger(\omega)A_l(\omega) \tag{B.26}$$

which can be written in Lindblad form if we diagnonalize the matrix $\gamma_{kl}$

# APPENDIX C – Second Quantization

In this chapter, we follow the description of [2] of the second Quantization (or Fock space representation) for tight binding electron systems.

## C.1 Fermionic Anticommutation Relations

To each lattice site $j \in \Lambda$ and spin index $\sigma = \uparrow, \downarrow$ we associate a fermion operator $c_{j,\sigma}$. Those operators satisfy the anticommutation relations

$$\{c^\dagger_{j,\sigma}, c^\dagger_{l,\tau}\} = \{c_{j,\sigma}, c_{l,\tau}\} = 0 \tag{C.1}$$

and

$$\{c_{j,\sigma}, c^\dagger_{l,\tau}\} = \delta_{j,l}\delta\sigma, \tau \tag{C.2}$$

for any $j, l \in \Lambda$ and $\sigma, \tau = \uparrow, \downarrow$, where the anticommutator is defined as $\{A, B\} = AB + BA$. Eq. C.1 implies $c^2_{j,\sigma} = (c^\dagger_{j,\sigma})^2 = 0$. The operators $c^\dagger_{j,\sigma}$, and $c_{j,\sigma}$ may be considered the creation and annihilation operators,respctfully, of an electron at site $j$ with spin $\sigma$. We define the number operator (which represents the number of electrons with a determied spin state on a site) as

$$n_{j,\sigma} = c^\dagger_{j,\sigma} c_{j,\sigma} \tag{C.3}$$

From C.1 and C.2 we get

$$n^2_{j,\sigma} = c^\dagger_{j,\sigma} c_{j,\sigma} c^\dagger_{j,\sigma} c_{j,\sigma} = c^\dagger_{j,\sigma}(1 - c^\dagger_{j,\sigma} c_{j,\sigma}) c_{j,\sigma} = c^\dagger_{j,\sigma} c_{j,\sigma} = n_{j,\sigma}. \tag{C.4}$$

Therefore we obtain $n_{j,\sigma}(1 - n_{j,\sigma}) = 0$, which implies that $n_{j,\sigma}$ have only the eigenvalues 0 and 1, which is a consequence of Pauli's exclusion principle. Other properties of the number operators are

$$[n_{j,\sigma}, c^\dagger_{l,\tau}] = \delta_{j,l}\delta_{\sigma,\tau} c^\dagger_{j,\sigma} \tag{C.5}$$

and

$$[n_{j,\sigma}, n_{l,\tau}] = 0 \tag{C.6}$$

for any $j, l \in \Lambda$ and $\sigma, \tau = \uparrow, \downarrow$.

The number operator for a single site $j$ is defined as $n_j = n_{j,\uparrow} + n_{j,\downarrow}$, and the total number operator is defined as

$$N := \sum_{j \in \Lambda} n_j = \sum_{j \in \Lambda, \sigma = \uparrow, \downarrow} n_{j,\sigma}. \tag{C.7}$$

## C.2 Hilbert Space

To construct the Hilbert space for many-electrons. Let $|\psi_{vac}\rangle$ be a normalized state which represent the state where the lattice has no electrons. This is respresented by

$$c_{j,\sigma}\,|\psi_{vac}\rangle = 0. \tag{C.8}$$

For an electron system, the total number of particles,$N$, is such that $1 \leq N \leq 2|\Lambda|$. We define a state where $N$ arbitrary sites, $j_1, j_2, ..., j_N \in \Lambda$ with spins $\sigma_1, \sigma_2, ..., \sigma_N = \uparrow, \downarrow$ are occupied by

$$\left|\psi_{(j_1,\sigma_1),...,(j_N,\sigma_N)}\right\rangle = c^\dagger_{j_1,\sigma_1}...c^\dagger_{j_N,\sigma_N}\,|\psi_{vac}\rangle\,. \tag{C.9}$$

All possible states of type C.9 are allowed, given that the anticommutation relations C.1,C.2 are sattisfied. In particular, the state C.9 vanishes whenever $(j_i, \sigma_i) = (j_k, \sigma_k)$ for some $j \neq k$ (which is nothing but Pauli Exclusion principle).

Supposing that $\left|\psi_{(j_1,\sigma_1,...,(j_N,\sigma_N)}\right\rangle$ is nonvanishing, we find by using C.5 and $n_{j,\sigma}\,|\psi_{vac}\rangle = 0$ that

$$n_{j,\sigma}\left|\psi_{(j_1,\sigma_1),...,(j_N,\sigma_N)}\right\rangle = \begin{cases} \left|\psi_{(j_1,\sigma_1),...,(j_N,\sigma_N)}\right\rangle \text{ if } (j_i,\sigma_i) = (j,\sigma) \text{ for some i} \\ \\ 0 \text{ otherwise} \end{cases} \tag{C.10}$$

The hilbert space which contains all possible eclectron numubers, namely

$$\mathcal{F} := \mathcal{H}_0 \oplus \mathcal{H}_1 \oplus ... \oplus \mathcal{H}_{2|\Lambda|} \tag{C.11}$$

is known as Fock space. Both the operators $c_{j,\sigma}$ and $c^\dagger_{j,\sigma}$ act on this space, which is why this formalism of quantum mechanics is called the Fock space representation.

## C.3 Bosonic Second Quantization

The derivation of Fock Space representation for bosons is analogous to the development made in the last sections. The difference being that the creation, $a^\dagger_{j,\sigma}$ and annihilation,$a_{j,\sigma}$, operators must satisfy the commutation relations

$$[a^\dagger_{j,\sigma}, a^\dagger_{l,\tau}] = [a_{j,\sigma}, a_{l,\tau}] = 0 \tag{C.12}$$

$$[a_{j,\sigma}, a^\dagger_{l,\tau}] = \delta_{j,l}\delta_{\sigma,\tau} \tag{C.13}$$

# APPENDIX D – 3-particle and 1-particle Loss Dissipation

## D.0.1 3-Particle Loss

It is common for 3 body loss events to occur on different kinds of many body systems, usually leading to undesired effects which may jeopardise the control over the system being studied. Neverthelss it is an interesting result that strong dissipative processes may be used in AMO systems which undergo three-body loss events in order to induce effective three body interactions that are normally difficult to produce in dilute quantum gases. This is possible due to the quantum Zeno effect that can be used to suppress three-body losses in these systems. Under proper approximations the systems which have such loss processes may be described by a Markovian master equation, as was the case shown for two-body loss events in the last section.

A typical way to picture three-body loss processes is shown in figure 26. There, collision processes between two atoms give rise to molecules which have a large binding energy when compared to the trap potential. As a result of the three-body interaction between a particle and a molecule a three body loss happens and they are ejected from the system. In the case where the binding energy released in the collision is much greater then the trap energy and the particles are ejected immediately after the interaction, the system evolution can be described by a master equation which is given by

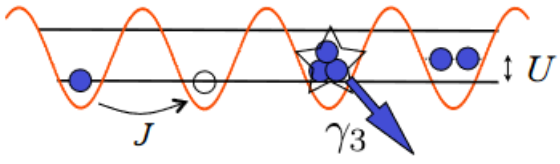


Figure 26 – Schemetics of bosons in an optical lattice in the presence of three-body loss at a rate $\gamma_3$. Figure extracted from [8]

$$\frac{d\rho}{dt} = -i(H_{eff}\rho - \rho H_{eff}^{\dagger}) + \frac{\gamma_3}{6}\sum_i a_i^3 \rho (a_i^{\dagger})^3 \tag{D.1}$$

where the effective Hamiltonian is given by:

$$H_{eff} = H_{BH+} - i\frac{\gamma_3}{12}\sum_i (a_i^{\dagger})^3 a_i^3 \tag{D.2}$$

where $H_{BH+}$ is the Bose-Hubbard Hamiltonian with an elastic interaction term:

$$H_{BH+} = -J\sum_{\langle j,l\rangle} a_j^\dagger a_l + \frac{U}{2}\sum_l a_l^\dagger a_l(a_l^\dagger a_l - 1) + \sum_i \epsilon_i a_i^\dagger a_i \tag{D.3}$$

According to Daley et al. [8], in the regime where $\gamma_3 \gg J, U$ it is possible to use perturbation theory in order to derive an efective Hamiltonian in terms of the subspace where the system has at most two particle per site. The effective Hamiltoninan, given by second order perturbation theory, is

$$H_{eff}^P \approx PH_{BH+}P - i\frac{6J^2}{\gamma_3}P\sum_i c_i^\dagger c_i P \tag{D.4}$$

where $c_i = (a_i^2/\sqrt{2})\sum_{j\in N_i} a_j$, $N_i$ is the set of nearest neighbours of the site i, and P is the projector onto the subspace of states which have a maximum number of two atoms per site. The first term on the right handside of equation D.4 describes the Hubbard dynamics with the constraint $(b_\dagger)^3$. Moreover, it can be shown that the effective loss rate decreases as $\frac{J^2}{\gamma_3}$ which is also expected when the quantum Zeno effect happens in systems which undergo two-particle loss [4, 40].

In ref [8] the study of the full non-equilibrium dynamics of the system was realized with a combination of t-DMRG and the quantum trajectories technique. After a close look at the behavior of the system in the limit of large $\gamma_3$ (so as to to have an account of the phase transitions for the projected Hamiltonian $PHP$), it was observed that, for $U/J > 0$, the system had the Mott-Insulator and Atomic Superfluid Phases. Nevertheless, the three-body loss constraint also had the system stabilized for $U/J < 0$ where a dimmer superfluid phase was found. The dimmer superfluid phase arises when the order parameter, which indicates superfluidity of single atoms (ASF) ($\langle b_i\rangle = 0$), vanishes while a dimmer superfluidity (DSF) order parameter continues to be observed ($\langle b_i^2\rangle \neq 0$). According to Romans et al. [45] these regimes are assotiated with quantum phase trasitions that lead to the spontaneous braking of a discrete $Z_2$ symmetry. Figure 27 shows a phase diagram of $U/J$ as a function of the density $n$ of particles with the constraint $n \leq 2$. The diagram was obtained using mean-field theory via the homogeneous Gutzwiller ansatz wavefunction. We can see that for $n \to 1$ the ASF-DSF transitions occur at the same coupling strength as the ASF-MI transition with opposit sign.

In order to understand the dynamics of the material undergoing phase transition from Mott insulator to Dimmer superfluid, the quantum trajectories approach was used. The results of the simulations are shown in figure 28. The change of the total energy(sum of the kinetic and interaction energies) for two types of lattices were analysed, i.e. for "lossless" (meaning only the evolution of effective Hamiltonian was considered) and "lossy" (evolution of the complete master equation) processes. Figure 28 (a) (i) shows the first

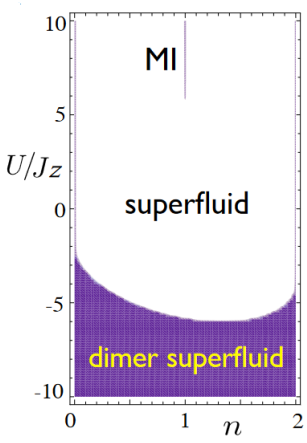


Figure 27 – Mean-field phase diagram of $U/J$ as a function of the density, n, for the projected Bose-Hubbard model. Figure extracted from [8]

lattice type, which is a Mott Insulator with one particle on each site. The second lattice type is shown in figure 28 (a) (ii) where a superposition of lattices rose the energy of certain sites and formed a Mott insulator with two particles per site in the lowest wells. The interaction strength was adiabatically altered as the systems evolved in order to reach the dimmer superfluid regime. In lattice (i) $U/J$ was ramped from $U/J = 30$ to $U/J = -8$ whereas the initial value of $U/J$ in (ii) was changed to the value $U/J = -8$ in a timescale much faster than the tunnelling between the lowest wells, then the superlattice was ramped down.

In figure 28b,c the sum of kinetic and interaction energies vs time is shown for single trajectories. Two types of trajectories were evaluated for each ramp type, the first is a "lossless" trajectory where the ground state is reached adiabatically and the second in a "lossy" trajectory, where three particle ejections happen in the system as it evolves creating heat. The probability of each type of lattice to produce a "lossless" trajectory (which means that after the evolution of a "lossy" trajectory no quantum jumps occured) is shown in figure 28 d. It is clearly seen that the type (ii) lattice is much more likely to decay to the ground state without losing particles on the time span considered.

Finally, figure 29 shows the the local density versus time and the matrix $D(i, j)$ which represents the matrix elements of $\langle a_i^\dagger a_i^\dagger a_j a_j \rangle$ which are the off diagonal elements that characterize the dimmer superfluid phase. Part $(a)$ represents a lossless trajectory while part $(b)$ a "lossy" one for the systems of figure 28. It can be seen that even with loss of particles some elements of the dimmer matrix persist which indicates that dimmer superfluid behavior can be seen experimentally.

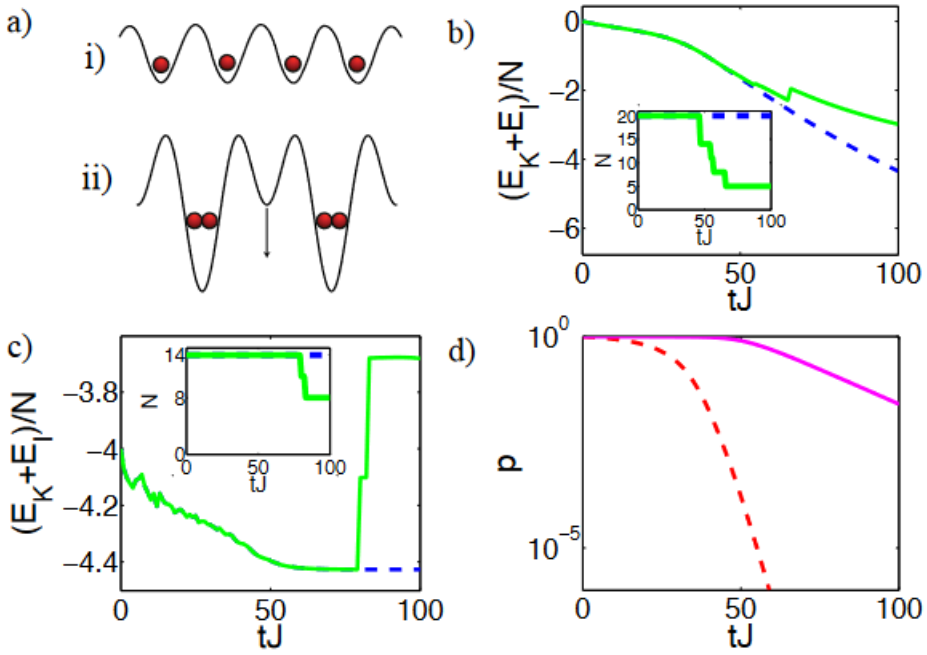


Figure 28 – Dynamics of adiabatic ramps into a dimer superfluid regime. (a) We begin with (i) a Mott-insulator state (ramping U/J), and (ii) a state with pre-prepared dimers in a superlat- tice (removing the superlattice). (b)-(c) The sum of kinetic ($E_K$ ) and interaction ($E_I$ ) energy and (inset) particle number as a function of time for two example trajectories, one with no loss events (dashed lines) and one with several loss events (solid lines). Here, (b) shows a ramp from $U/J = 30$ to $U/J = -8$, with $U(t) = \alpha J/(100 + 3tJ) + \gamma$, with $\alpha$ and $\gamma$ ramp parameters, and (c) shows a ramp with a superlattice potential, $\epsilon_l = V0cos(2\pi l/3)$, where $V_0 \approx 30Jexp(-0.1tJ)$, adjusted so that $V_0(tJ = 100) = 0$, with fixed $U/J = -8$. In each case, $\gamma_3 = 250J$. For (b), we use 20 atoms on 20 lattice sites, for (c), 14 atoms on 23 lattice sites. (d) Plot showing the probability that no loss event has occurred after time t for the ramps in (b) (dashed line) and (c) (solid). Image extracted from [8]

### D.0.2 1-Particle Loss

Single particle loss events can be seen in a variety of setups, such as ionizing atoms in a Bose Einstein condensate (BEC) with an electron beam [46, 47] as is illustrated in figure 30 and driving atoms to momentum states that have greater energy than the lattice depth through photon scattering [54, 55]. Localized single particle losses have been achieved experimentally using high-resolution electron microscopy to probe a BEC with high precision [46]. The one dimensional Bose-Einstein condensate may be represented (in a considerable parameter range) by the Bose-Hubbard model

$$H_{BEC} = \sum_l \Big[ - J(b_l^\dagger b_{l+1} + b_{l+1}^\dagger b_l) + \frac{U}{2} n_l(n_l - 1) \Big] \tag{D.5}$$

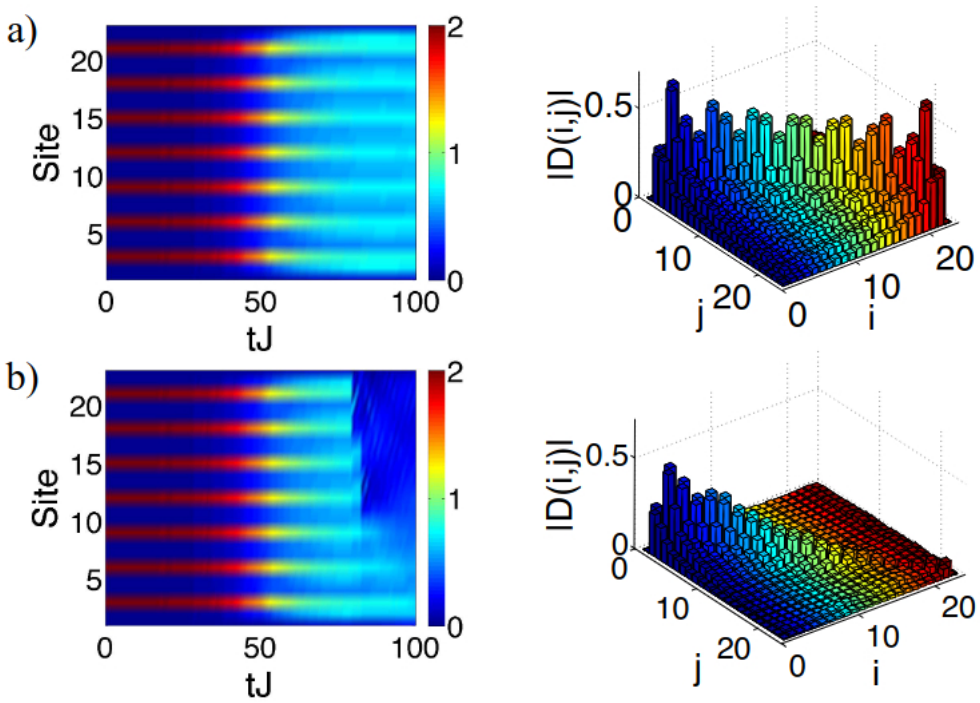


Figure 29 – Comparison of (a) lossless and (b) lossy trajectories from figure 28. The mean density $\langle n_i \rangle$ is shown as a function of position and time, and the magnitude of the dimer correlation at the $\|D(i,j)\|(i \neq j)$. Figure extracted from [8]

where we consider a system with open boundaries ranging from $l = -(L-1)/2$ to $l = (L-1)/2$ (L being the number of sites).

In an experiment the initial state of the system without any dissipative effects may be set to the BEC ground state. Considering an electron beam or a scattering light beam is used to probe this condensate at site $l = 0$ at time $t = 0$ the interactions with the BEC gas lead to particle loss in the system, i.e. the emission of single particles from site 0. If the the atoms are expelled quickly enough, we can use the approximations needed to describe the system dynamics with a master equation:

$$\dot{\rho} = -i[H_{BEC}, \rho] + \Gamma(b_0 \rho b_0^\dagger) - \frac{\Gamma}{2}(n_0 \rho) - \frac{\Gamma}{2}(\rho n_0). \tag{D.6}$$

According to Barmettler and Kollath [10] the strength of dissipation will depend on the cross-section of the scattering between the atoms and the type of probing method e.g. the electron beam. The master equation can then be solved by using quantum trajectories with effective Hamiltonian $H_{eff} = H_{BEC} - i\Gamma n_0$ which should represent the dynamics of the system given that no atom loss is detected, and, as in the case with 2 and 3 particle losses seen in the last sections, atom loss detection can be simulated by stochastically applying annihilation bosonic field operators to the system state vector. This was done in [10] by using t-DMRG to evolve the system state between quantum jumps, which

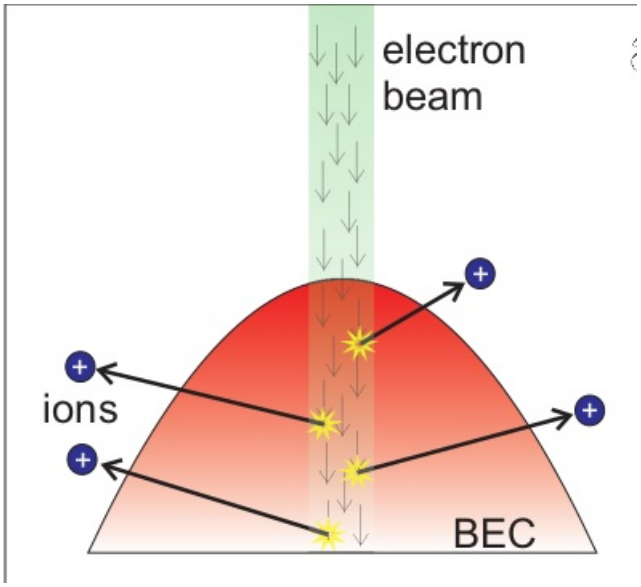


Figure 30 – Illustrative image of the ionization of atoms of a Bose Einstein condensate by an electron beam. Figure extracted from [9]

allowed for the simulation of a system with a considerable number of sites ($L = 105$). To study how the system behaves at long times we can focus on how occupation density at site 0 affects the total state of the BEC, this is shown in figures 31, 32 for weak and strong dissipations, respectfully. In Figure 31(a-b) the normalized occupation density is presented for three different times and for different interaction parameters. In the strong interaction limit a dark density modulation caused by the loss at site zero propagates at sound speed (close to $2Jat/\hbar$ where a is the distance between sites), this behavior is seen both for a Tonks-Girardeau gas [1] and Mott Insulator states [10]. On the other hand, in the weak interaction limit there is a formation of a shock wave which travels at a speed that strongly exceeds $Jat/\hbar$, only after the this wave the dark density modulation caused by dissipative effects propagates as expected. Analysing single trajectories in which atom losses have been both detected ,$\psi_{hole}(t)$, and not detected ,$\psi_{nd}(t)$, as is shown in figure 31(a) it is possible to see that the non detection dynamics has the most important role to explain the origin of the shock wave, eventhough $\psi_{hole}(t)$ causes a larger perturbation than $\psi_{nd}(t)$.

In figure 31(c) it is possible to see that the the underlying dynamics of the system goes unnoticed i.e. has no apparent effect on the evolution of the total loss number $(N(t)/n_{in})$ in short time scales the evolution of $N(t)$ is given by $N(t) = 1 - e^{-\Gamma t}$ as expected for any type of system. More interestingly, the initial state, interaction strength, as well as the initial number of particles have little effect on the total number of particles detected in time. It can also be seen that the time dependence of $N(t)$ is approximately linear. In order to see clearly the differences in the behavior of $N(t)$ the occupation

[1] A Tonks-Girardeu gas is a one dimensional bose gas with hard-core constraint in the strong interaction regime

number at site 0 ($n_0(t)$) was plotted as a function of time. The figure shows $n_0$ reaches a quasi-steady state after a slowly decaying regime for the respective interaction strengths shown in Figure 31(d). Barmettler and Kollath [10] have found through the analysis of these results that this behavior (short time exponential decay followed by a long time linear rise) is general and should be encountered in a broad range of parameters for this system type.

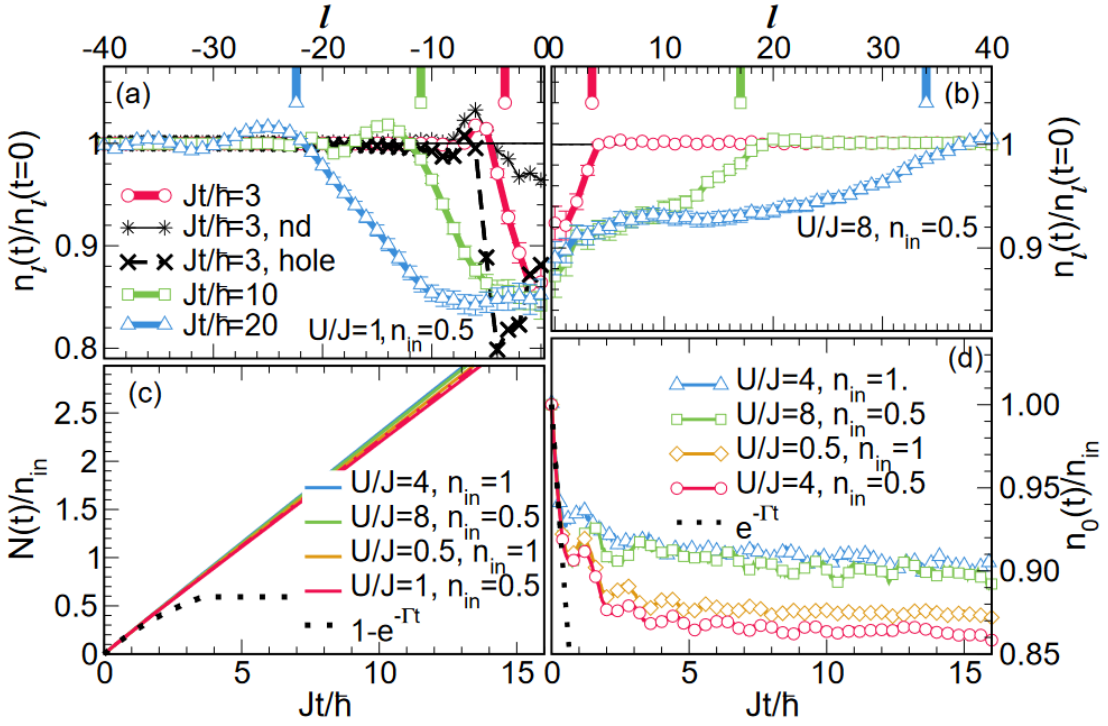


Figure 31 – Weak dissipative coupling $\Gamma/J = 0.25$, L = 105 and 53 or 105 particles. (a) and (b) show density profiles at different times. Densities are rescaled by their initial values and size-dependent features in the vicinity of the edges of the systems are discarded. The 'light- cone' of waves moving with the sound velocity [20] is depicted by vertical lines. Star and cross symbols represent $|\psi_{nd}\rangle$, $|\psi_{hole}\rangle$ respectively. In the lower panels the total atom loss is ploted in (c) and the central density in (d), both rescaled by the initial density nin. In (c) 4 curves almost lie on top of each other. Boundary effects are eliminated by interrupting simulations before reaching the recurrence times. Statistical errors are either marked by bars or smaller than line width or symbol size. Image extracted from [10]

Figure 32 (a,b) shows that the behavior of the BEC for strong dissipative effect ($\Gamma \gg J, U$) is very similar to the one observed for weak dissipation. The major difference is that now the total number of particle loss is very sensitive to the initial state as is shown in figure 32(c). In this case the Von Neumann entropy was also calculated (Figure 32(d)) and it is shown to have an interesting behavior i.e. the site 0 defect can generate strong entanglement increase between the sub systems formed by it. In small time scales the entropy decreases due to the projection performed by the measurements and , after that,

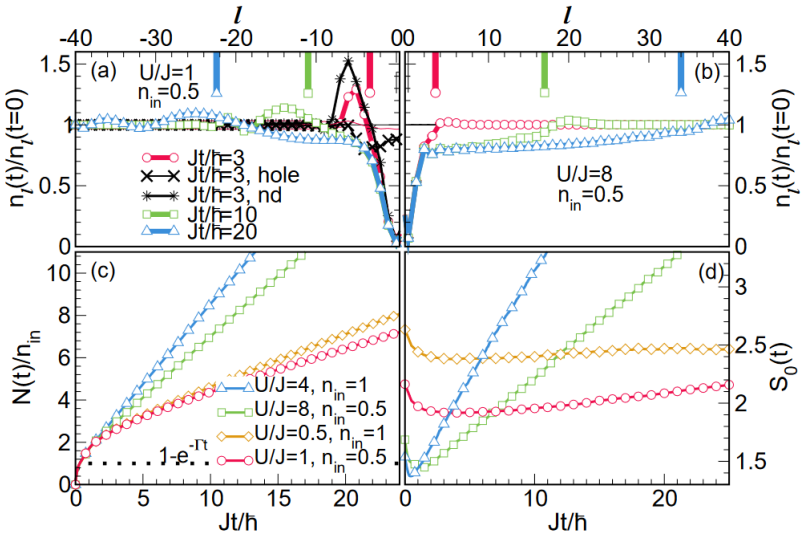


Figure 32 – Numerical results for strongly dissipative coupling, $\Gamma/J = 8$. (a-b) are explained in figure 31. (d) represents the Von Neunmann entropy between the bipartite system formed by the defect at $l = 0$.

it grows approximately linearly. It is also seen that this dissipative system presents the quantum Zeno effect. In fact, using perturbation theory to analyse the master equations behavior considering an adiabatic particle loss process at the center of the lattice we find that [10]:

$$\dot{N}(t \gg \hbar/J) \approx \frac{8J^2}{\Gamma} n_{\mp(L-1)/2}(t=0) \tag{D.7}$$

the effect was also numerically avaluated by Barmettler and Kollath and is shown in figure 33

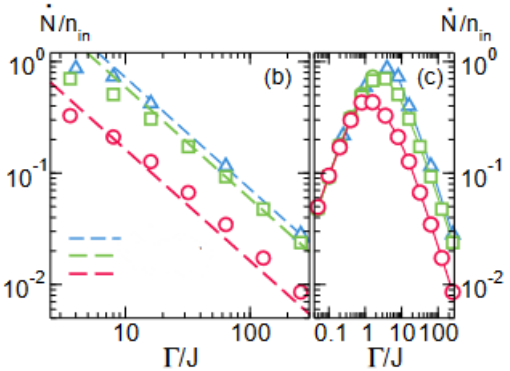


Figure 33 – Zeno effect perceived in the total loss rate for various three initial total occupation numbers ($n_{in} = 1(triangle)$ *and* $n_{in=0.5}(circle\ and\ square)$ and also interaction strengths ($U/J = 4(triangle)$, $U/J = 8(square)$ *and* $U/J = 1(circle)$)

# APPENDIX E – Further Results on the Dynamics of Particle Density of Section 4.2.2.2

We use the one dimensional Hubbard model given by Eq. 4.10 to otain the particle density of the sites of a 5-site lattice that starts its evolution with 5 bosons. The results are shown in figure 34 .

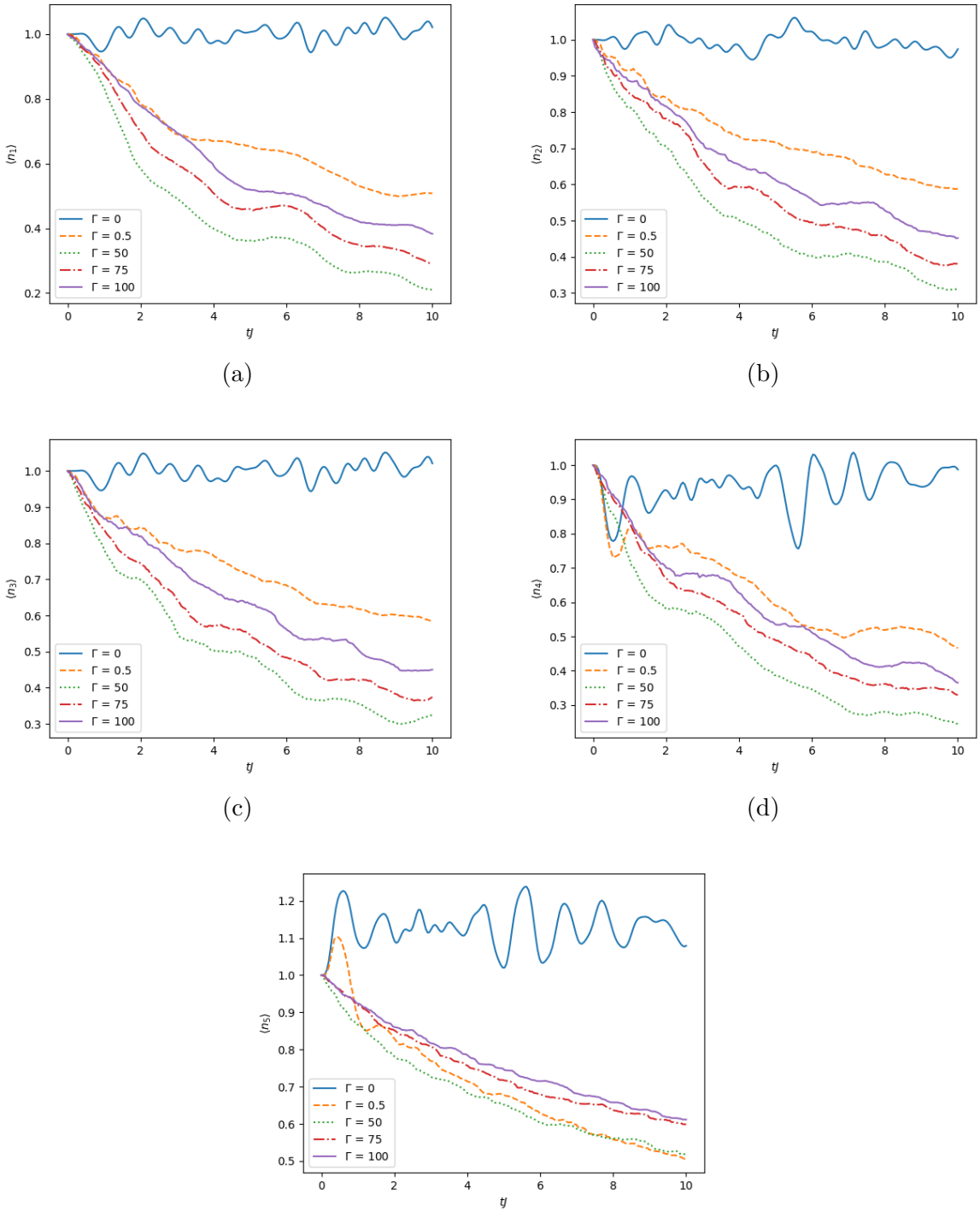


Figure 34 – Particle density dynamics for different Γ at each site of a lattice with 5 sites and (initially) 5 bosons. The Evolution was done using quantum trajectories. Here we see that the average density at each site tend to decay more slowly with time as we increase the dissipation strength (see green, red and purple lines). As a means to comparison, we have obtained the dynamics of the density for weak dissipation(Orange dashed lines). It is clear from the figures that as we increase dissipation strength the particle density loss over time get close to the case of weak dissipation.